NTNU

Norwegian University of
Science and Technology

Analysis and Design of Bjørnafjorden TLP Supported Suspension Bridge Subjected to Large Ship Collisions and Extreme Environmental Loads

Ole Harald Moe

NTNU

Analysis and Design of Bjørnafjorden TLP Supported Suspension Bridge Subjected to Large Ship Collisions and Extreme Environmental Loads

Ole Harald Moe

June 2016

MASTER THESIS

Department of Marine Technology

Norwegian University of Science and Technology

Supervisor: Professor Jørgen Amdahl

MASTER THESIS 2016

For

Stud. Techn. Ole Harald Moe

Analysis and Design Bjørnefjorden TLP Supported Suspension Bridge subjected to Large Ship Collisions and Extreme Environmental Loads

Analyse og dimensjonering Bjørnefjorden TLP understøttede hengebro utsatt for støt fra store skip og ekstreme miljøkrefter

The Norwegian Public Roads Administration (NPRA) is running a project "Ferry free coastal route E39", where the where suspension bridges, floating bridges or submerged tunnels would be installed across fjords in Western Norway. The straits are up 5 kilometres wide and will call for significant extension of present technology. Several innovative crossing concepts have been proposed. One of these is the TLP bridge concept, which consists of a 3-span suspension bridge, supported by two tension leg moored floaters and two fixed traditional concrete Pylons. The 3 main spans of the bridge have a length of 1385m. The side span on the south is approximately 300m and 353m at the northern end. The water depth is 550m at one floater and 450m at the other. The sketch below illustrates the technical concept of the Bridge
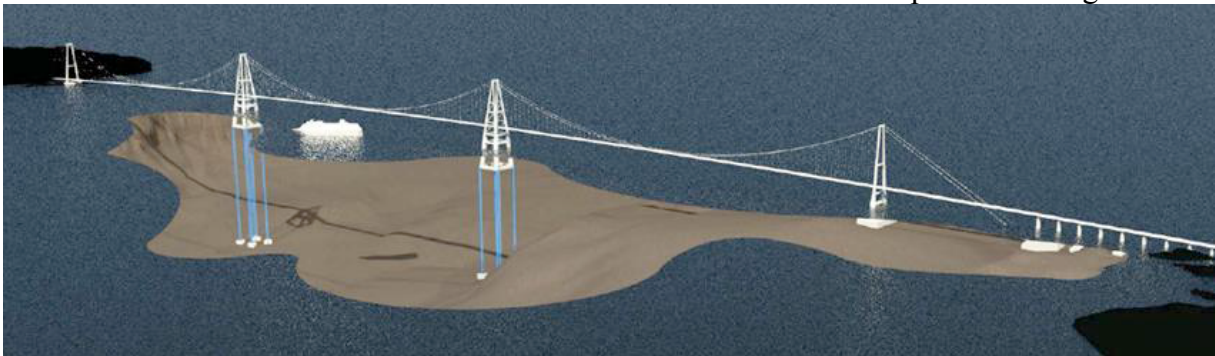
The bridge has to resist extreme environmental loads and accidental actions with acceptable safety levels. One of the concerns are accidental ship collisions with energies 100-1500 MJ. The proposed concepts cannot be designed adequately using existing methods and design rules. Consequently, advanced scenario-based analyses have to be conducted based on accurate simulation of the governing physical processes.

This TLP will be single leg floater with arms below the free surface for attachment of the tension legs. A floating ring structure at the free surface, which is connected to the tension leg attachment points and shall ensure sufficient stability in transport and installation phase, is intended to act as a device to absorb energy during a ship impact event. The ring will be pushed forward and due to this motion be submerged. The increased buoyancy and hydrodynamic drag should dissipate the major part of the collision energy.
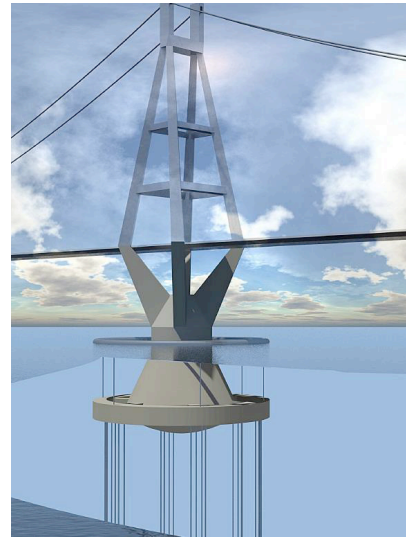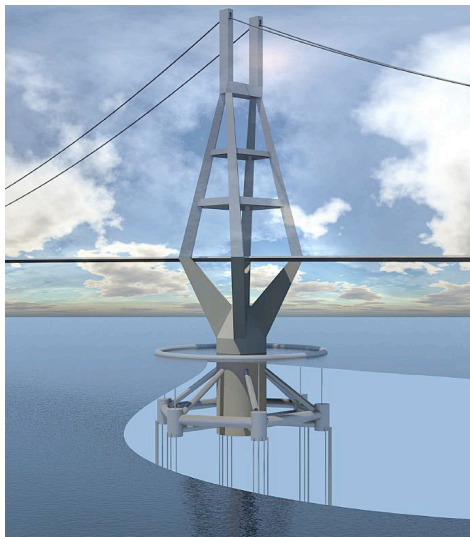
The purpose of the work is to quantify the energy absorption of the protection device and the forces transmitted to the TLP support during collision.

Scope of work:

1. Establish a finite model of the entire bridge and the protection device for USFOS analysis based on input from TDA. Conduct eigenperiod analysis and compare with the results obtained with alternative software (e.g. MD Bridge).

2. Conduct simulation of the complete system during collision. Ship force-deformation curve obtained form LS_DYNA analysis shall be modelled with a nonlinear spring and the ship with a nodal mass with initial velocity. Central collisions shall be assumed initially. Assess the forces transmitted to the TLP bridge and compare the results with those from simplified analysis. Evaluate if it is possible to split the analysis into two steps:

   i)   Collision response of protection device (fixed at tower base and
   ii) Response of the bridge based on force-time histories transferred to the tower base.

   Perform analysis with varying collision energies. Depending on the collision energy it may be necessary to vary the size of the protection barrier. To the extent possible, compare results obtained with the MATLAB program.

3. If the barrier should contact the tower, introduce a second nonlinear spring(s) that account for this situation.

4. Perform analysis of non-central impacts, where ship may be deflected away from the TLP. Use a new model for global ship motions if this becomes available during thesis period.

5. Propose a barrier design that is sufficiently strong to maintain the global behaviour during collision with the bow. The local model of the barrier should be analysed for bulbous bow impact with LS_DYNA.

6. Perform collisions directly on the tower and compare the results with those obtained with the protection barrier. Propose a design for a steel tower that is strong enough to crush the ship bow. Verify the design by local analysis with LD_DYNA.

7. Perform dynamic, time domain response analysis of the bridge subjected to extreme wind and waves. Turbulent wind may be created with the program WINDSIM. Stochastic waves may be based on relevant sea spectra forf the site. Check the utilization of critical members.. Compare the results with corresponding values obtained with other computer programs. Apply the contour method or similar approaches to determine the extreme response. Scripting should be sued to facilitate a large no. of simulations.

8. Conclusions and recommendations for further work

Literature studies of specific topics relevant to the thesis work may be included.

The work scope may prove to be larger than initially anticipated. Subject to approval from the supervisor, topics may be deleted from the list above or reduced in extent.

In the thesis the candidate shall present his personal contribution to the resolution of problems within the scope of the thesis work.

Theories and conclusions should be based on mathematical derivations and/or logic reasoning identifying the various steps in the deduction.

The candidate should utilise the existing possibilities for obtaining relevant literature.

The thesis should be organised in a rational manner to give a clear exposition of results, assessments, and conclusions. The text should be brief and to the point, with a clear language. Telegraphic language should be avoided.

The thesis shall contain the following elements: A text defining the scope, preface, list of contents, summary, main body of thesis, conclusions with recommendations for further work, list of symbols and acronyms, references and (optional) appendices. All figures, tables and equations shall be numerated.

The supervisor may require that the candidate, in an early stage of the work, presents a written plan for the completion of the work. The plan should include a budget for the use of computer and laboratory resources, which will be charged to the department. Overruns shall be reported to the supervisor.

The original contribution of the candidate and material taken from other sources shall be clearly defined. Work from other sources shall be properly referenced using an acknowledged referencing system.

The report shall be submitted in two copies:
  - Signed by the candidate
  - The text defining the scope included
  - In bound volume(s)

- Drawings and/or computer prints which cannot be bound should be organised in a separate folder.

Supervisor NTNU:
Prof. Jørgen Amdahl

Deadline:, June 10 2016

Trondheim, January 25 2016

Jørgen Amdahl

Preface

This master thesis is the result of the work done by stud. techn. Ole Harald Moe at the Norwegian University of Science and Technolog during the spring of 2016. The work builds on the project thesis which was written during the autumn of 2015, with scope of work and problem description formulated by Professor Jørgen Amdahl. The scope of work was updated continuously throughout the process. This was necessitated based on evaluation of the preliminary results in understanding with Prof. Jørgen Amdahl as the work progressed. The main change in scope was to turn the focus away from local modelling and towards the global response of the bridge when subjected to environmental loading. In addition to this glancing ship impacts were not studied as the model for global ship motions was not available.

Trondheim, June 9, 2016

Ole Harald Moe

Abstract

The objective of this thesis is to study the global response of a tether anchored floating suspension bridge over Bjørnafjorden when it is subjected to ship impacts and extreme environmental loads. Bjørnafjorden south of Bergen is one of the fjords, where the ferry crossing is proposed to be replaced by a bridge. The proposed crossing has a length of over 4 000 metres and depths of over 450 metres. Due to the length and depth of this fjord it is not possible to use a conventional bridge. Instead the proposed design is to build a three span suspension bridge supported by two TLP floaters. Each of the main spans has a length of 1 380 metres, and the sailing height is 45 metres. One of the features of this design is a circular tube at the sea surface. This is connected to the floater through tethers and is thought to give stability in the installation phase and act as a barrier against ship impacts. The bridge has eigenperiods spanning from 100 to 4 seconds, making it behave dynamically for many types of loads.

The geometry of the barrier was established based on simplified methods in order to find a combination minimising motions and strain energy. One of the key questions in this thesis is how this barrier influences the response of the bridge due to ship impacts. In order to establish this, several collision analyses were conducted with energies spanning from 50 to 1 200 [MJ]. With the vessels both colliding against the barrier and directly against the floater. In the analyses the ship was modelled as a nodal mass given an initial velocity. It was connected to the bridge through springs. One of these where one was given the force deformation characteristic of the vessel, while the other spring was used to ensure that the system did not have any tensile stiffness. One of the key results from these analyses was that the barrier increased the global motions, making it disadvantageous for the global response.

Another key question in this thesis was to investigate the response of the bridge when subjected to extreme environmental loads. The load components used were the 100 year wind speed, and the second order drift force in the 100 year sea state. A stochastic wind model was used to account for the time and spatial variability of the wind speeds. Since both the wind and wave loads are of a stochastic nature, 30 one hour simulations were conducted. This made it possible to use extreme value statistics to find the 100 year response to environmental loads. The 90 % percentile was used to account for short term variability. These analyses showed that environmental loading yields a larger global response than ship collisions, making it governing for design against global response.

Norsk sammendrag

Hovedformålet med denne masteroppgaven er å studere den globale responsen til en TLP understøttet flytende hengebro når den blir utsatt for ekstreme laster. Broen som blir analysert er et designforslag for krysning av Bjørnafjorden sør for Bergen, og har en lengde på over 4000 meter. På grunn av lengden på krysningen og vanndybden på stedet er det ikke mulig å krysse fjorden med en konvensjonell løsning. Løsningen er å bygge en hengebro med tre spenn som blir understøttet av to TLP flytere. Dette gir en lengde på hovedspennene på 1380 meter, og en seilingshøyde på 45 meter. Dette designet har en flytende ring i vannoverflaten, som er festet til flyteren gjennom strekkstag. Hovedideen bak denne ringen er å gi stabilitet i installasjonsfasen, samt være en barriere ved skipskollisjoner. Designet gir broen egenperioder som spenner fra 100 til 4 sekunder, noe som gjør at en rekke forskjellige laster kan eksitere en respons. For å analysere dette er alle analyser dynamiske og i tidsplanet.

Barrierens geometri ble funnet ved å bruke forenklede metoder med tanke på å redusere tøyningsenergi og bevegelser av barrieren. Et av hovedspørsmålene i oppgaven er hvordan denne barrieren påvirker broens respons på skipskolliskjoner. Dette ble studert ved å simulere en rekke kollisjoner hvor kollisjonsenergien varierte fra 50 til 1200 M, både mot barrieren, og direkte mot flyteren. I analysene ble skipet modellert som en punktmasse med en initialhastighet som var forbundet med broen ved hjelp av to fjærer. Den ene fjæren ble gitt kraft deformasjonskarakteristikken til skipet, mens den andre sørget for at det ikke var noe stivhet i strekk. Dette resulterte i en av hovedkonklusjonene i denne oppgaven: at barrieren øker broens utbøying, i stedet for å redusere den.

Et annet spørsmål som oppgaven ser på er hvordan broen oppfører seg i ekstremvær. For å gjøre ble 100 års vind og andre ordens driftkrefter i 100 års stormen brukt. Vinden ble modellert som et stokastisk vindfelt for å ta hensyn til dens tids og stedsvariasjon. Da både bølgelaster og vindlaster er stokastiske ble det kjørt 30 simuleringer a en time. Dette gjorde det mulig å lage en ekstremverdi statistikk til å etablere en sannsynlighetsfordeling for broens respons. Designresponsen ble tatt som 90 % persentilen til denne fordelingen for å ta hensyn til den kortsiktige variabiliteten. Disse analysene viste at miljølaster ga større utbøying av broen og at de ville være dimensjonerende for design mot global respons. Skipstøt vil på sin side være viktigst for lokalt design av flyterne.

Contents

List of Figures

List of Tables

Nomenclature

Abbreviations

TLP	Tension leg platform
DAF	Dynamic amplification factor
ULS	Ultimate limit state
ALS	Accidental limit state
FLS	Fatigue limit state
SLS	Servicability limit state
JONSWAP	Joint North Sea Wave Project (wave spectrum)
pdf	Probability density function
SDOF	Single degree-of-freedom
STD	Standard deviation
LOA	Length over all
WA	Water plane area

Latin Symbols

Symbol	Units	Description
A	[m^2]	Area
m	[kg]	Mass
r	[m]	Response
c	[Nms]	Damping coefficent
k	[N m]	Stiffness coefficent
F	[N]	Force
t	[s]	Time
P	[N]	Tension force
L	[m]	Length
x	[m]	Displacement of TLP
E	[Pa]	Youngs modulus
I	[m^3]	Second area moment
C_d	[-]	Drag coefficent
c_m	[-]	Mass coefficent
D	[m]	Diameter

d	[m]	Cross-sectional diameter
T	[s]	Eigenperiod
m_s	[kg]	Mass of ship
a_s	[kg]	Added mass of ship
u_s	[m s^{-1}]	Velocity of ship
t	[m]	Wall thickness
E_s	[J]	Kinetic energy of ship
m_i	[kg]	Mass of installation
a_i	[kg]	Added mass of installation
u_i	[m s^{-1}]	Velocity of installation
E_2	[J]	Joint kinetic energy after impact
V	[m s^{-1}]	joint velocity after impact
E_ϵ	[J]	strain energy
R_s	[N]	Ship resistance to indentation
R_i	[N]	installation resistance to indentation
w_s	[m]	Ship indentation
w_i	[m]	Ship indentation
I_t		Torsional area moment
Wp	[m^3]	Plastic bending moment
Sh	[m^2]	Shear area
GM	[m]	Metacentric height
BM	[m]	Distance from the centre of buoyancy to the metacenter
B	[m]	Beam
$MT1$	[N m m^{-1}]	Unit trim moment
g	[m s^{-2}]	Gravitational acceleration
R_c	[N]	Critical resistance
f_y	[Pa]	yield strength
B	[m^2]	impacted area
r	[m]	radius
A_j	[m]	Amplitude of wave component j
T_{jk}		second order transfer function
N		Number of discrete points
U_{ref}	[m s^{-1}]	Reference wind speed
Z_{ref}	[m]	Reference height
U	[m s^{-1}]	Wind speed

Z	[m]	altitude
C_D	[-]	Drag coefficent
C_L	[-]	Lift coefficent
C_M	[-]	Moment coefficent
S_{ii}		Spectral value
I_i	[-]	Turbulence intensity in direction i
U_{10min}	[m s^{-1}]	10 minute mean wind speed
L_i	[m]	Length scale
f	[Hz]	Frequency
coh		Coherence
c_i	[-]	coherence factor in direction i
s	[m]	Distance between points
F_Y	[-]	Cummulative distribution
S_m	[-]	Sample standard deviation
$\bar{x_m}$		Sample mean

Greek Symbols

Symbol	Units	Description
α	[-]	power coefficient
β	[rad]	angle
γ	[-]	Peakedness parameter (JONSWAP spectrum)
Δ	[kg]	Displacement
δt	[m]	trim
$\Delta \omega$	[rad s^{-1}]	Frequency step
ε	[-]	strain
ζ	[m]	Surface elevation
ζ_A	[m]	Wave amplitude
θ	[rad]	Rotation
λ	[-]	Damping ratio
λ	[m]	Wave length
ρ	[kg m^{-3}]	Density
σ	[-]	Broadness parameter (JONSWAP spectrum)
ϕ	[rad]	Phase angle
ω	[rad s^{-1}]	frequency

ω_i	$[\mathrm{rad\,s^{-1}}]$	frequency of component i
ω_{max}	$[\mathrm{rad\,s^{-1}}]$	maximum frequency
ω_{min}	$[\mathrm{rad\,s^{-1}}]$	minimum frequency
ω_n	$[\mathrm{rad\,s^{-1}}]$	Natural frequency

1 Introduction

This thesis will look at the global response of a proposed bridge over the Bjørnafjorden just outside Bergen, when it is subjected to extreme loads. The loads includes both ship impacts and environmental loads

Given that the initial framework given by the government indicated a start of construction of these crossings in 2018 there is a lot of research and engineering work happening on these projects. As a result, designs and concepts change rapidly, which means that some of the solutions presented herein already are obsolete. It is however possible to gather insight to general challenges by looking at a specific design. This is the goal of this thesis.

The thesis will start by presenting the background for the problem addressed, before defining the scope and objective. Then theory relevant for the analyses herein are presented in chapter 2. In chapter 5 the method and modelling of the ship collisions is presented, as well as the results from these analyses. Chapter 6 contains the method and results from the analyses of environmental loading. After this, the results are discussed, then the conclusions and recommendations for further work are presented.

1.1 Background

In 2014 the Norwegian parliament voted for a new national plan of transport. Here it was decided to replace all ferries on the main road between Kristiansand and Trondheim, E39, with fixed straight crossings. As a part of this project a collaboration of Teknisk Data, Cowi, Aas Jackobsen and Aker Solutions has proposed a design for the crossing of the Bjørnafjorden, situated south of Bergen. The proposed design is to support the bridge by two tension leg platforms. This concept that has not been implemented on any bridges yet, highlighting the need for more research. As a consequence Statens Vegvesen had a call for bids to do a more detailed analysis of this concept, ending on the 23rd of November 2015 (Eidem, 2015).

1.1.1 E39

In the national plan for transport spanning the years 2014 to 2023 the Norwegian government has decided to realize a "ferry free E39". E39 is the main road on the west coast of Norway stretching from Kristiansand in the south to Trondheim in the north, as can be seen in figure 1.

Figure 1: E39 (Statens vegvesen, 2012b)

As of today the road includes eight ferry crossings which are to be replaced by fixed straight crossings(Statens vegvesen, 2012b). Out of these eight, five are considered extreme crossings, meaning that a conventional single span crossing would require new technology and innovation. In addition these crossings are too deep for a conventional tunnel. Fixed straight crossings of these five fjords would therefore have to be done by one of three solutions: single span suspension bridge, floating bridge, submerged tunnel, or a combination of the three.

One of the things to consider when selecting a concept for straight crossings is ship traffic. The west coast of Norway is busy with traffic by vessels of all sizes and speeds The heavy traffic both along the coast and into the fjords pose a unique challenge for the described straight crossings.

2

1.1.2 Extreme straight crossings, today's status

As mentioned in the previous section five of the straights in question are characterized as extreme. Currently three concepts are being evaluated for the crossings, and in a report published by Statens Vegvesen all concepts are deemed feasible (Statens vegvesen, 2015b).

The most well known concept is the single span suspension bridge, which for instance is used on the Golde Gate bridge. However, the longest span built today is less than 2000 metres and belongs to the Akashi Kaikyo bridge in Japan, with a main span of 1991 metres (Roadtraffic-Technology, 2015).

Figure 2: The Akashi Kaikyo Bridge (Roadtraffic-Technology, 2015)

Most of the extreme crossings on E39 are considerable longer, requiring a main span in excess of 3000 metres(Statens vegvesen, 2012a).

The greatest advantage with this solution is that it doesn't influence the ship traffic. Another advantage is that the construction procedures are well established. However, the large span will result in large dynamic effects, which requires new materials and technology to make it feasible(Statens vegvesen, 2012a).

An alternative concept is a submerged tunnel bridge. Here cars will drive through a submerged tube tunnel, well below the draught of any ships. A submerged tunnel bridge has been proposed for several straight crossings, for example over the Norwegian Høgsfjorden (Sekse, 2015), but has yet to be realized. This concept can be split up into two sub concepts, tether stabilized and pontoon stabilized (Sekse, 2015).
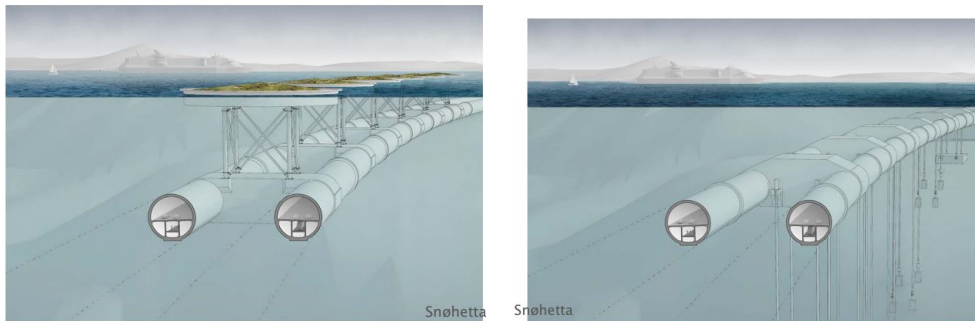
(a) Pontoon stabilized (Sekse, 2015)   (b) Tether stabilized (Sekse, 2015)

Figure 3: Submerged tunnel concepts

Both possesses unique advantages and challenges. The tether stabilized tunnel has the advantage that it does not have any elements at or close to the sea surface, thus not influencing ship traffic. The disadvantage is a more complex installation and a dependency on the sea floor conditions. If one decides instead to go for the pontoon stabilized bridge the sea floor conditions are not as important, but now large surface structures are necessary. This means that ship collisions will be of great importance. A challenge that both concepts possesses is the installation process, which will require innovation and planning (Sekse, 2015).

A third concept is a floating bridge. Here the bridge towers are placed on floating pontoons, thus avoiding the need of one large span. However, it makes the bridge susceptible to ship collisions and increased environmental loads. One of the advantages of a floating bridge is that it can draw from the offshore expertise already established in Norway. In addition, floating bridges have already been realized, including two in Norway, namely the Bergøysund bridge and the Nordhordaland bridge (Villoria, 2015). Both of these bridges are utilizing one of the two proposed sub concepts for floating bridges, namely the pontoon supported floating bridge. This is also the case for the longest floating bridge in the world, the Evergreen Point floating bridge with a floating section of 2310 metres(Villoria, 2015). The concept is based upon using several pontoons, usually in concrete, to give the bridge the required buoyancy.

The other sub concept is relying upon the experiences drawn from platforms in The North Sea. Here the bridge pillar is supported by a tension leg platform, or TLP for short. A tension leg platform is connected to the sea floor with tethers. These are long steel pipes which is pre-tensioned such that the tension forces gives the platform added stiffness, significantly reducing the motions. This concept makes it possible to reduce the number

4

Figure 4: A pontoon floating bridge (Villoria, 2015)

of pontoons, thus lowering the risk of ship collisions, while not increasing the dynamic effects.
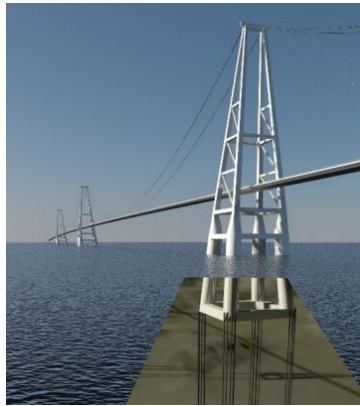
Figure 5: A TLP supported floating bridge (Veie, 2015)

1.1.3 The Bjørnafjorden

One of the crossings that are classifieds as extreme is the Bjørnafjorden. which is situated south of Bergen. The crossing is proposed to go from Eldholm on the south side, to Røtinga on the north, see figure 6. The crossing has a length of over 4000 metres, with depths of over 500 metres(Villoria, 2015).

The fjord itself is the sea route to the city of Os, as well as several other villages and factories. In addition to this the sea route to Bergen is parallel to the inlet of the fjord. Currently the ship traffic inside the fjord is dominated by small vessels, like fishing vessels and leisure crafts, with the exception of a large container vessel(Forsman, 2015). The traffic running parallel to the proposed straight crossing is more dense, and consisting of larger vessels than the traffic inside the fjord.
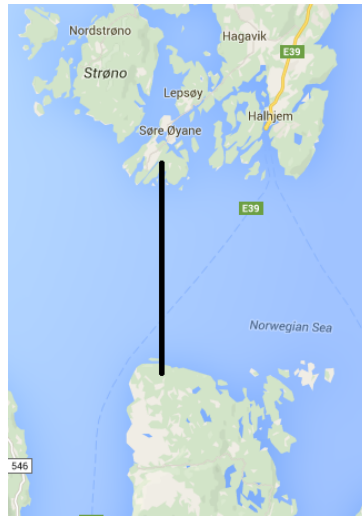
Figure 6: Map of the proposed crossing location (Google Maps, 2015)
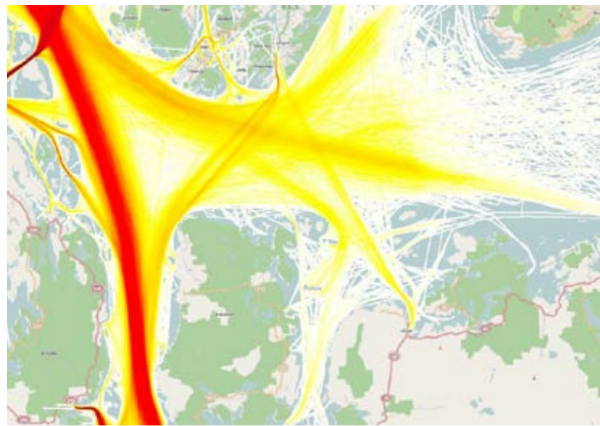
Figure 7: Ship traffic in the area (Villoria, 2015)

This parallel ship traffic will however have a distance to the straight of 1 nautical mile at the south side, and 2 nautical miles at the north side (Forsman, 2015).

1.1.4 Proposed concept

The concept that will be investigated further in this report is a five span suspension bridge supported by two tension leg platforms (Teknisk Data AS, 2014). The three main spans have a length of 1385 metres each and is in addition to the two TLPs supported by a fixed concrete pylon at each end. The water depth where the two TLPs are situated is approximately 550 and 450 metres. At each shore side there is a side span of 300 and 353 metres respectively(Teknisk Data AS, 2014). The proposed bridge is shown in figure 8

6
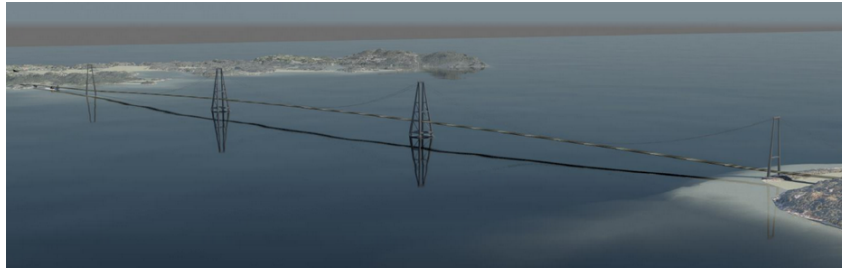
Figure 8: Proposed bridge design (Teknisk Data AS, 2014)

The two floating TLPs which will be subjected to analysis herein, are one legged structures, with design as showed in figure 9. The sailing height in the proposed concept is 45 metres and the total height of the superstructure is approximately 200 metres.
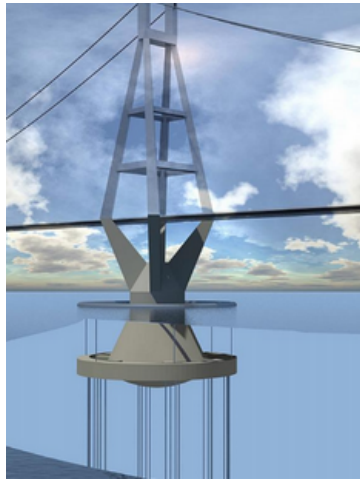
Figure 9: Proposed floater design (Teknisk Data AS, 2014)

The floaters are anchored to the ground through tethers. As figure 9 shows, the tethers are placed in four groups of three. As mentioned the TLPs will be monopiles, with the pillar stretching from the base to below the bridge girder, seen in figure 9.

One of the key features of this design is the circular ring at the sea surface, as is seen in figure 9. This provides stability in the installation phase, and acts as a fender for ship collisions. It is connected to the floater through tethers and the idea is to dissipate energy through drag forces as the barrier moves.

The floater will be built in either steel or concrete, where the concrete alternative is heavier than the steel one. The weight of the floaters influences the response to ship collisions which means that the choice of materials are important for the response. In this thesis a steel floater is assumed, and the concrete alternative will only be discussed

qualitatively.

1.2 Objective

The objective of this thesis is to study a floating bridge when it is subjected to extreme loads. Two key questions that are being studied in this thesis are:

1. How the collision barrier described in section 1.1.4 influences the response of the bridge to ship impacts.

2. How the impact energy, in relation to the speed and size of the ship affects the response of the bridge.

3. How the bridge responds to extreme environmental loads.

As mentioned in section 1.1.1, ship traffic poses a unique challenge to the extreme crossings of the ferry free E39. This is also true for the Bjørnafjorden. Finding measures to mitigate the effects on the bridge caused by ship impacts will thus be important to realize these crossings. The proposed barrier aims to do just this. If this is successful, the barrier design can be implemented in other crossings as well.

The ship traffic in the area of the crossing consists of vessels with different speeds and sizes. Both size and speed influences the impact energy in the collision. How this affects the motion of the bridge is important to establish in order to ensure a robust design of the bridge. In addition, ship collision against tether stabilized floating bridges is a novel problem and studying the response to different impact energies will help create an understanding for how these structures responds to ship impacts.

If the bridge is realized it will be a vital part of critical infrastructure, with a long expected life. It is therefore necessary that it can withstand extreme environmental loads. Because of the length and the proposed design it faces unique challenges that are not common for conventional bridges. One of these challenges is motions of the floaters, which can lead to large dynamic displacements and accelerations. In order to construct a safe and reliable bridge, the exact nature of these responses have to be known. Furthermore, since the environmental loads are inherently random, it is important to have conducted a sufficient amount of simulations to be able to conclude.

1.3 Scope and limitations

The scope of this thesis is limited to the global response of the bridge. As a result, local analyses of the bridge and ship will only be discussed qualitatively. Furthermore, the scope is limited to studying the response to extreme loading. This means that fatigue and serviceability concerns are not included, even though these can have a large influence on the design.

For more information on local structural analysis, and ship impacts see e.g. Storheim (2016). At the end of June 2016 a new report addressing the local response will be available as a result of a more detailed concept study for the crossing. When conducting the analysis, the bridge was considered a strength design. This implies that the bridge shall not be damaged when subjected to a ship collision. How this can be achieved is not part of the scope of this thesis.

2 Theory

This section will start by giving some theoretical background about the motion of the TLP floaters. Later theory for solving the dynamic equation of motion in the time domain is presented.. For theory specific for ship collisions or environmental loads, see the respective sections, 5.1 and 6.1.

2.1 Movement of a TLP

As noted in section 1.1.4 the bridge will be supported by two floating TLPs. The motion of such a TLP can be described by the dynamic equation of equilibrium, equation 1 (Faltinsen, 1990).

$$m\ddot{r} + c\dot{r} + kr = F(t) \tag{1}$$

In equation 1 m is the mass of the platform plus the added mass, c is a damping coefficient and k is the stiffness.

A tension leg platform is a structure that has positive net buoyancy, meaning that the tethers anchoring it to the ocean floor is pretensioned. Figure 10 shows a TLP given a horizontal displacement.
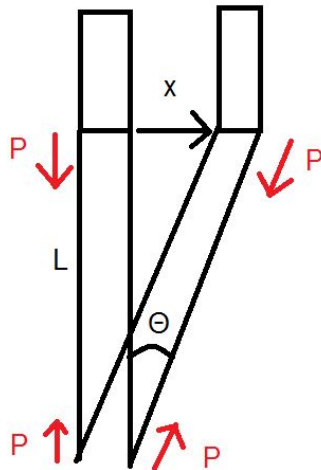
Figure 10: Horizontal displacement of a TLP

If the pretension is denoted P and the TLP is given an excitation as shown in figure 10,

the force counteracting the motion will be given by equation 2.

$$F_{x_{pretension}} = P \sin \theta = P\frac{x}{L} \tag{2}$$

This gives the stiffness of the system in lateral translations $K = \frac{P}{L}$. Vertically, any excitations require an elongation of the tethers. As a result the stiffness of the system against vertical motions is given by equation 3.

$$k = \frac{EA}{L} \tag{3}$$

In equation 3 E is the youngs modulus, A is the cross sectional area of the tethers and L is the length of the tethers.

The bridge will in addition have a second stiffness contribution, namely the bending resistance of the bridge girder. This can be expressed as in equation 4 (Leira, 2014).

$$K_{bending} = \frac{EI}{L} \tag{4}$$

As the floater moves the motion will induce forces counteracting the motions. These can be estimated by the morison equation, equation 5 (Faltinsen, 1990).

$$F = \frac{1}{2}\rho C_d D\dot{r}|\dot{r}|h + \rho C_m A\ddot{r}h \tag{5}$$

In equation 5 C_d and C_m are dimensionless constants, D is the diameter of the monopile, A is the water plane area, h is the draught of the floater and ρ is the density of water.

The eigenperiod for a single dof system can be calculated by equation 6.

$$T = 2\pi\sqrt{\frac{m}{k}} \tag{6}$$

The eigenperiod of the system is important in order to find the dynamic amplification of the loading. A ship impact represents an impulse load on the structure and the response is then relying on the ratio between the eigenperiod of the system and the period of the loading.(Haver, 2011)

2.2 Time domain analysis

All analyses in this thesis will be dynamic time domain analyses. The reason for this is that the response will be non-linear which makes this the only viable solution method. There are several strategies for solving a dynamic problem in the time domain. Common for all of them is that they solve the dynamic equation of motion, equation 7, stepwise.

$$\mathbf{M\ddot{r}} + \mathbf{C\dot{r}} + \mathbf{Kr} = \mathbf{Q}(t) \tag{7}$$

In addition, these strategies use the conditions $\mathbf{\ddot{r}_n}, \mathbf{\dot{r}_n}, \mathbf{r_n}$ to calculate the conditions at the next time step $n + 1$.

The software used for analyses in this thesis, USFOS, uses the Hilber-Hughes-Taylor-α method, or HHT-α for short (Marintek, 2001). This method is based on the Newmark's β-family, which uses equation 8 and 9 to calculate the response at time step $n + 1$

$$\mathbf{r}_{n+1} = \mathbf{r}_n + h\mathbf{\dot{r}}_n + \frac{h^2}{2}[(1 - 2\beta)\mathbf{\ddot{r}}_n + 2\beta\mathbf{\ddot{r}}_{n+1}] \tag{8}$$

$$\mathbf{\dot{r}}_{n+1} = \mathbf{\dot{r}}_n + h[(1 - \gamma)\mathbf{\ddot{r}}_n + \gamma\mathbf{\ddot{r}}_{n+1}] \tag{9}$$

The Newmark's β-family method is unconditionally stable if 10 is fulfilled

$$\gamma \geq \frac{1}{2} \quad , \quad \beta \geq \frac{(\gamma + \frac{1}{2})^2}{4} \tag{10}$$

The HHT-α method uses equation 8 and 9 to formulate the displacement and velocity at time step $n + 1$. However the dynamic equilibrium equation is changed by using the parameter α to equation 11 (Negrut, Ottarsson, Rampalli, & Sajdak, 2005).

$$\mathbf{M\ddot{r}}_{n+1} + (1 + \alpha)\mathbf{C\dot{r}}_{n+1} - \alpha\mathbf{C\dot{r}}_n + (1 + \alpha)\mathbf{Kr}_{n+1} - \alpha\mathbf{Kr}_n = \mathbf{F}(\tilde{t_{n+1}}) \tag{11}$$

In equation 11, $\tilde{t_{n+1}}$ is given by equation 12.

$$\tilde{t_{n+1}} = t_n + (1 + \alpha)h \tag{12}$$

This method is unconditionally stable given that equations 13, 14 and 15 are fulfilled

(Marintek, 2001).

$$-\frac{1}{3} \leq \alpha \leq 0 \tag{13}$$

$$\gamma = \frac{1}{2}(1 - 2\alpha) \tag{14}$$

$$\beta = \frac{1}{4}(1 - \alpha)^2 \tag{15}$$

The reason why an unconditionally stable method is preferable is because numerically stable ones are dependent on the length of the time step. To be accurate the ratio of the length of the time step divided by the eigenperiod, as can be seen in figure 11.
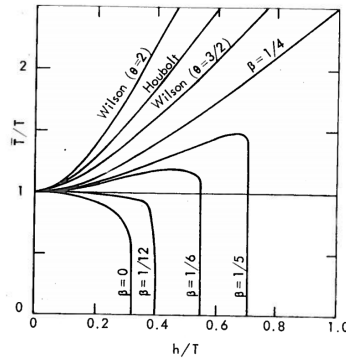
Figure 11: Period error for different time domain solvers(Ivar Langen, 1978)

For a large system, the smallest eigenperiod will thus be governing for stability. This results in one having to use a very small time step, which increases computational time (Marintek, 2001).

The parameter α in the HHT-α method introduces an artificial damping to the system which is largest for higher order vibration modes. This means that it eliminates parasitic higher order frequencies and noise. The damping is largest for small αs and zero for $\alpha = 0$, which also yields the Newmark-β method.

Another advantage of the HHT-α method is that it is second order accurate(Negrut et al., 2005).

This method can be used both with direct integration and predictor-corrector approach. Where the latter predicts the displacements, velocities and accelerations at the next step before the "real" values are found by solving the dynamic equilibrium equation iteratively.

3 The bridge model

To investigate the response of the bridge, a model was created in USFOS. This model was based on input given by TDA and Statens Vegvesen, such that it had a correct representation of the design. However, modelling the bridge without making some assumptions was impossible. These assumptions both reduced the computational time and sources for errors, without decreasing the validity of the result.

3.1 Geometry

As mentioned above the geometry of the bridge was imported to USFOS from a model created by TDA and Statens Vegvesen in RM Bridge. The model consisted of the location of the nodes and elements of the bridge girder, main cables and hangers, in addition to the superstructures at both shores and for the floaters. A representation of the bridge in USFOS is shown in figure 12.
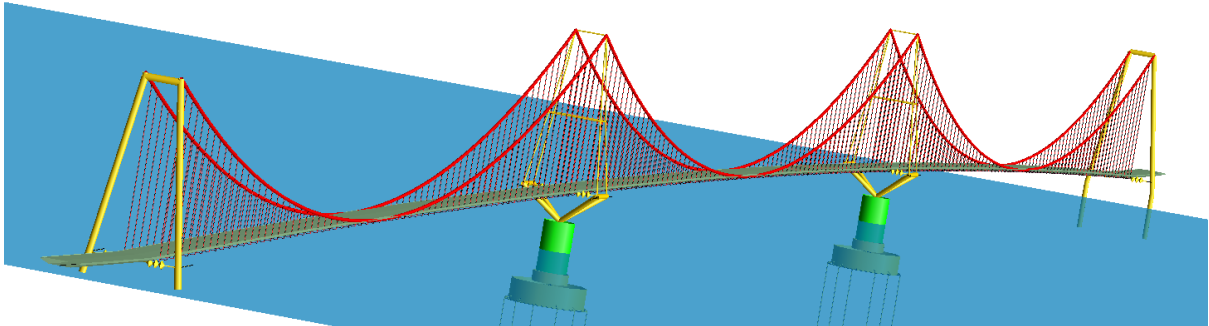
Figure 12: USFOS model of the bridge

The floaters in the model were four legged structures, see figure 13a, but these were changed to monopiles, which is shown in figure 13b. The switch was only made for the floater as the superstructure was kept as four legged. This change is necessary as the monopile configuration is the most likely candidate for construction.

The monopile is modelled as a pipe with an equivalent thickness and diameter. It is further assumed that the monopile will be made of steel, as discussed in chapter 1.1.4. This is not a given as concrete is another viable option. If the steel alternative is chosen it would be similar to the column of a semi-submersible or TLP, with stiffness contributions from both longitudinal stiffeners, ring stiffners, as well as walls and bulkheads. Using equivalent thickness and diameter will give an inaccurate torsional resistance, local

(a) Four legged hull (b) Monopile
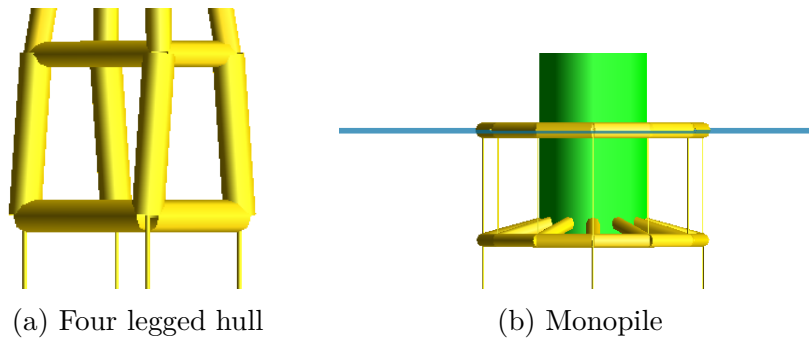
Figure 13: Floater geometries

stresses, as well as piercing resistance. However, the error for global behaviour is not significant.

In the model both the bridge girder and the main cable are modelled as beam elements with a constant length longitudinally of 2.5 metres. The hangers are modelled as only one element over the length, and thus the element length varies greatly.

At this stage the design has one bridge girder, with a cross-sectional shape as shown in figure 14. The girder has an aerodynamic shape to reduce the wind loads.
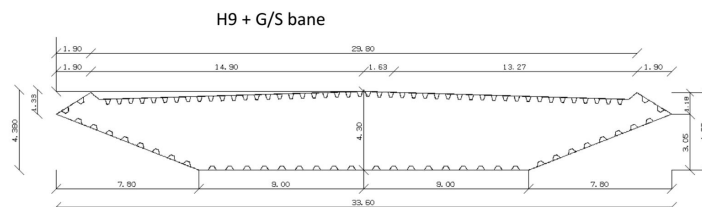
Figure 14: Drawing of the proposed design of the bridge girder

In order to get torsional stiffness of the cross-section it contains several longitudinal stiffeners as well as longitudinal bulkheads. As a comparison to figure 14, figure 15 shows how the visual representation in USFOS.

Figure 15: USFOS representation of the bridge girder

15

It is clear from this comparison that just using the shell of the cross-section would yield a torsional stiffness far too low. As a result all the elements imported from the TDA model was given a general cross-section. This meant defining the following values: cross-sectional area, shear area, second order moments and torsional moments, as well as plastic bending moment. Figure 15 is thus only a visual representation of the cross-section.

The same was done for the main cables and hangers . These elements consists of wires in different configurations, and using pipe elements would therefore be inaccurate. An example of the cross section of a main cable is presented in figure 16.

Figure 16: Example of cross section of a main cable used on suspension bridges

Table 4 lists the cross-sectional parameters for all the imported elements.

The geometry of the floater superstructure is a four legged structure as can be seen in figure 17.

Figure 17: USFOS model of the superstructure at the floaters

Figure 17 shows that a simplification has been made in the modelling of the transition

Table 4: Cross-sectional parameters

Item	Tethers	Main cable	Hangers
Area [m^2]	0.3717	0.423	0.003
It [m^4]	0.022	0.044	1.8E-6
Iy [m^4]	0.011	0.022	9.2E-7
Iz [m^4]	0.011	0.022	9.2E-7
Wpx [m^3]	0.023	0.046	1.89E-6
Wpy [m^3]	0,012	0,023	9.63E-7
Wpz [m^3]	0.012	0.023	9.63E-7
Shy [m^2]	0.32	0.258	0.002
Shz [m^2]	0.32	0.258	0.002
	Bridge Girder	**Fixed pylons**	**Superstructure**
Area [m^2]	1.042	25.94	1.25
It [m^4]	7.67	582.37	12.3
Iy [m^4]	96.95	352.9	8.2
Iz [m^4]	2.99	395.23	8.2
Wpx [m^3]	8.05	611.5	12.95
Wpy [m^3]	101.8	370.5	8.6
Wpz [m^3]	3.14	415	8.6
Shy [m^2]	0.019	9.96	0.52
Shz [m^2]	0.63	12.89	0.546

between superstructure and monopile. This transition has been modelled as four separate pipe beams that have been given an extra stiffness and yield strength. This enables the forces to be transferred from the superstructure to the monopile without the transition yielding. As a consequence the local stresses and forces here will not be accurately represented, but this error has a negligible impact on the global behaviour. The different parameters for these four beams are presented in table 5.

Table 5: Parameters for monopile to superstructure conenction

Item	Value
Diameter [m]	5.0
Thickness [mm]	30
Length [m]	49.55
Youngs modulus [MPa]	2.1E9
Yield Strength [Mpa]	3.55E8

Additional assumptions are needed for the connection between the bridge girder and the floaters. For the floaters the bearings allow for some motions vertically and longitudinally, while restraining all transversal motions This was modelled as a non-linear spring

with different characteristics in the three translational directions, and no stiffness in rotation. The connection characteristics given in "Multi-span suspension bridge on floating foundations", and the spring characteristics used in the model is shown in table 6.

Table 6: Bearing characteristics at the floaters

Direction	Allowed motion[m]		Spring stiffness [N]			
	Max	Min	Min+0.1[m]	Min	Max	Max+0.1[m]
X	1.0	-1.0	-3.5E16	-37.4E3	37.4E3	3.5E16
Y	0	0	NA	-1E10	1E10	NA
Z	1.0	0.6	-1E12	-6E6	1E7	1E12

It is seen in table 6 that the spring is given some stiffness even when inside the threshold of allowed motion. The effect of this can be questioned, but is not looked into at this stage. Though it is assumed that the bearing will carry some force between the bridge girder and the floater even when inside the motion limits.

In addition the connection between the superstructure and bridge girder consists of wires. These are pre-tensioned to 30 MN and have a length of 40 metres on either side of the bearings. At the floater the wires are connected to the superstructure, while they are connected to the bridge girder via an eccentricity. This allows the wires to be parallel to the bridge girder, and transmit the forces correctly. The effect of this is both to give an axial stiffness and a geometrical vertical stiffness in the connection. These are shown in figure 18.
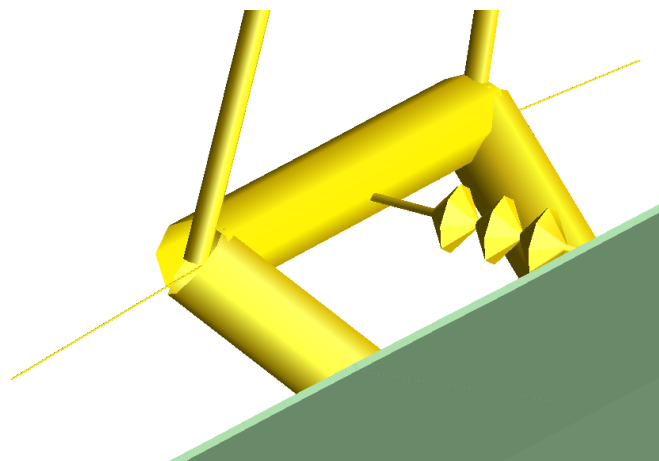
Figure 18: USFOS model of the tension wires

At the fixed pylons the bearing are pendulum bearings(Statens vegvesen, 2015a) This allows some movements, but only to a given threshold, as is seen in figure 19 which shows

a principle sketch of a pendulum bearing.
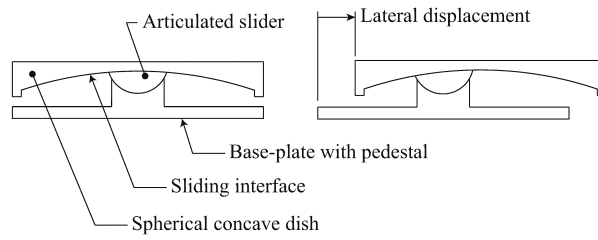
Figure 19: A sketch of a pendulum bearing (Warn & Ryan, 2012)

In the design, each floater has four groups of three tethers anchoring it to the ground, but in the computational model these groups were replaced with an equivalent tether. This does not however introduce a significant for the response. One source of error can be the morrison load, which will be different for the equivalent tethers than for the real tether configuration. However, these deviations will be small and negligible for the response of the bridge.

The equivalent tethers as used in the calculations are shown in figure 20, and have dimensions as shown in table 4.
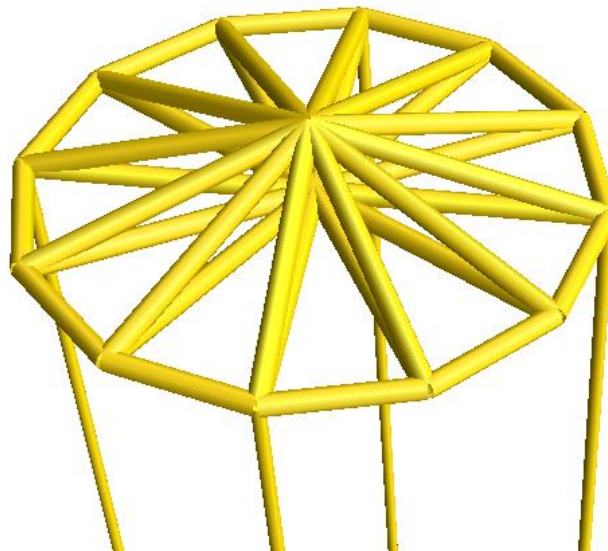
Figure 20: Equivalent tethers

Figure 20 also shows another assumption, namely the layout of the connection between the bridge pillar and the anchoring tethers. In the model this was designed as a truss

work. If the bridge is built as a monopile it will have another configuration, which is shown in figure 8. This will not have a great influence upon the result in this scope, since the buoyancy and weight of the floaters are the same as in the proposed design.

The model has boundary conditions at the sea floor at each tether, at each end of the bridge girder and at the pillars of the fixed towers. The tethers are assumed to be simply supported, i.e. free to rotate but fixed against translations, this is also the case for the bridge girder. However, the shore side pillars are assumed to be clamped, i.e. completely fixed against both rotations and translations. The red circles in figure 21 show the location of the applied boundary conditions.
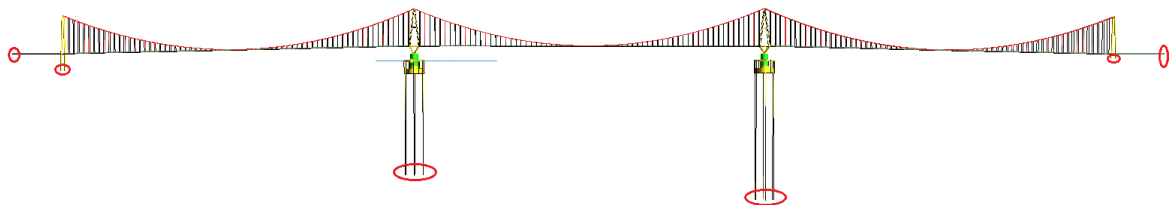
Figure 21: Location of boundary conditions

Assuming that the tethers and bridge girder are simply supported is conservative. For the tethers this also gives the most physical representation. For the bridge girder it is more unclear if simply supported is the best physical representation. Given that the boundary conditions are applied after the fixed pillars, they have little influence on the results. The assumption that the shore side pillars are clamped is based on the physical connection between the pillars and the ground. In the real world the pillars would be casted in concrete, giving a clamped behaviour.

At the midspan the cables are supported by cable lockers. These are truss works that lock the cable in place, ensuring that the geometry does not change too much, and reduce the fatigue load on the hangers. In the analyses they are modelled by giving the hangers close to the midspan an artificial stiffness. This is shown in figure 22 where the hangers marked in red are the ones given the added stiffness. The model gives a stiff connection between the main cables and the bridge girder, and also between the main cables at the midspans. Modelling it in this way does not give a correct representation of the local forces and stresses, but does not yield significant errors for the global response.

Beam elements are defined as a one-dimensional line given the properties of the cross

Figure 22: Model of chain locker

section. This means that eccentricities have to be used to get a correct representation of the global behaviour. It is especially important in order to get the contribution to the torsional resistance of the bridge girder from the cables. These eccentricities were modelled as stiff beams from the hangers to the bridge girder. In figure 23 the eccentricities are marked by the red ellipsis.
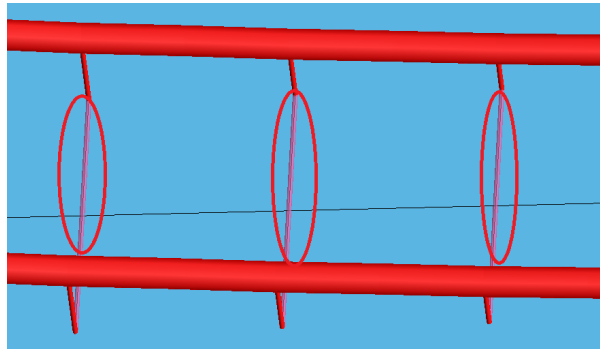
Figure 23: Eccentricities

3.2 Materials

In the calculations the material assumed for all elements is S355. This has a characterstic as shown in table 7.

Table 7: Material properties

Parameter	Value
Yield strength [MPa]	355
Youngs modulus [GPa]	210
Poisson ratio [-]	0.3
Density [kg/m^3]	7850

21

3.3 Loading

Some of the applied loads will vary from analysis to analysis, while other loads are equal for all analyses. One of these constant loads is weight, another is the live loads from traffic. This is approximated as a line load with a constant amplitude of 9 kN per meter.

The constant loads such as weight, buoyancy and live loads are applied quasi-statically. After these have been applied the ship impact and envrionmental loads were applied in the dynamic domain. The model given by TDA and Statens Vegvesen are given for the fully loaded bridge. When loading the structure it will deform. To resolve this discrepancy a command called HJHANSEN was used. This command allows USFOS to update the forces withot updating the coordinates. The result is that the input geometry will remain after loading the structure, which ensure that the distribution of forces will be correct.

3.4 Updated model

Parallel with the work done on this thesis, a collaboration consisting of among others COWI and Moss Maritime looked into and refined the design of the crossing. Some of these changes were included in the calculation model used in this thesis, the most important being the design of the floater. Figure 24 shows the updated design with some dimensions.
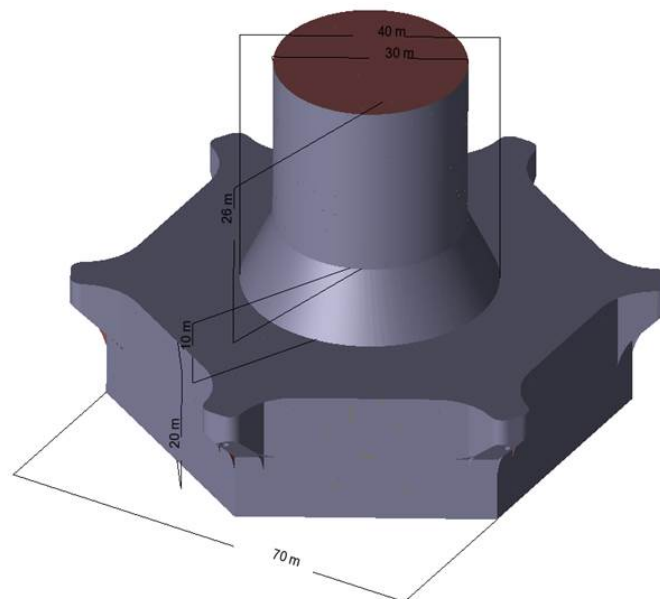
Figure 24: Updated floater design

For the global response the weight and buoyancy characteristics are most important. This is given in table 8.

Table 8: Weight characteristics new floater

Item	Weight [ton]	Centre of gravity [m]
Lightship weight	23 150	16.6
Ballast	32 850	9.14
Displacement	111 400	15.2

In USFOS the floater was modelled by pipe elements as shown in figure 25.
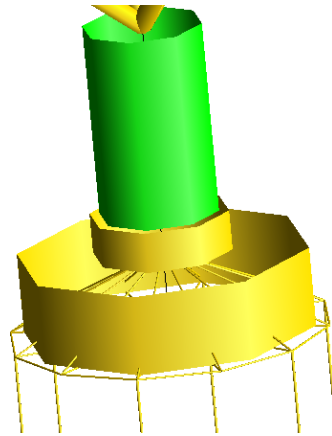
Figure 25: Updated USFOS model

To get the correct weight, displacement and centre of gravity the pipe elements were given equivalent wall thickness and density. The properties of the pipe elements used in the USFOS model are shown in table 9.

Table 9: USFOS elements

Element	Diameter [m]	Thickness [mm]	Density $[\frac{kg}{m^3}]$
Pillar	30	112	7850
Transition	35	200	7850
Box	73.3	200	17100

Another difference in the new design is the number of tethers. Previously the tethers were mounted at four points, see figure 20, in the new model this has increased to six, as can be seen in figure 25.

When comparing the new design and the USFOS representation it is seen that the new design has a hexagonal shape while the USFOS model is cylindrical. To account for

this, the added mass coefficient for the USFOS model was changed. This was done by modelling the floater in GeniE, importing it to Wadam and calculating the added mass of the bottom part of the structure. Figure 26 shows the added mass coefficient for the hexagonal box.
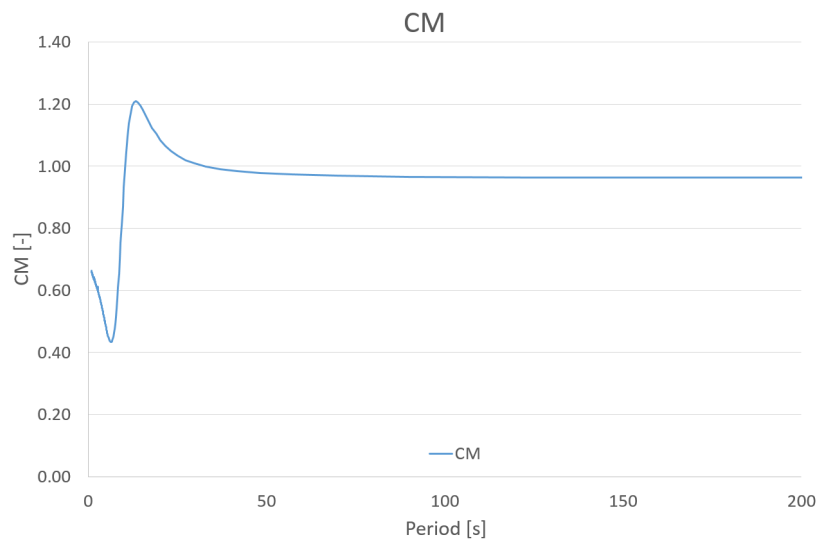
Figure 26: Added mass coefficient hexagon box

Based on figure 26 the added mass coefficient was selected to 0.96, since the response is assumed to be dominated by low frequency loads.

3.5 Points of interest

In order to extract the most critical results, some key points on the bridge were selected for a detailed output. These are shown in figure 27, and includes the bridge girder at the floaters, node 11246 and 11174, and the top of the towers, node 13246 and 13174, as well as the midspan, node 11211. The tether forces are taken in elements 10131 to 10136, while the forces in the main cable were taken in element 13248 and 12248.

These points were selected based on where the displacements, accelerations and forces was assumed to be most critical.
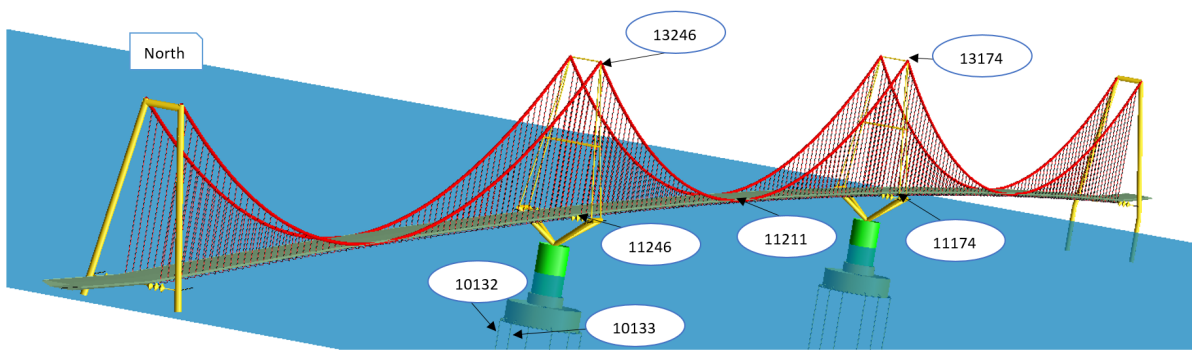
Figure 27: Nodes for output

4 Eigenvalue analyses

An eigenvalue analysis was conducted in order to get a better understanding for how the bridge will behave. In addition, the eigenperiods yields requirements as to the solution technique one can use when subjecting the bridge to loads.

4.1 Method

The eigenvalue analysis was done using the model created in USFOS by calculating the eigenvalues with the corresponding mode shapes for the ten highest eigenperiods. Both the eigenvalues and the mode shapes were then compared to the results which Statens Vegvesen had obtained using Orcaflex.

It should be noted here that the software used, USFOS, does not account for the stiffness contribution of the waterplane area. As the floater is a TLP this will not have a significant effect on the results. The reason for this is that the stiffness contribution from the tethers are much larger than the contribution from the waterplane area. This can be seen by using equation 16 and 17 for the tether contribution, and water plane area contribution respectively.

$$k_{tethers} = \frac{EA}{L} \ [N/m] \tag{16}$$

$$k_{WA} = \frac{1}{4} \rho g \pi D^2 \ [N/m] \tag{17}$$

Using equation 16 and 17 the contribution from the waterplane area is calculated to be approximately 2% of the tethers. Which means that the effect of the waterplane area is negligible.

Another assumption made in USFOS is that the added mass is constant, and frequency independent. Figure 28 shows the added mass for the floater, calculated in Wadam.

The largest eigenperiods are assumed to be high for this structure. In figure 28 it is seen that for periods over 40 seconds the added mass of the floater is constant. This means that the assumption of constant added mass will not yield significant errors.
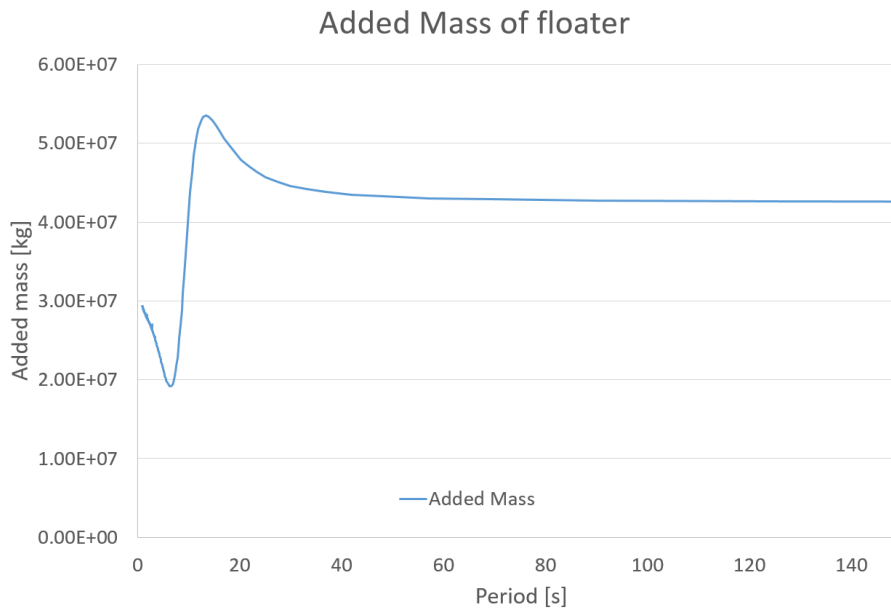
Figure 28: Added mass of floater

4.2 Results

As described in chapter 4.1 an eigenvalue analysis was conducted for the bridge. Such an analysis gives a good insight in the behaviour of the bridge. All results in this chapter is with the updated floater geometry.

The largest eigenperiod found for the system was 104.4 seconds and the corresponding mode was a lateral displacement of the two floaters such that it formed one half wave over the bridge. This is shown in figure 29.
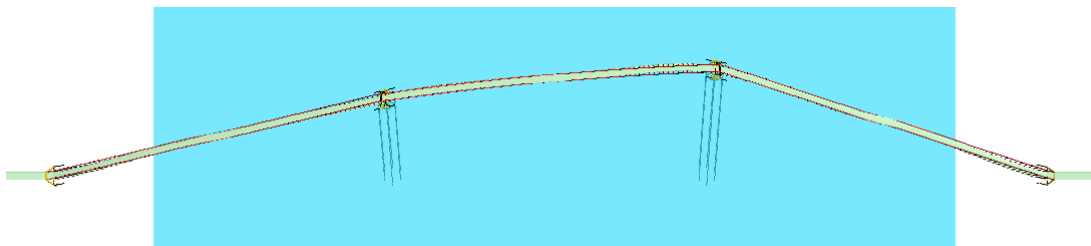
Figure 29: Modeshape corresponding to largest eigenperiod

For the second largest eigenperiod, which was 81.5 seconds, the floaters moved laterally out of phase such as to create two half waves over the length. This is presented in figure 30.

27
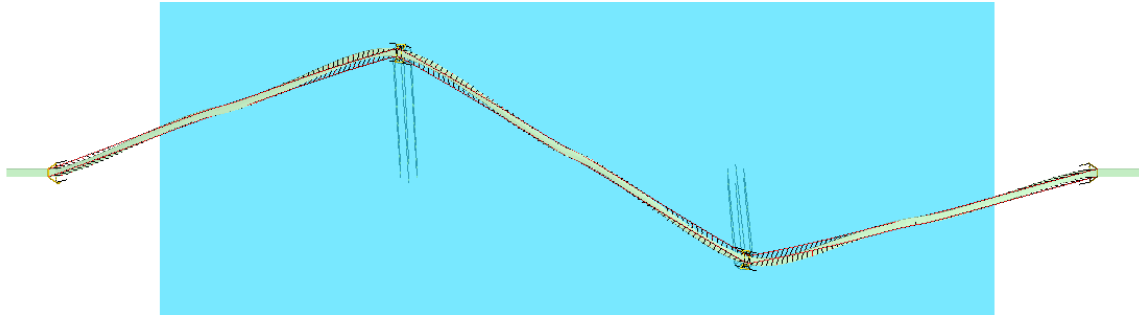
Figure 30: Modeshape corresponding to the second largest eigenperiod

The two largest motions, which consist of lateral motion of the bridge girder is important for the response of the bridge to a ship impact. However, as is observed the eigenperiods are quite high. The impulse from the ship impact will thus be very short compared to the eigenperiod, which will reduce the dynamic effects. As a control these eigenvalues were verified by forcing the bridge to displace in the given modeshapes and then releasing it, such that it vibrates freely. The test gave good correspondance with the calculated values, as the first modeshape gave a period of 101.2 seconds and the second a period of 78.8 seconds.

The next eigenvalue was at 23.6 seconds where the corresponding mode is shown in figure 31. This shows that this eigenperiod is important for functional loads.
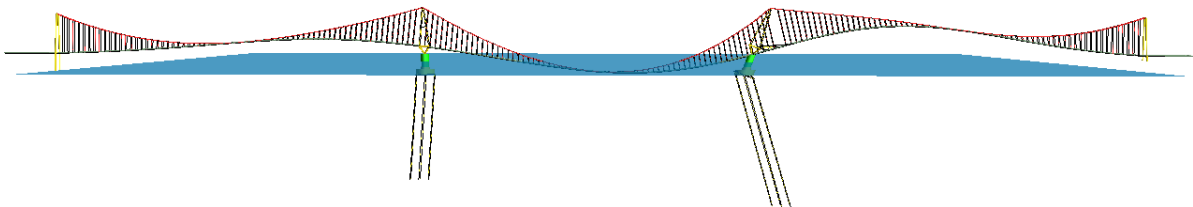
Figure 31: Modeshape corresponding to the third eigenperiod

The same is true for the next eigenmode with a corresponding period of 22.2 seconds, which is the mirrored motion of the previous one.

For enviromental loading, and wind loading in particular, 22.1 seconds was found to be a critical eigenperiode. The corresponding modeshape consists of local bending of the bridge girder between the supports, creating three half-waves over the bridge. It is hence the largest eigenperiod with local bending of the bridge girder, and is shown in figure 33.

Another eigenperiod that can influence the response against environmental loads is 20.7
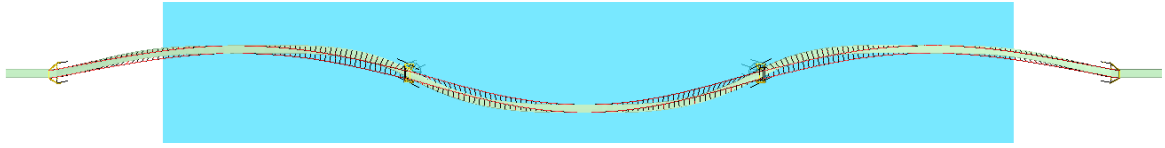
Figure 32: Modeshape corresponding to the first local bending eigenperiod

seconds. The corresponding eigenmode for this yields local bending of the bridge girder in the same direction, as shown in figure
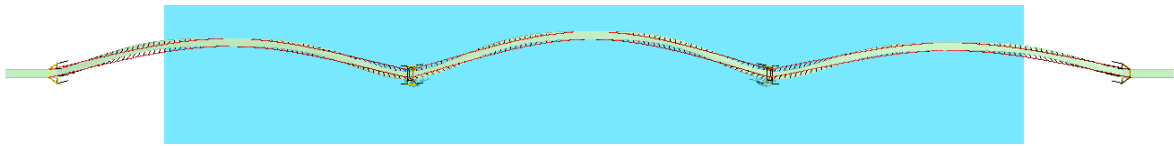
Figure 33: Modeshape corresponding to the second local bending eigenperiod

In addition to these the bridge have torsional eigenmodes with corresponding periods of 13.3, 11.2 and 8.8 seconds, and local bending modes of the bridge girder with periods 8, and 6 seconds. For a full list of eigenmodes with corresponding periods see appendixC.

The two translational eigenmodes for the barrier, shown in figure 34a, have a corresponding period of 12.7 seconds. In addition to these it has an torsional eigenmode, figure 34b, with a corresponding period of 10.1 seconds.
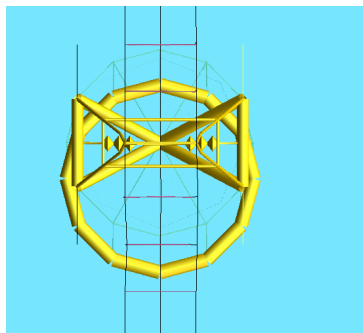
(a) Translational eigenmode
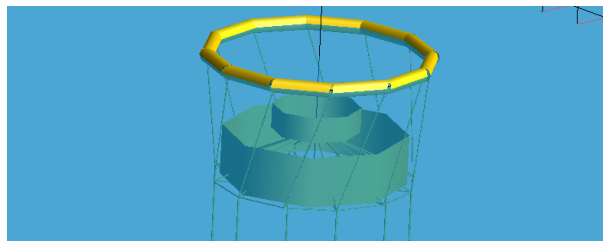
(b) Torsional

Figure 34: Eigenmodes of the barrier

4.2.1 New model vs Old.

As mention in section 3.4 the only change in the design accounted for in this thesis is the updated floater design. This means that only those eigenvalues involving motion of the

floaters will change with the updated design. Table 10 shows the eigenvalues for the old and new floater design for the four largest eigenperiods.

Table 10: Comparison of eigenvalues

Eigenmode	Old	New
1	85.2	104.4
2	69.7	81.5
3	27.3	23.6
5	22.6	22.2

As expected, the three largest eigenperiods are the ones with the greatest change. For the two largest, which involves horizontal motion of the floaters the eigenperiod has increased. This is expected, as the mass of the new design is larger than for the old one, and the increased buoyancy does note make up for the change in mass. The third eigenmode which is shown in figure 31 actually has a lower eigenperiod for the new design. This is because the new design has a lower centre of gravity than the previous one, which increases the stiffness against rotations.

5 Ship Collision

One of the key goals in this thesis is to study the influence the barrier proposed in section 1.1.4 has on the response to ship impacts. Another question to be studied was how the impact energy affected the response. Both of these were studied by running a series of collisions with different energies against the bridge both with and without the barrier. In addition to the aforementioned questions, this chapter looks at the effects of the barrier vessel interaction and barrier floater interaction, as well as how the geometry of the barrier influences the response.

This section will start by presenting theory for ship collisions, before the choice of design ships and impact energies are discussed. The MATLAB script that was created to find the geometry of the barrier will then be presented. Later the method used in modelling the ship collisions and the results of these will be presented and discussed.

5.1 Theory

As noted in section 1, no floating TLP anchored bridges have yet been realized. A result of this is that ship collisions against such bridges is a new problem and is not given in any regulations. However, similar analyses are common in the offshore industry and are covered by the NORSOK code N-004 (Norsk standard, 2004). In the Norsok code it is distinguished between three types of design with regards to strain energy dissipation: strength design, ductility design and shared energy design (Norsk standard, 2004). These three designs are pictured in figure 35. The difference between the three is the amount of strain energy that is dissipated by the structure itself.
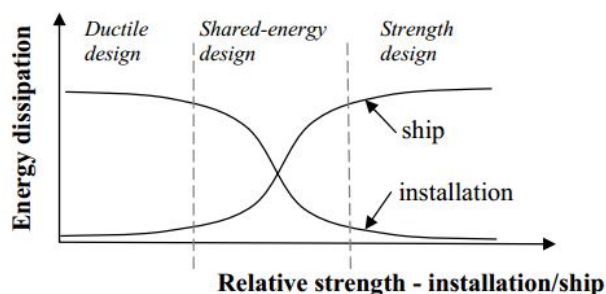
Figure 35: Share of energy dissipation (Norsk standard, 2004)

For convenience either strength or ductility design is assumed, as it yields simpler calculations. In reality the shared energy design is more probable. However, if the installation

is able the bow of the vessel, the error introduced by assuming strength design will be small.

Given that a TLP is a compliant structure all the energy from the ship impact need not be dissipated as strain energy. Instead a large portion of it will be taken up as kinetic energy. This makes it possible to split the collision problem up into two parts. Namely the external and internal collision mechanisms.

5.1.1 External collision mechanisms

External collision mechanisms gives the amount of energy that is dissipated by kinetic and strain energy respectively. This is done by using two important physical principles, namely conservation of energy and conservation of momentum.

The kinetic energy of the ship that has to be dissipated in the collision is calculated from equation 18

$$E_s = \frac{1}{2}(m_s + a_s)u_s^2 \tag{18}$$

Where E_s is the kinetic energy of the ship, m_s is the mass of the ship, a_s is the added mass of the ship and u_s is the velocity in $[\text{m s}^{-1}]$. The added mass for the ship is taken as $0.1m_s$. This is a value that is commonly adopted and e.g Petersen showed that this is a conservative assumption with actual values lying in the area 0.02 to 0.07 times the mass, for forward motion (Petersen, 1982).

Equation 19 shows the equation for conservation of momentum.

$$(m_s + a_s)u_s + (m_i + a_i)u_i = (m_s + a_s)v_s + (m_i + a_i)v_i \tag{19}$$

In equation 19 m_s and m_i are the mass of the ship and installation respectively, u_i and u_s are the speed of the installation and ship before collision and v_i and v_s are the speeds after collision. Assuming that the initial speed of the installation is zero, and that the collision is perfectly inelastic the joint speed after collision is given in equation 20.

$$V = \frac{(m_s + a_s)u_s}{(m_s + a_s) + (m_i + a_i)} \tag{20}$$

The total kinetic energy after the collision is calculated by equation 21.

$$E_2 = \frac{1}{2}(m_s + a_s + m_i + a_i)V^2 \qquad (21)$$

The strain energy or the energy that has to be dissipated by deformation of the ring and ship is calculated by equation 22.

$$E_\varepsilon = E_s - E_2 \qquad (22)$$

This gives the same result as the Norsok regulations, if the masses include added mass, which states that the amount of strain energy that has to be dissipated is defined in equation 23 (Norsk standard, 2004).

$$E_\varepsilon = \frac{1}{2}(m_s + a_s)\frac{(1 - \frac{V_i}{V_s})^2}{1 + \frac{m_s + a_s}{m_i + a_i}} \qquad (23)$$

5.1.2 Internal collision mechanisms

The internal mechanisms deal with how the strain energy will be dissipated, both by the vessel and the structure. Generally this can be found from looking at the force displacement curve for both the vessel and platform. A generic example is shown in figure 36.
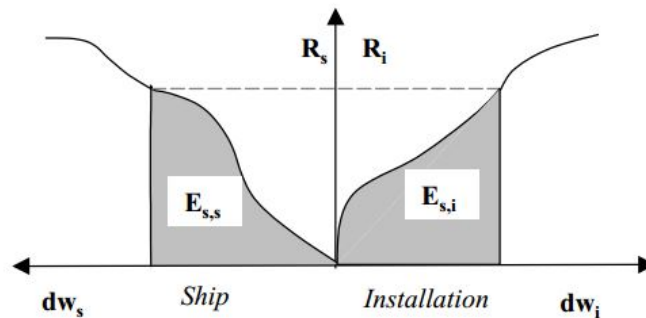
Figure 36: Force displacement curve (Norsk standard, 2004)

The share of strain energy being dissipated by the ship and installation can then be calculated by solving equation 24 iteratively, as the load level is not usually known (Norsk

standard, 2004).

$$E_{strain} = \int_0^{W_{ship,max}} R_{ship} dw_{ship} + \int_0^{W_{installation,max}} R_{installation} dw_{installation} \qquad (24)$$

5.2   Choice of design ship

As mentioned in section 1.1.3 there is a lot of ship traffic in the area of the crossing. This can potentially increase over the next 20 to 50 years (Forsman, 2015). To get an understanding of the risks related to ship collisions for this bridge, the Swedish company SSPA has conducted a risk analysis of the ship traffic (Forsman, 2015).

Here it was clear that the largest vessels operating in the area are cruise ships like AIDALuna shown in figure 37.

Figure 37: The cruise vessel AIDALuna (Wikimedia - Commons, 2015)

These vessels have a length of over 200 metres, a displacement greater than 28 000 m^3 and a transit speed of around 24 knots. However, these vessels operate very rarely in this area, with 28 yearly passages today and an expected 50 in 2035 (Forsman, 2015). Combined with the fact that these passages are parallel to the span and hence with a clearance of over one nautical mile, the likelihood of a collision is negligible.

The most frequent users of the shipping lane alongside the fjord is dominated by small tank and bulk vessels with lengths of less than 100 metres. The vessels passing into the fjord and under the proposed crossing mainly consist of small general cargo vessels and some bulkers, with lengths up to 80 metres and speeds of less than 16 knots(Forsman, 2015). These ships pose a much lower threat to the bridge although the likelihood of collision is much larger.

In the risk analysis it was clear that a container vessel sails to Fusa every week, yielding around 100 yearly crossings of the proposed bridge. This ship, which has main dimensions as presented in table 11 is called Maersk Flensburg. It will thus both have a significant

likelihood of collision, and a high impact energy.

Table 11: Principle characteristics of Maersk Flensburg (Forsman, 2015)

	Value	Unit
LOA	160	[m]
Beam	23	[m]
Displacement	16 900	[m^3]
Speed	22	[knots]

This means that the Maersk Flensburg, as is shown in figure 38, is a possible candidate for collision, and will in this thesis represent a worst case scenario.

Figure 38: The container vessel Maersk Flensburg (Braker, 2011)

Maersk Flensburg will likely be replaced by 2035 but with no major ports inside the crossing it is fair to assume that the replacement will be of the same size. It is also proposed to impose a speed restriction at the crossing of 12 knots (M. Storheim, personal communication, April 27, 2016). This will decrease the impact energy and the effect of this will be included in the analysis.

The design vessel to be used in ship impact calculations has varried greatly. In the first risk reports, it was assumed to be a vessel with approximately 200 [MJ], while an updated risk report shows that the design vessel might only have an impact energy of 50 [MJ] (M. Storheim, personal communication, April 27, 2016).

To account for this discrepancy several ships will be used in the simulations. The Maersk Flensburg at full speed will be used as a worst case scenario. Furthermore the same vessel with restricted speed will be analysed, as well as some vessels with smaller energies.

The vessels used in the analysis in this thesis are presented in table 12.

Table 12: Vessels used in analysis

Mass [tonnes]	Speed [knots]	Energy [MJ]
16 905	22	1191
16 905	12	354
20 000	9	235
3 450	10	50,2

5.3 MATLAB script

At the present stage the barrier described in section 1.1.4 is only at the idea stage. As a result a MATLAB script was created to establish its geometry. An additional incentive to create the script was to get an understanding of how the barrier works. This includes both the resulting displacements, but also the amount of strain energy, and how the kinetic energy is dissipated.

5.3.1 Method

To get find adequate dimensions for the barrier, and get an initial feel for the behaviour of the barrier a MATLAB script was created This script was based on the theory outlined in section 2, and was constructed such that the assumptions would equal that in USFOS.

The idea behind the script was to calculate the initial speed and kinetic energy of the ring. After this the kinetic energy was dissipated by buoyancy and drag forces, as the barrier moved. The maximum response of the barrier was found at the point were the kinetic energy was zero. The Morrison equation, equatuion 5, with coefficents $C_d = 0.7$ and $C_m = 1.0$ was used to calculate drag and mass force on the ring. The choice of $C_d = 0.7$ and $C_m = 1.0$ was made to use the same coefficients as in USFOS. The input to this script was .

1. D: the diameter of the ring
2. d: the diameter of the cross section
3. t: wall thickness
4. ρ: the density of the material
5. l: the length of the tethers
6. m_s the mass of the ship
7. u_s the speed of the ship

All of these were allowed to change in order to come up with a combination that gave the dimensions of the collision barrier.

For the full theoretical background of the MATLAB script see Appendix A and for the MATLAB code see appendix B.

5.3.2 Results

The first step was to conduct a parameter study by varying all input parameters in the script. The dimensions of the ring was chosen based on these results, as well as the preliminary dimensions of the floater. For simplicity the wall thickness was taken as an equivalent thickness to account for weight of stiffeners. The dimensions were chosen with the aim to minimize the strain energy and the motion of the barrier and are presented in table 13.

Table 13: Principle characteristics of ring

Parameter	Value	Unit
Diameter of ring	80	[m]
Cross-sectional diameter	6	[m]
Wall thickness	125	[mm]
Density of metal	7850	$[\mathrm{kg\,m^{-3}}]$
Length of tethers	50	[m]

Using the worst case scenario identified in section 5.2 and an added mass of 0.1 times the ship mass the impact energy was calculated to E_s=1190 [MJ]. This gave an initial speed of the ring of over V=10 $[\mathrm{m\,s^{-1}}]$

The resulting movement of the ring in, x-direction as calculated in the MATLAB algorithm, is shown in figure 39a and the movement in z is presented in figure 39b.

(a) x-direction

(b) z-direction
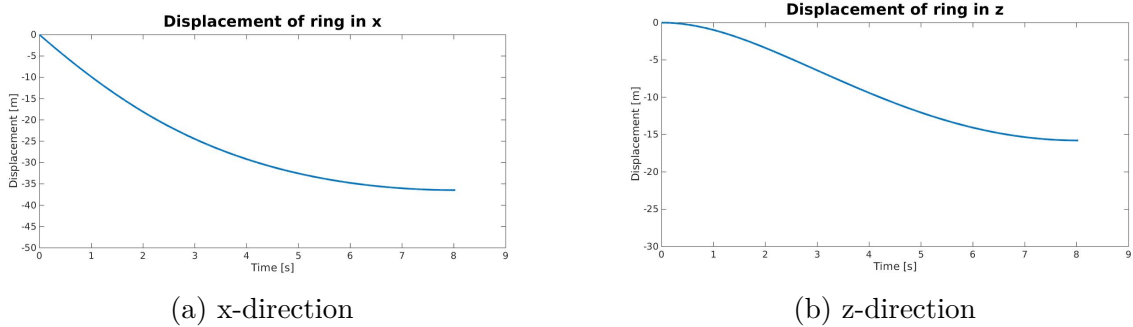
Figure 39: Displacement for the worst case scenario in MATLAB

As figure 39b shows, the maximum submersion of the ring is 15.8 metres, and a maximum horizontal displacement of 35.5 metres.

37

A model of the barrier in USFOS was used to verify the findings from the MATLAB algorithm The worst case scenario was then used to calculate the resulting displacement of the barrier. Figure 40 shows the displacement of the barrier as calculated in USFOS.

(a) x-direction

(b) z-direction
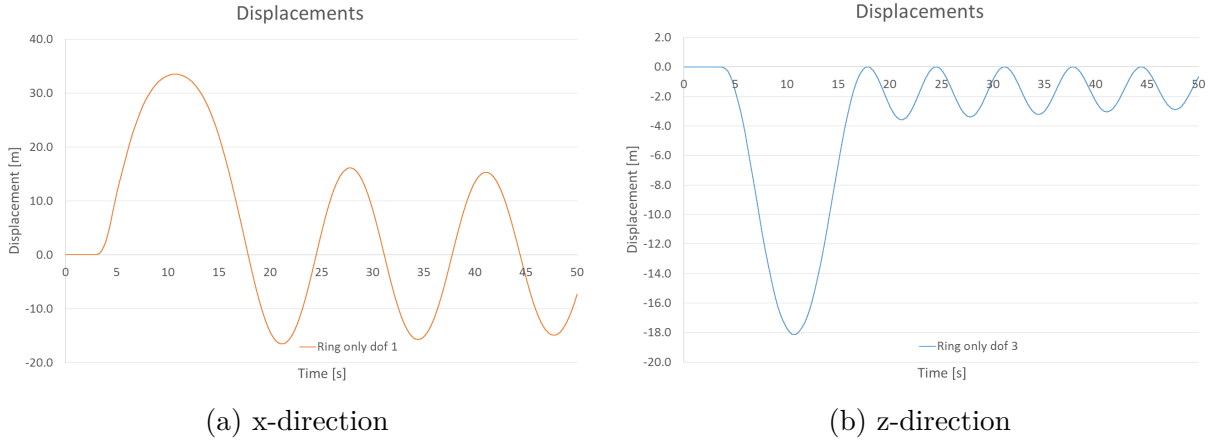
Figure 40: Displacement for the worst case scenario in USFOS

The maximum vertical displacement in USFOS, figure 40b is 18 metres this is 2.2 metres more than in MATLAB. Furhtermore the maximum horizontal displacement is 33.4 metres which is 2.1 metres less than the MATLAB script. It is expected to be some discrepancies between the two approaches, and a difference of 12 and 7% for vertical and horizontal motion respectively can be accepted.

5.4 Method

The modelling and methodology used for analysing the various ship impacts in USFOS will now be presented. As mentioned in section 1.1.4 the water depth is different for the two floaters. In this thesis all collisions are on the floater at the largest water depth, as the stiffness against horizontal motions is less for this floater.

5.4.1 Ship model

In USFOS, the ship was modelled as a nodal mass with an initial velocity. This was connected to the bridge by a non-linear spring which was given similar force deformation characteristic to the ship. The force deformation characteristics were obtained by modelling the ship bow with shell elements. The bow model was collided against both a rigid wall and a rigid ring with the same diameter as the one which is proposed for the barrier. The collision against a rigid wall represents the collision against the bridge pillar.

38

The reason why two separate collisions were conducted was that the initial point of impact and the deformed area are different for the two scenarios. This work was conducted by Yanyan Sha who used the MS Maersk Flensburg for modelling for the ship bow(Amdahl & Sha, n.d.). The force deformation characteristics for this vessel was used for all collisions investigated.

Figure 41 shows how the ship bow is deformed in a collision with the ring. It can also be seen that the initial point of contact is under the water line. The effect of this will be investigated further in section 5.4.4

(a) First Impact   (b) Midway   (c) Final state
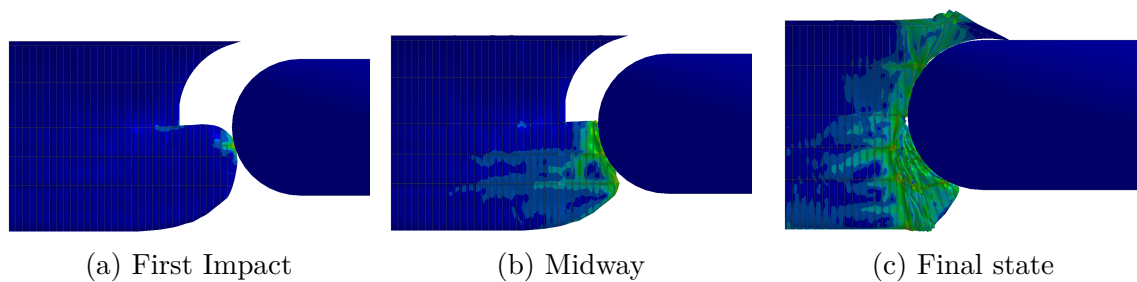
Figure 41: Impact on ring

As a comparison figure 42 shows the deformation of the ship bow when colliding against a rigid wall. This shows that the impact is dissipated over a different area, which gives the necessity of two distinct force deformation characteristics.

(a) First impact   (b) Midway   (c) Final state
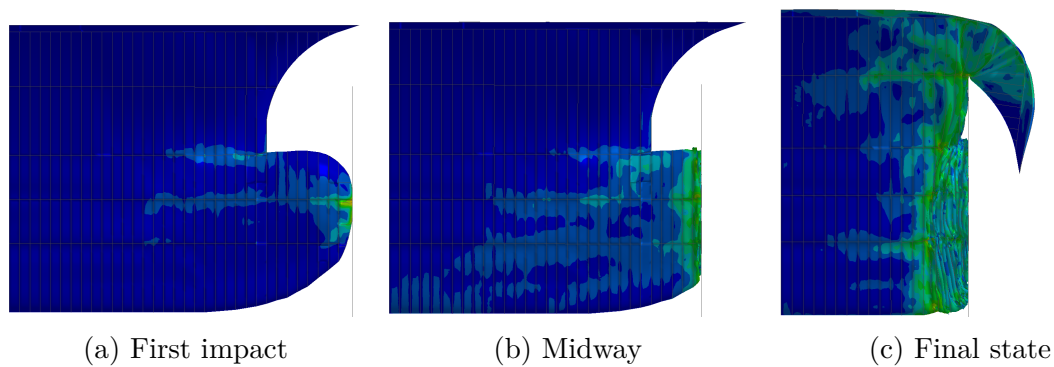
Figure 42: Impact on Wall

The resulting force deformation curve as well as the approximation for the collision against a ring is presented in figure 43.

Similarly both the true and approximated force deformation curve for the collision against a rigid wall is presented in figure 44. It should be noted that a collision against a pillar
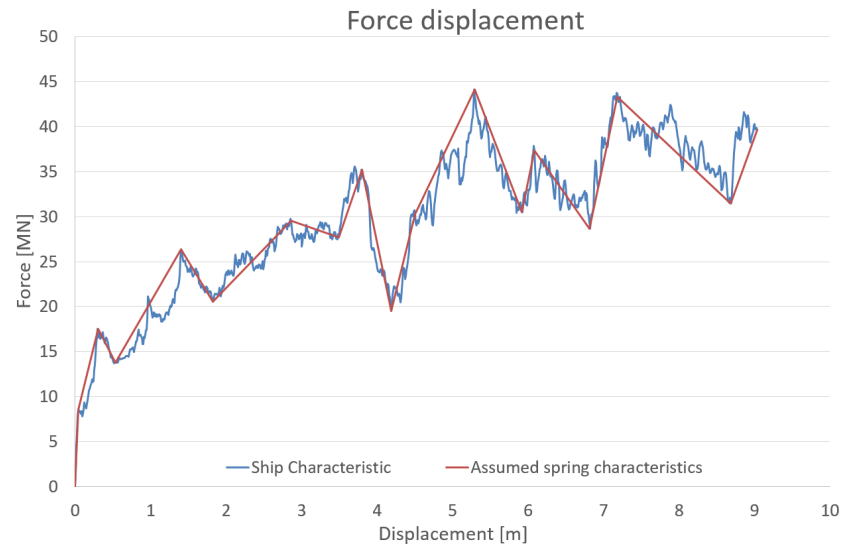
Figure 43: Force deformation curve, against a ring

with the same diameter as the bridge pillar could give a more realistic force deformation. However the diameter of 30 metres means that the error of not including the curvature would be negligible.
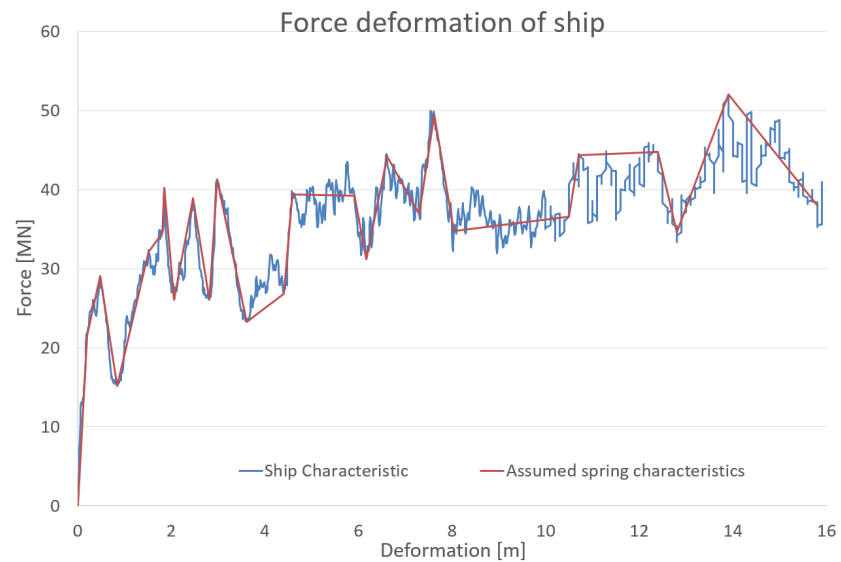
Figure 44: Force deformation curve, against a rigid wall

5.4.2 Barrier design

Part of the scope of this thesis is to evaluate the effect of using a collision barrier on the global response of the floaters. The idea behind the design of this barrier is described in

section 1.1.4. Here it is given that the barrier is a floating ring with tethers down to the base of the floater. The USFOS representation is shown in figure 45 whereas the original design is presented in figure 9.
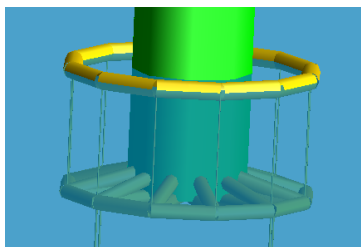
Figure 45: USFOS model of the ring

As figure 45 shows the ring is modelled as 12 beam elements with 12 tethers connecting it to the base. These have a length of 50 metres. Given that the collision barrier is at the idea stage no dimensions are currently determined and the MATLAB script, in section 5.3 was used to derive the initial dimensions. This gave an outer diameter of 80 metres, as well as a cross-sectional diameter of 6 metres with an equivalent thickness of 25 mm.

The boundary conditions of the ring tethers are not given. In these analyses it is assumed that the connections are hinged, i.e. that there are no rotational stiffness in the joints. This has several advantages in the analyses, firstly it enables the tethers to only take up the forces axially, eliminating the emergence of plastic hinges. Secondly it allows for easy comparisons between the MATLAB script, section 5.3 and the ring behaviour connected to the full bridge model.

5.4.3 Parameter study

As mentioned in section 5.4.2 the dimensions of the barrier was selected based on a parameter study conducted in MATLAB, see section 5.3. To investigate how the geometry of the barrier affected the response of the bridge a parameter study was conducted in USFOS. The parameters investigated was cross-sectional diameter and equivalent thickness. Changing the diameter will affect the buoyancy, added mass and drag forces on the barrier. It will in addition increase the tension force in the tethers connecting the floater to the sea floor. This change can be compensated for by ballast, but this is not done in these analyses. Changing the equivalent thickness will affect the mass of the barrier, and thus the amount of energy dissipated as strain energy. In addition it will also change the net buoyancy of the barrier and hence the tension force in the tethers. The different diameters and equivalent thickness's looked at are presented in table 14.

Table 14: Combinations Parameter study USFOS

Combination	Diameter [m]	Thickness [mm]
1	4	25
2	4	50
3	4	75
4	6	25
5	6	50
6	6	75
7	8	25
8	8	50
9	8	75
10	10	25
11	10	50

5.4.4 Trimming moment

The main idea of the barrier, is as described in section 5.4.2 to dissipate energy by drag forces when it is subjected to ship impacts. There are however two aspects that can change the effectiveness of the barrier.

Firstly the interaction between the barrier and the vessel is uncertain. Figure 46 shows the initial point of contact between the barrier and the vessel. Here it is seen that the contact is such that it is probable that the vessel and barrier will lock together.
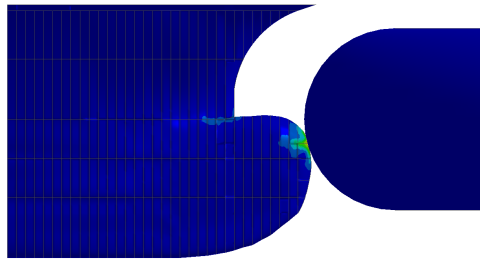
Figure 46: First impact

If they do lock together the bow has to be submerged for the ring to move. This will induce a trim of the vessel, which creates a vertical force on the barrier.

The force required to submerge the bow one metre is defined by equation 25 (Amdahl et al., 2011).

$$MT1 = \frac{\partial MR_L}{\partial \delta t} = \frac{\Delta GM_L}{L} \tag{25}$$

In equation 25 MR_L is the longitudinal righting moment, δt is the trim, and GM_L is the longitudinal metacentric height. By assuming that $GM_L \approx BM_L$ equation 25 gets simplified into equation 26.

$$MT1 = \frac{\rho I_L}{L} \tag{26}$$

Rewriting equation 26 and multiplying with g, and 1 metres to find the force one gets.

$$MT1 = \rho g L^2 B C_{IL} \ [N/m] \tag{27}$$

Here C_{IL} is an dimensionless constant accounting for the shape of the vessel, if the waterline was a perfect rectangle $C_{IL} = 0.083$. For the vessel selected in section 5.2 a C_{IL} of 0.06 was assumed. This gives a vertical stiffness from trimming the vessel of:

$$K_T = 355.23 \cdot 10^6 \ [N/m]$$

In USFOS this stiffness was modelled in two ways: first as a spring between the node connecting the ship to the ring and the base of the floater. Then as an additional spring "on top" of the spring representing the ship. This was then given only a vertical stiffness with no horizontal stiffness. The first approach is shown in figure 47.
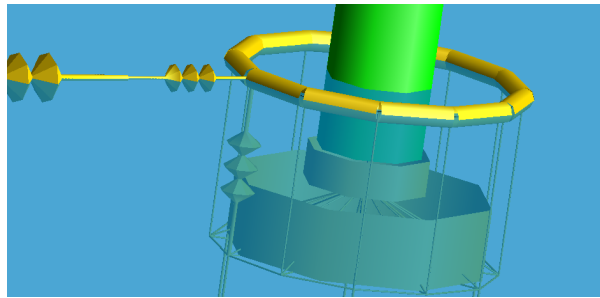
Figure 47: USFOS model of first approach

5.4.5 Barrier floater impact

Another potential problem is that the barrier might come into contact with the pillar. Given the dimensions on the pillar and the barrier, a horizontal displacement of 22 metres will result in a collision between the two. This is not accounted for when using beam

elements in USFOS. To remedy this a spring was introduced between the ring and the pylon. The spring was given properties such that it only gets activated when the horizontal motion exceeds 22 metres.

To calculate the stiffness of the spring when it was activated it was assumed that the stiffness stemmed from denting of the tubular members of the barrier. The resistance, R, to denting of tubular members is defined in NORSOK N-004 by equation 28 (Norsk standard, 2004). This assumes that the member is unstiffened.

$$\frac{R}{R_c} = kc_1(\frac{w_d}{D})^{c_2} \tag{28}$$

Here k, c_1 and c_2 are dimensionless constants, w_d is the depth of the dent, D is the cross-sectional diameter and R_c is the critical resistance, defined by equation 29. The constants c_1 and c_2 are defined by equation 30 and 31 respectively.

$$R_c = f_y \frac{t^2}{4} \sqrt{\frac{D}{t}} \tag{29}$$

$$c_1 = 22 + 1.2\frac{B}{D} \tag{30}$$

$$c_2 = \frac{1.925}{3.5 + \frac{B}{D}} \tag{31}$$

In equations 30 and 31 B is the width of the contact area, k is calculated based on the design axial compressive force and resistance. Assuming that the design force is less than 0.2 times the resistance, k is found to be equal to 1.0.

Assuming that the area of impact is much less than the diameter, and inserting the given data for the barrier the spring got characteristics as presented in figure 48.

Figure 49 shows the USFOS model of the spring. The spring representing the collision between the barrier and pylon goes from the barrier to the pylon at the water line. It is then given a local coordinate system such that a stiffness in the global direction of the impact can be defined. The spring has a low stiffness before the barrier collides with the pylon, and starts behaving as shown in figure 48 from the moment of impact.
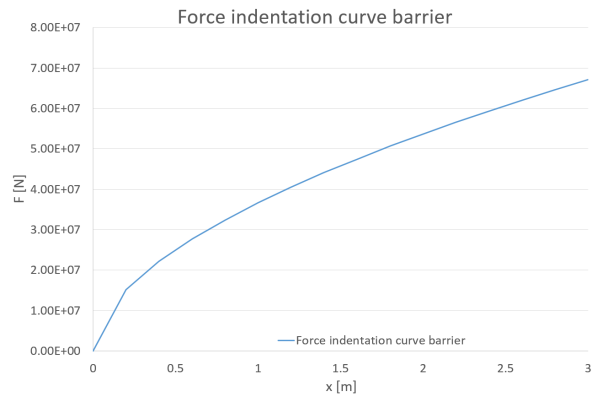
Figure 48: Force deformation characteristic barrier
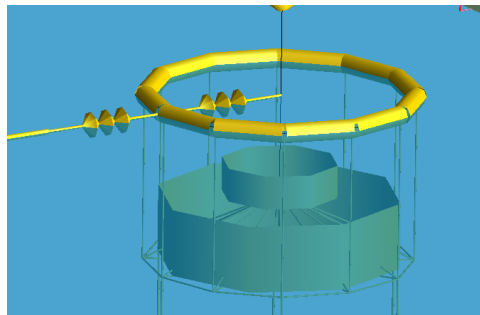
Figure 49: Spring model of barrier pylon collision

5.4.6 Splitting the analysis

The first step in the two step analysis was to collide the ship against a model of the barrier connected to the ground. The barrier model used here is the same as for the full bridge model, with the difference that the barrier for this case is tethered to the ground and not to the floater. This means that the base will not move during the analysis. The boundary conditions for the ring are the same as described in section 5.4.2. Figure 50 shows the USFOS model used in the analysis.
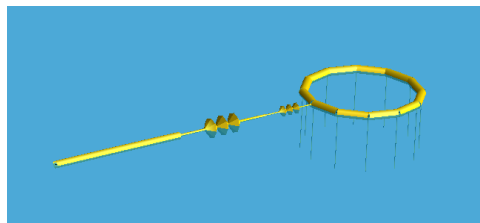
Figure 50: USFOS model of the barrier

From this analysis the reaction base shear force was calculated as a force-time history.

This was sampled every 0.1 seconds and was used as a time history input for a nodal force at the base of the floater, in the analysis of the bridge model. Two different approaches was used in the analyses. First only the initial impulse, as shown in figure 51 was used as input. The next step was to use the first 50 seconds as input, and compare the two approaches with the combined analysis.
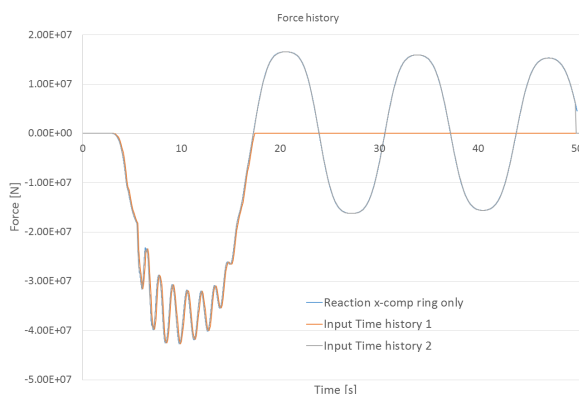
Figure 51: Resulting base shear force from barrier

5.5 Results

As mentioned in section 5.4 the bridge was subjected to several ship collisions with different energy levels. The analysis consisted of collisions against the barrier with the entire bridge model, analysis against the collision barrier only, and collisions directly against the bridge pillar. All results herein is from the updated model if it is not otherwise specified.

All results presented in graphs in this thesis are labelled as follows, if not stated otherwise: Nodenumber_dofSM=Mass of shipSS=Speed of vessel Ring/WORing or Without ring. "Ring" shows that the results is from a case with a collision against a barrier, whereas "WORing" or "Without ring" is from a collision directly against the floater. An example, which is taken from figure 52 is: 11246_1SM=16905_SS=22Ring. This is then the nodal displacement of node 11246 in x-direction when the ship impact is from a vessel with a mass of 16905 tonnes, travelling at a speed of 22 knots, with a barrier.

5.5.1 Bridge model with barrier

In section 5.2 the collision energies to be used in the analyses were presented. Of this a container vessel, the MS Maersk Flensburg at full speed was selected as a worst case

scenario. The key results for this scenario is presented in table 15.

Table 15: Key results worst case scenario

Item		Units	Min	Average	Max
Floater 1	Displacement Bridge Girder	[m]	-15.6	0.0	20.4
	Acceleration Bridge Girder	[m s^{-2}]	-0.37	0.0	0.54
	Displacement Tower	[m]	-15.3	0.0	20.3
	Acceleration Tower	[m s^{-2}]	-0.57	0.0	0.69
Floater 2	Displacement Bridge Girder	[m]	-12.8	0.0	14.2
	Acceleration Bridge Girder	[m s^{-2}]	-0.08	0.0	0.08
	Displacement Tower	[m]	-12.6	0.0	14.0
	Acceleration Tower	[m s^{-2}]	-0.09	0.0	0.08
Cable force		[MN]	120	131	139
Tether force		[MN]	37.0	49.6	68.4

Figure 52a shows the responding motion of the impacted floater for the worst case scenario, whereas figure 52b shows the motion of the second floater.

(a) Impacted floater

(b) Second floater
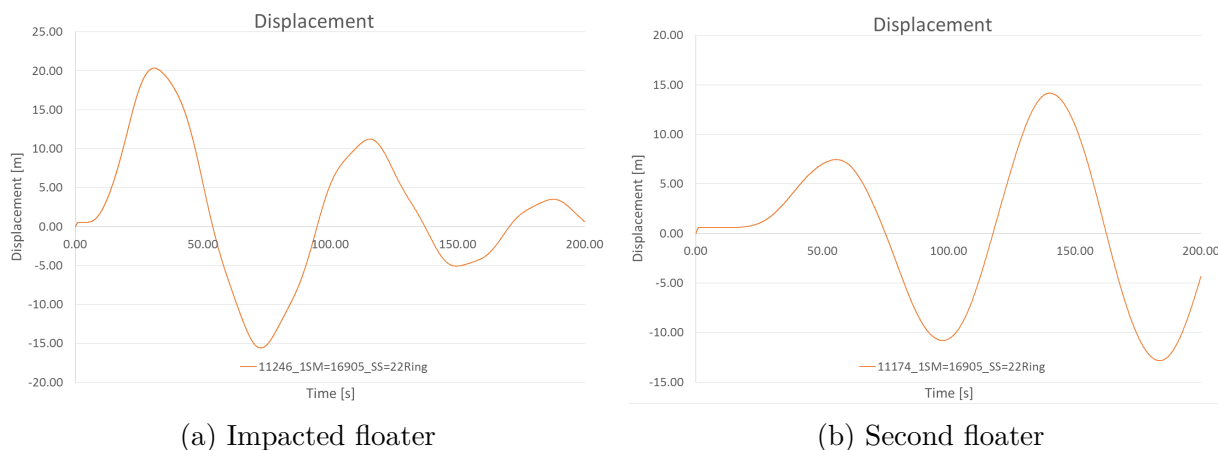
Figure 52: Displacement

From figure 52a it is clear that the maximum displacement in the worst case scenario is 20 metres. For the other collision scenarios the maximum displacement is 11.5 metres for the container vessel with speed restriction, 350 [MJ], 10.3 metres for the 200 [MJ] impact and 2.2 metres for the 50 [MJ] impact. The behaviour of the bridge is similar for all impacts. For figures of the resulting displacements for the other collision scenarios see appendix D. Figure 52b shows that the reaction of the second floater is similar to that of the first floater, albeit with a time lag. Another important result is the acceleration of the bridge girder at both floaters. For the worst case scenario this is shown in figure 53a and figure 53b respectively.
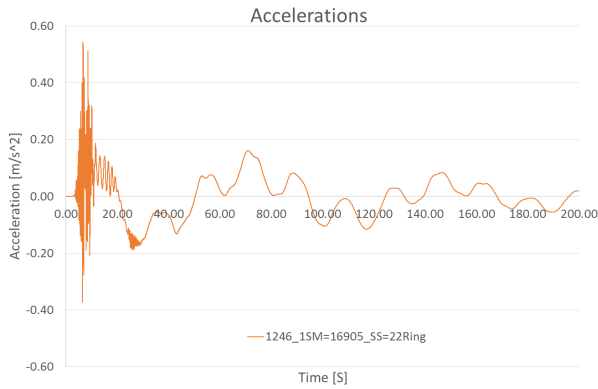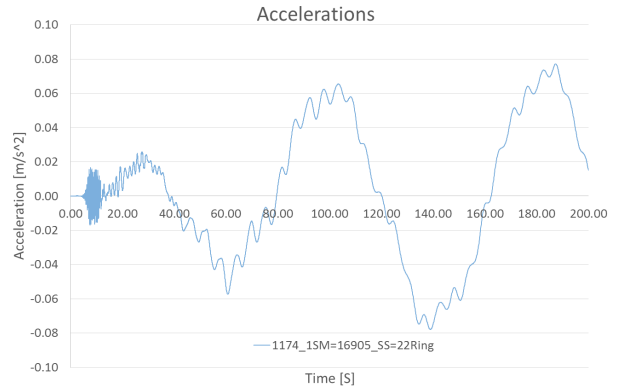
(a) Impacted floater (b) Second floater

Figure 53: Acceleration of floaters with barrier

In figure 53a it is seen that the largest acceleration for the worst case scenario is approximately 0.54 $[\mathrm{m\,s^{-2}}]$. Meanwhile the second floater experiences an acceleration of about 0.08 $[\mathrm{m\,s^{-2}}]$ or less than 1 % of gravity. With the speed restriction the acceleration of the impacted floater is $0.3[\mathrm{m\,s^{-2}}]$, while for the 50 and 200 [MJ] impact it is 0.23, and 0.22 $[\mathrm{m\,s^{-2}}]$ respectively.

Figure 54 shows the accelerations at the top of the superstructure for the impacted floater.
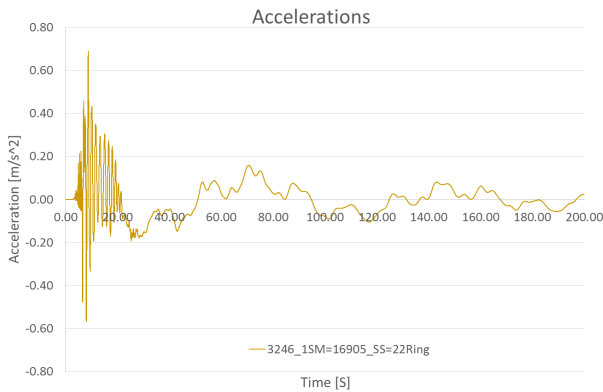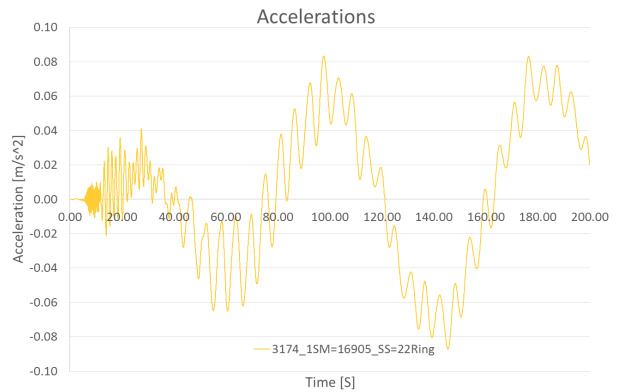
(a) Superstructure at impacted floater (b) Superstructure at second floater

Figure 54: Acceleration of the superstructure with barrier

Comparing figure 54 to the acceleration at the bridge girder it is seen that it is 0.15 $[\mathrm{m\,s^{-2}}]$ larger. This is an increase of 30%, and is also present for the other impact scenarios. The reason for this increase is that the impulse on the floater is not in the rotational center. This leads to a rotational motion of the floater, which gives an acceleration that increases with increasing distance from the rotational center. As the top of the towers are further

from the center of rotation the accelerations here are thus larger than at the bridge girder. How much the acceleration increases depends on the distance between the point of impact and the rotational centre, and the height of the tower.

The exact location of the rotational centre of the floater is not easily established. It is however assumed to be close to the tether plane.

An additional result that needs to be evaluated is the force in tethers and main cables. The force levels in these components have to be within the yield level, and for the tethers it is also important to avoid slack. Figure 55a and 55b show the forces in the tether closest to the impact and the main cable close to the saddle at the impacted floater for the worst case scenario.

(a) Tether Force

(b) Force in main cable
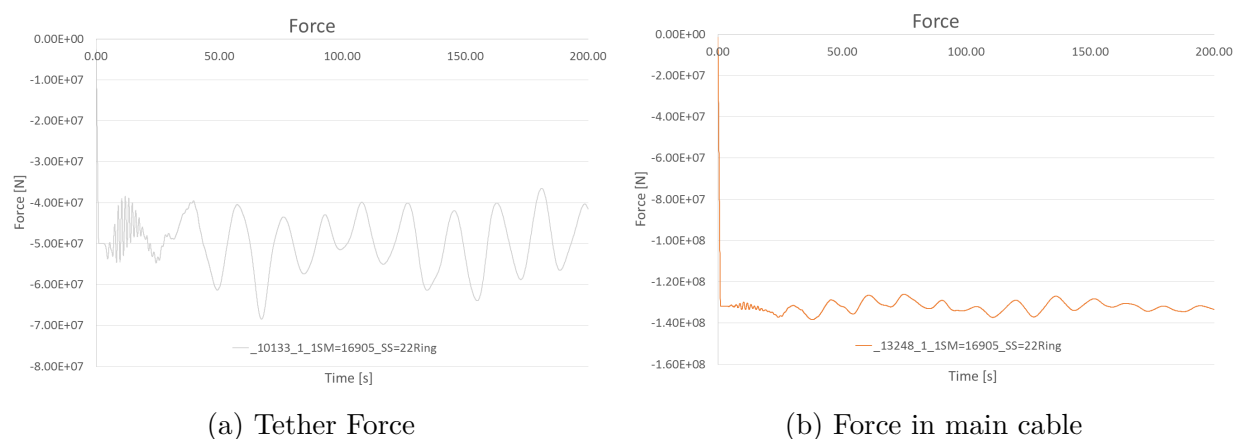
Figure 55: Forces

The cable force is not affected by the impact as is seen in 55b. For the tethers the collision has an effect, but as figure 55a shows, not a significant one. Even for the worst case scenario there is no risk of slack or yielding.

In order to investigate how the barrier worked the, motion of the ring was also assessed. Figure 56a and 56b show the vertical and horizontal displacement of the ring. These show that for the worst case scenario the ring will submerge almost 24 metres. This could allow the ring to slip underneath the incoming vessel and reducing the potential efficiency of the barrier. Reducing the impact energy to 350 [MJ] reduces the maximum submergence to 7.3 metres, whereas the 200 and 50 [MJ] has even less vertical motion, with 4.8 and 0.3 metres respectively.

From figure 56b it is clear that the horizontal displacement of the ring is large. This might cause an impact between ring and bridge pillar, which will also reduce the barriers

(a) Vertical displacement
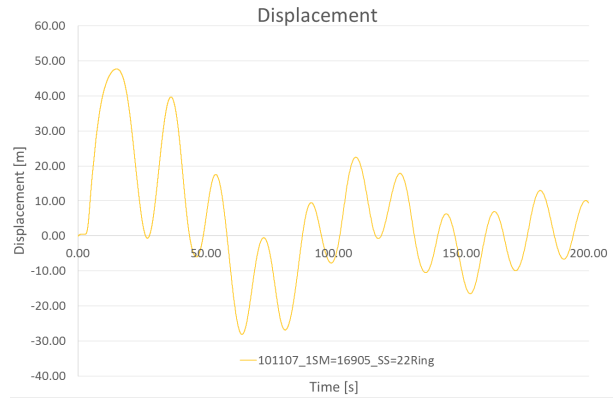
(b) Horizontal displacement

Figure 56: Displacement of barrier

efficiency.

For the analysis to be valid, the interaction between the vessel and the barrier has to be correct. To check this, the force deformation curve of the ship and the force time history of the ship are looked at. These are shown in figure 57a and 57b for the worst case scenario.
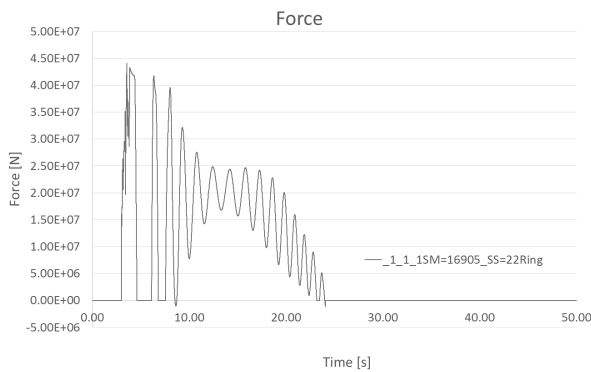
(a) Force history for ship element
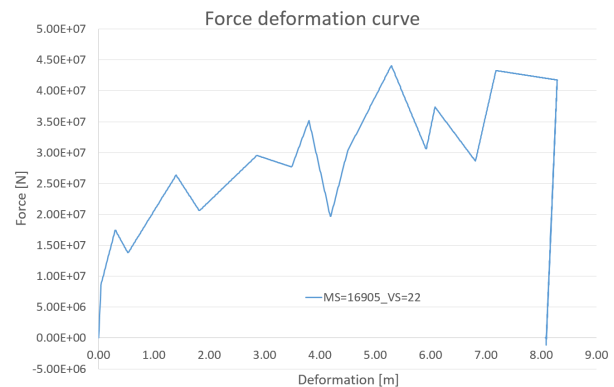
(b) Force deformation for ship element

Figure 57: Ship results

The area under the force deformation curve of the ship gives the strain energy absorbed by the ship. In the MATLAB script this was calculated to 225 [MJ] for the worst case scenario, while an integration under the curve in figure 57b gives 240 [MJ]. This gives a difference of 6% between the two approaches, which shows that they both yields a good estimate of the strain energy.

The impulse on the bridge barrier from the ship has a maximum peak of approximately

50

44 [MN] , and has a duration of 22 seconds. When compared with the eigenvalues of the system, this impulse is short, i.e. less than one quarter of the largest and one third of the second largest eigenperiod. This means that the dynamic amplification factor will be small.

A full set of results for all energy levels can be found in appendix D.1.

5.5.2 Bridge model without barrier

To investigate the effect of the collision barrier the same collisions as described in section 5.5.1 were conducted directly on the floater.

Some key results for the worst case scenario is presented in table 16.

Table 16: Key results worst case scenario

Item		Units	Min	Average	Max
Floater 1	Displacement Bridge Girder	[m]	-8.5	0	15.1
	Acceleration Bridge Girder	[$\mathrm{m\,s^{-2}}$]	-1.11	0.0	1.24
	Displacement Tower	[m]	-8.4	0.0	15.0
	Acceleration Tower	[$\mathrm{m\,s^{-2}}$]	-1.35	0.0	1.31
Floater 2	Displacement Bridge Girder	[m]	-7.8	0.0	9.9
	Acceleration Bridge Girder	[$\mathrm{m\,s^{-2}}$]	-0.06	0.0	0.07
	Displacement Tower	[m]	-7.7	0.0	9.8
	Acceleration Tower	[$\mathrm{m\,s^{-2}}$]	-0.13	0.0	0.14
Cable Force		[MN]	130	131	135
Tether Force		[MN]	25.6	41.6	57.7

If one compare the results in table 16 with the results for collision with the barrier, table 15, it is clear that the addition of the collision barrier has a negative effect on the global response. The resulting displacement of the impacted floater is reduced from 20 metres to 15 metres when the impact is directly on the pillar. For the 200 and 50 [MJ] impacts the displacement of the floater is now 8 and 2.4 metres respectively. An impacte energy of 350 [MJ] yields a maximum displacement of 8.8 metres.

These findings are substantiated by looking at figures 58a and 58b. Which show that the response is similar to that of the bridge with the collision barrier, but with a smaller amplitude.

The figures 59a and 59b show the accelerations of the floaters when subjected to the worst case ship impact.
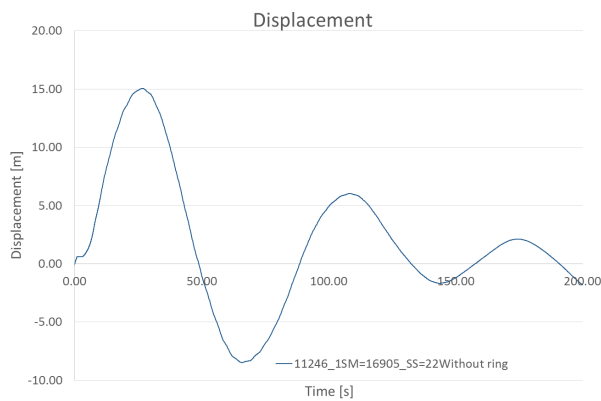
(a) Impacted floater
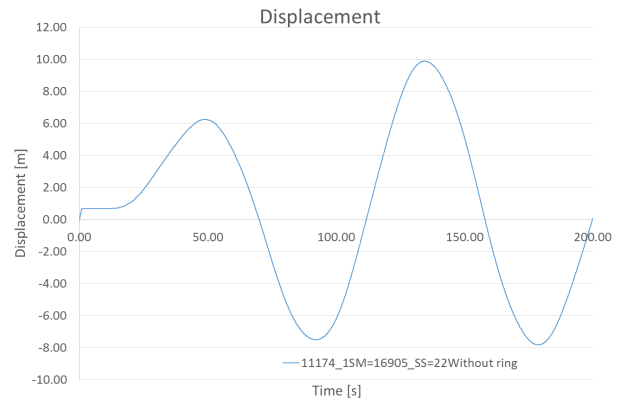
(b) Second floater

Figure 58: Displacement without barrier
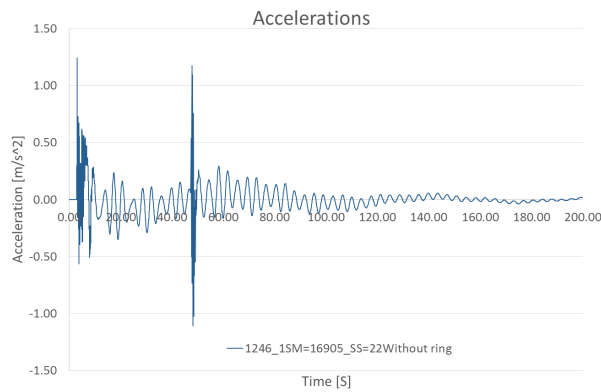
(a) Impacted floater
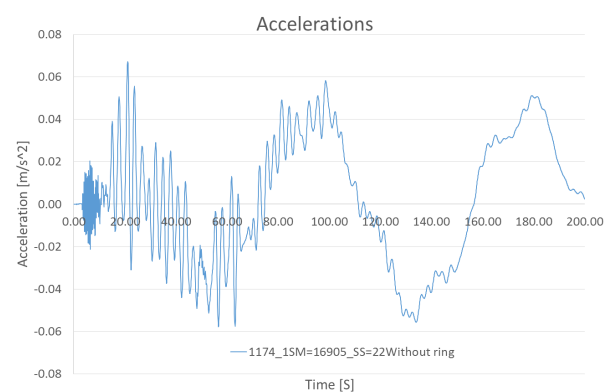
(b) Second floater

Figure 59: Acceleration of floaters without barrier

These show that the maximum accelerations of the floaters are much larger for a collision without the barrier, increasing from 0.54 to 1.24 $[\mathrm{m\,s^{-2}}]$ for the worst case scenario. For the other scenarios the accelerations are 1.08 for the 350 [MJ] impact, and 1.0 $[\mathrm{m\,s^{-2}}]$ for both the 200 and 50 [MJ] impacts. As figure 59a shows, the maximum acceleration occurs immediately after the first impact, which is at 3 seconds. This is in contrast to the peak acceleration of the floater with the barrier, which occurred later. The fact that the peak acceleration is right after the first impact is true for all energy levels. Another thing worth noting is that in these analyses the impact energy only has a modest effect on the acceleration of the bridge girder.

An interesting result is the acceleration of the impacted floater at 45 seconds. This corresponds with the second peak in the force history for the ship, see figure 62a. Which

will be discussed later.

Figure 60 shows that the acceleration of the superstructures corresponds with the accelerations of the bridge girder at the two floaters. The peak acceleration for the superstructure is similar to the peak acceleration at the bridge girder. However, figure 60 also shows that the superstructure experiences larger oscillating accelerations after the initial peak. The amplitude of these oscillations increases from 0.35 at the bridge girder to 1.05 $[\mathrm{m\,s^{-2}}]$ at the top of the tower. This was also seen for the case with the collision barrier, but the difference between superstructure and bridge girder is increased without the barrier. The reason for this is that the point of impact is further away from the centre of gravity when the collision is straight on the pylon instead of the barrier. This increases the moment and thus the rotation of the tower.
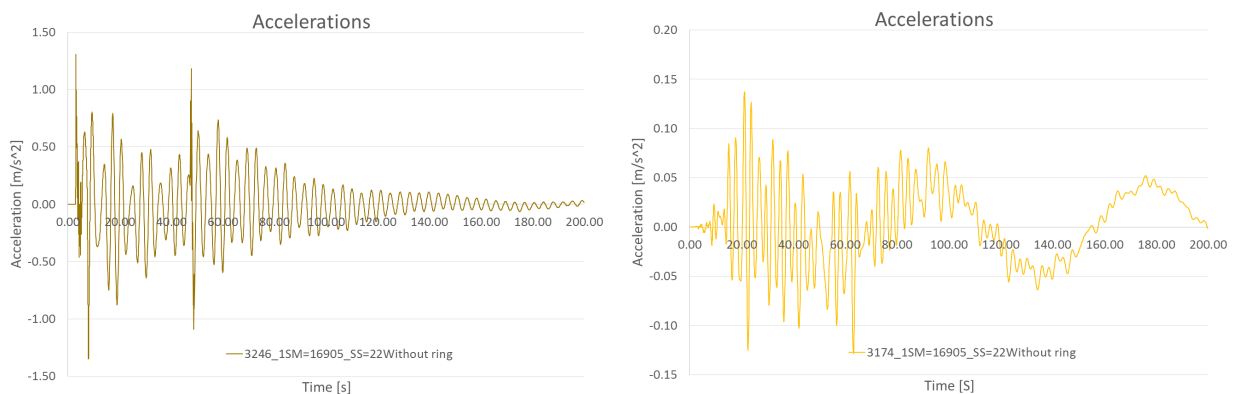
(a) Superstructure at impacted floater

(b) Superstructure at second floater

Figure 60: Acceleration of the superstructure without barrier

If one looks at the forces in the main cables and in the tethers, figure 61b shows that the force in the main cable is not affected by the impact. The tether force is however affected as figure 61a shows. Due to the ship collision the tethers get an oscillating tension force which oscillates between 25 MN to 55 MN.

(a) Tether Force

(b) Force in main cable
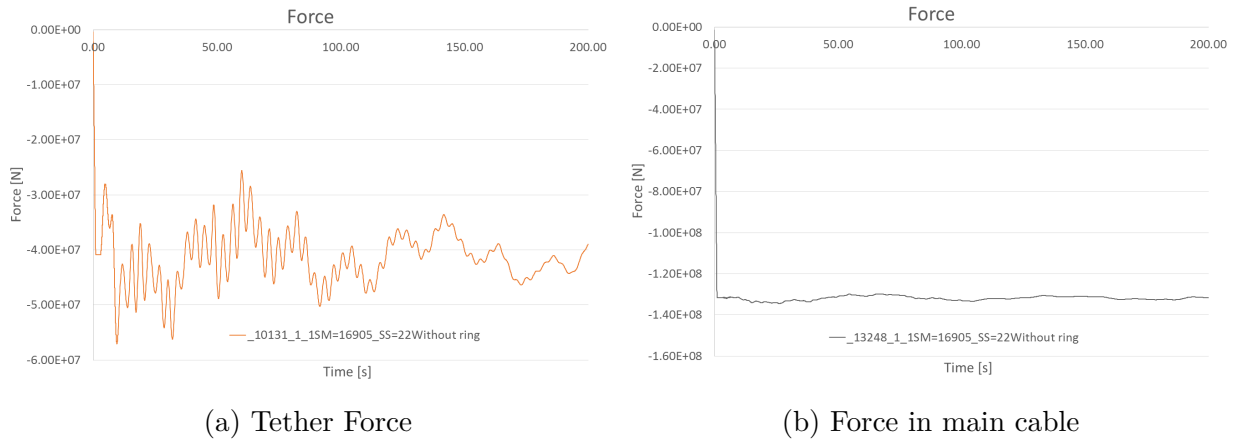
Figure 61: Forces without barrier

Figure 62 shows the force history and the force deformation characteristic of the ship for the worst case scenario.

(a) Force history for ship element

(b) Force deformation for ship element
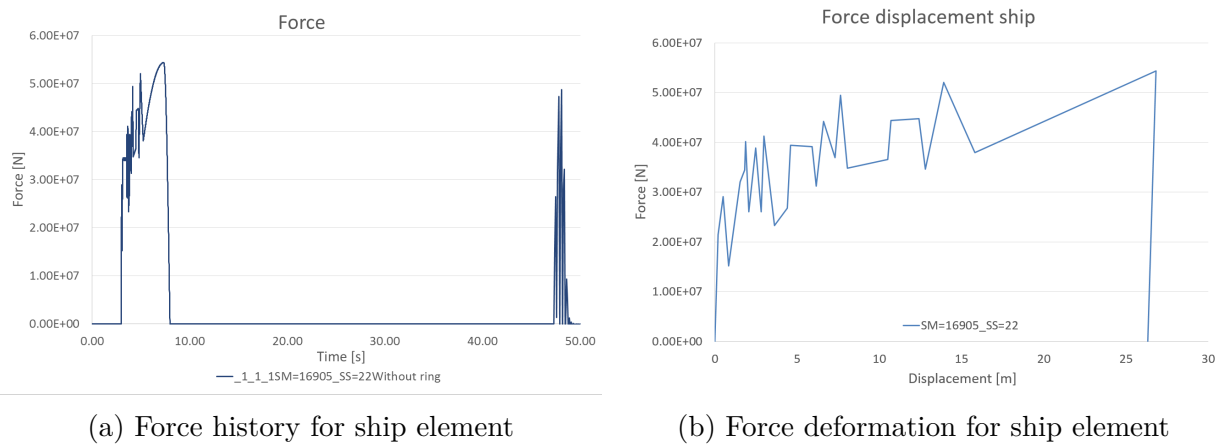
Figure 62: Ship results without barrier

Figure 62b shows that the ship indentation is 25 metres for the collision directly against the floater. The peak force as shown in figure 62a is 54.4 MN for the worst case scenario. For an impact energy of 350 [MJ] the ship indentation was 9.1 metres with a peak force of 49.5 MN. The 200 and 50 [MJ] impacts had ship indentations of 6.3 and 1.6 metres respectively with a maximum force of 41.3 and 34.6 MN.

Another thing to notice is the second force peak occurring at 45 seconds. This happens because the floater "pushes" the vessel after oscillating back from the initial displacement. The reason for this effect is the spring model of the bridge. As mentioned in section 5.4.1 this is made up of two springs in a series with one spring representing the ship, while the

other has a large stiffness in compression and a very small one in tension. In the collision the mass representing the ship stops after 7 seconds, as shown in figure 62a. From then on the springs are in tension and are elongated as the bridge moves, while the nodal mass remains at rest. After 45 seconds the bridge is back where it was when point mass stopped, and thus the springs once again becomes compressed. This creates the force acting on the ship which then reduces as the mass is accellerated, and the springs once again are in tension.

For a full set of results for all impact energies see appendix D.2.

5.5.3 Parameter study

The effect of changing the cross-sectional diameter of the barrier can be found by holding the thickness constant and only changing the diameter. This was done by selecting the thickness to be 50 mm and thus looking at the results for different diameters. Figure 63a shows the horizontal motion of the barrier, while figure 63b shows the response of the floater.

(a) Response of barrier   (b) Response of floater
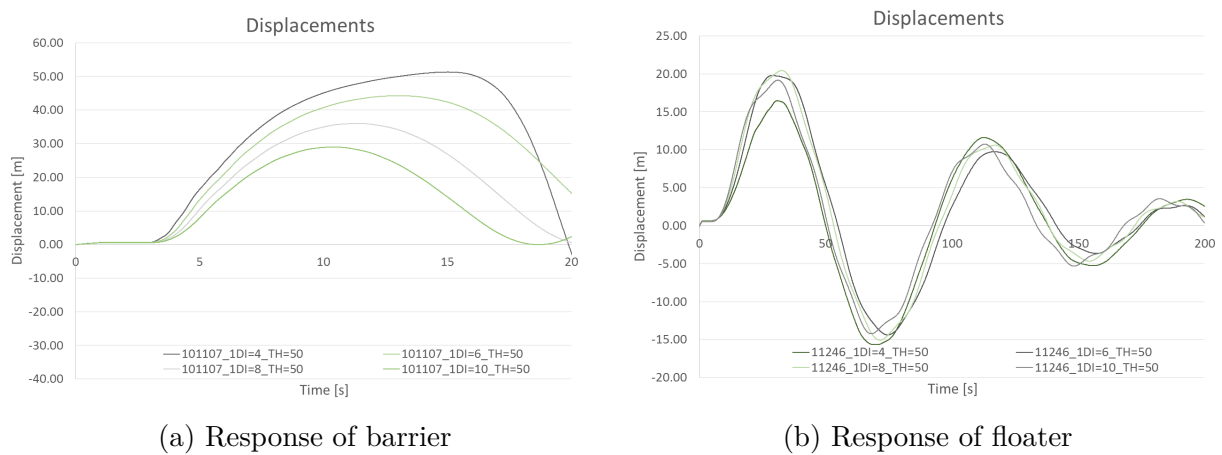
Figure 63: Changing Diameter

As figure 63 shows, changing the diameter greatly affects the behaviour of the barrier, but the effect on the floater is less dominant. This is due to the fact that with a larger cross-sectional diameter, more energy will be taken up as strain energy. Furthermore less motion is required to dissipate the same amount of energy in drag, and buoyancy. A small diameter on the other hand allows for a large motion of the ring and thus dissipate more energy by drag and buoyancy. In addition, the tension force in the tethers supporting the barrier is smaller. This leads to less force transfer to the bridge.

55

The fact that the change of diameter only has limited effect on the global response is further substantiated by looking at table 17.

Table 17: Key results diameter

Item		Units	Diameter [m]			
			4	6	8	10
Floater 1	Displacement Bridge Girder	[m]	16.5	19.8	20.4	19.2
	Acceleration Bridge Girder	[m s^{-2}]	0.54	0.73	0.53	0.40
Floater 2	Displacement Bridge Girder	[m]	13.9	14.2	14.3	13.0
	Acceleration Bridge Girder	[m s^{-2}]	0.12	0.07	0.07	0.08
	Ship deformation	[m]	5.2	7.4	9.5	11.6
	Cable force	[MN]	152	142	135	134
	Floater tether force	[MN]	59.5	58.5	59.2	65.4
	Barrier dof 1	[m]	51.3	45.61	36.0	32.3
	Barrier dof 3	[m]	31.0	19.9	11.9	7.1

Table 17 shows the key results for the global response for different diameters. Here it is evident that both a small and large diameter has its merits. A small diameter yields smaller ship indentation and displacements, while a large diameter yields smaller accelerations and cable force.

As mentioned in section 5.4.3 the equivalent thickness was also studied. Figure 64a shows the horizontal motion of the barrier with three equivalent thickness's. Similarly figure 64b shows the response of the floater for the same three wall thickness's.

(a) Response of barrier

(b) Response of floater
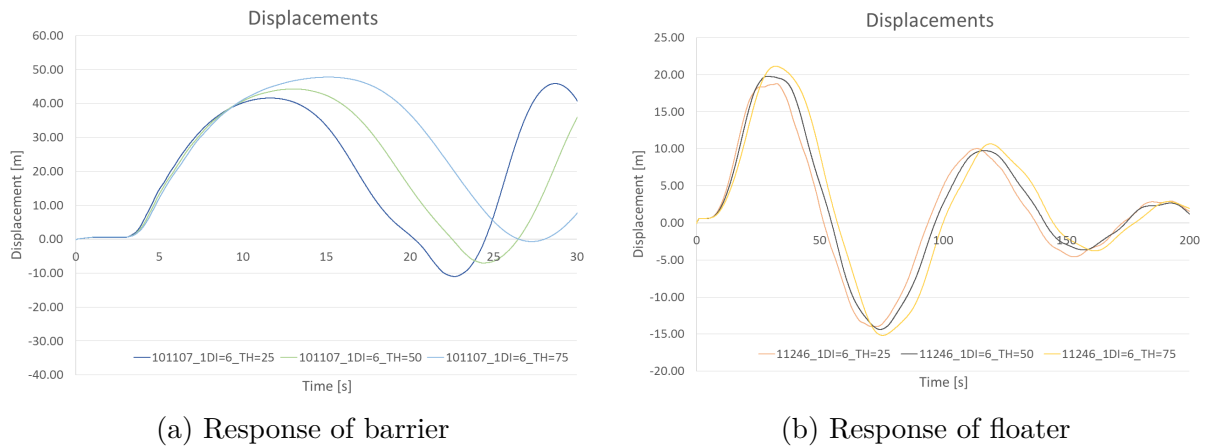
Figure 64: Changing thickness

Figure 64 shows the same trend observed in figure 63, namely that the response of the floater is not very dependent on the weight of the barrier. This is further verified by

looking at table 18 which shows the key results for the three scenarios depicted in figure 64.

Table 18: Key results thickness

Item		Units	thickness [mm]		
			25	50	75
Floater 1	Displacement Bridge Girder	[m]	18.8	19.8	21.1
	Acceleration Bridge Girder	[m s^{-2}]	0.45	0.73	0.52
Floater 2	Displacement Bridge Girder	[m]	13.6	14.2	15.3
	Acceleration Bridge Girder	[m s^{-2}]	0.10	0.07	0.07
Ship deformation		[m]	6.4	7.4	8.3
Cable Force		[MN]	145	142	138
Tether Force		[MN]	61.8	58.5	54.4
Barrier dof 1		[m]	45.5	45.6	47.8
Barrier dof 3		[m]	17.3	19.9	23.9

Table 18 shows that making the barrier as light as possible is advantageous for the response. This includes both the barrier and the motion and acceleration of the floaters. The only drawback with a light barrier is that the cable and tether forces increases. However all differences are small, i.e. less than 30%. The main reason for the reduced motions of the floaters are the increased tension force in the tethers. The difference in tension force is not big, but since the tethers are the main stiffness contribution the change is noticeable.

5.5.4 Trimming moment

As mentioned in section 5.4.2 there is a possibility that the ship will be locked onto the barrier as it starts to move. As a result, the bow of the vessel must be submerged for the barrier to displace. This was accounted for in two ways as stated in section 5.4.4. Figure 65 shows the vertical and horizontal displacement of the barrier when subjected to the worst case scenario impact. In addition to the two methods, the case where trim is not accounted for is also included in the figures. This is labelled Base case, while the two methods for accounting for trim are labelled Method 1 and Method 2 respectively.

From these figures it is clear that the difference the two approaches yield, are small in the horizontal direction. For the vertical motion the first approach gives a maximum submergence of 3.2 metres while the second approach gives 2.4 metres. In addition figure 65 shows that the effect on the motion of the barrier of accounting for trim is large. The

57

(a) Lateral displacement

(b) Vertical displacement
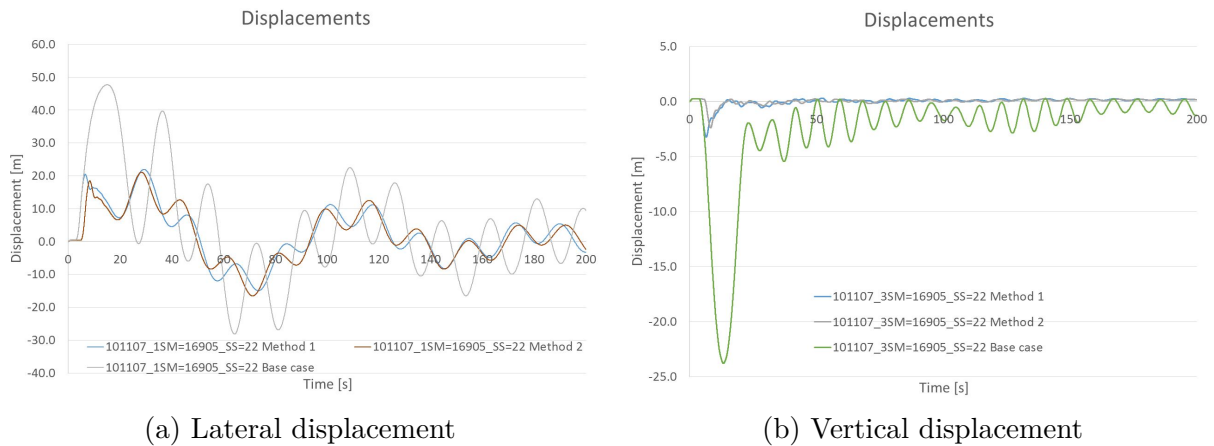
Figure 65: Displacement of barrier with trim both methods

vertical diplacement is reduced from 24 metres to 2.4 metres, while the horizontal motion is reduced from 48 to 18 metres.

Figure 65 shows that both approaches are viable when the displacement of the ring is considered. However the first approach has a significant risk by forcing the vertical force introduced by the trimming stiffness to go through the tether closest to the impact. If the barrier has a higher relative strength than the tethers supporting the barrier, the force will be evenly distributed over all tethers. Only if the tethers have much higher relative strength will the first approach give a realistic result.

Figure 66 shows the force in the tethers supporting the barrier closest to the impact for the same three analyses as in figure 65.
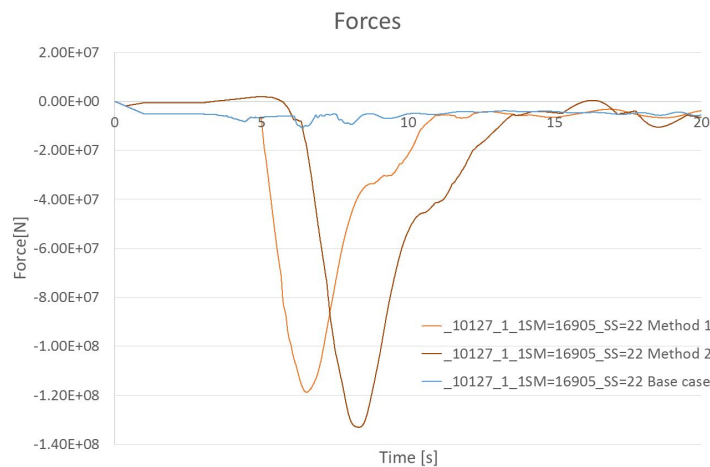
Figure 66: Ring tether forces with trim

58

This, figure 66, shows that the relative stiffness of the tethers supporting the barrier are higher than the barrier, which means that the force is taken up in the closest tether. As a result the first approach is viable for this case. However, since the second approach is valid for a wider range of parameters this is the one used for further comparisons. One thing to notice in figure 66 is that the vertical force introduced by trimming the vessel gives a large tension in the tether closest to the impact. This force, which is ten times larger than without trim is such that it can lead to yielding and possibly also failure of the tether.

For the impacted floater the introduction of the added stiffness reduces the global motion of the floater, but increases the accelerations, as shown in figure 67. The accelerations does not only increase in magnitude, but as the blue line in figure 67b shows, the accelerations oscillates at a higher amplitude for a longer duration as well.
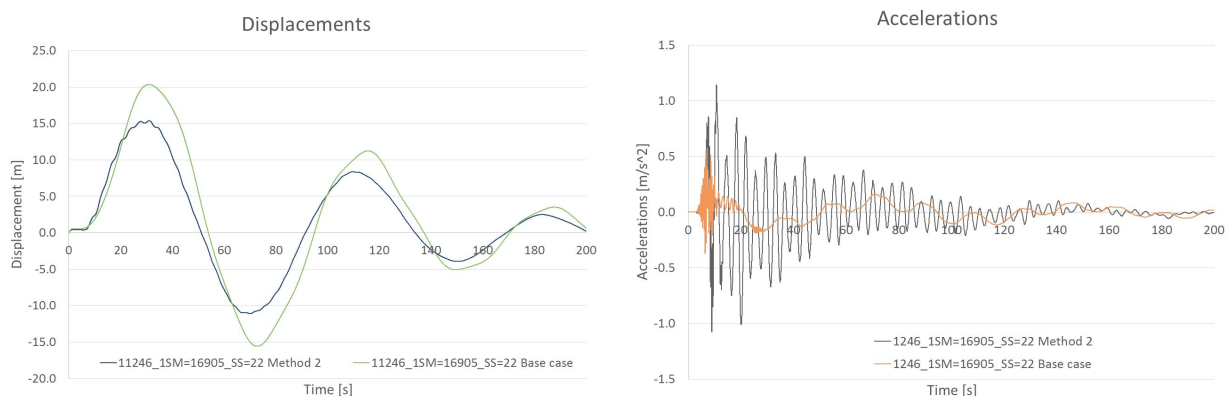
(a) Global displacement of impacted floater

(b) Accelerations of impacted floater

Figure 67: Displacement of barrier with and without trim

The increased acceleration is due to the transient effects induced by the impulse shown in figure 66. This is caused by a a short large amplitude impulse in one of the tethers connecting the barrier to the floater gives the system, Which then gives the floater a large acceleration

Since the impulse is located at the bottom of the floater it is interesting to see the response at the other extreme, i.e. at the top of the tower. This is shown in figure 68, and it is clear that the accelerations at the top of the tower is close to 3 times the accelerations at the bridge girder.
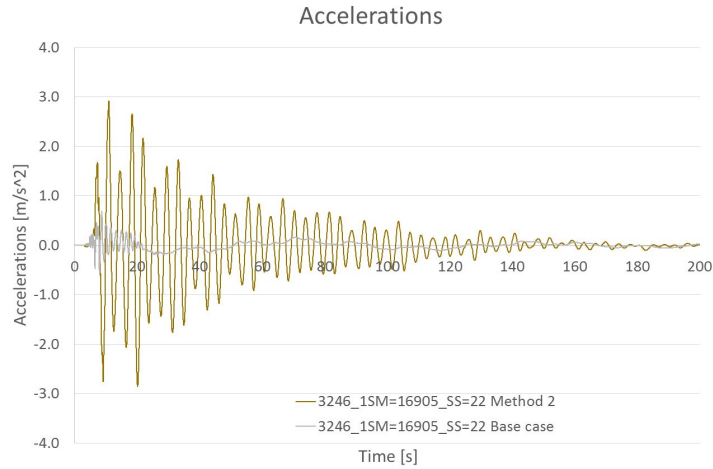
Figure 68: Acceleration of the tower

The reduction in global motion of the floater can be explained by looking at figure 69a where it is seen that the ship takes up more strain energy when trim is accounted for. The maximum indentation of the ship increases from around 8 metres to 23 metres. Furthermore figure 69b shows that the impulse from the ship on the ring has a longer duration when trim is not taken into consideration. This gives a longer impulse from the barrier on the floater. These two factors combined explains the change in motion.
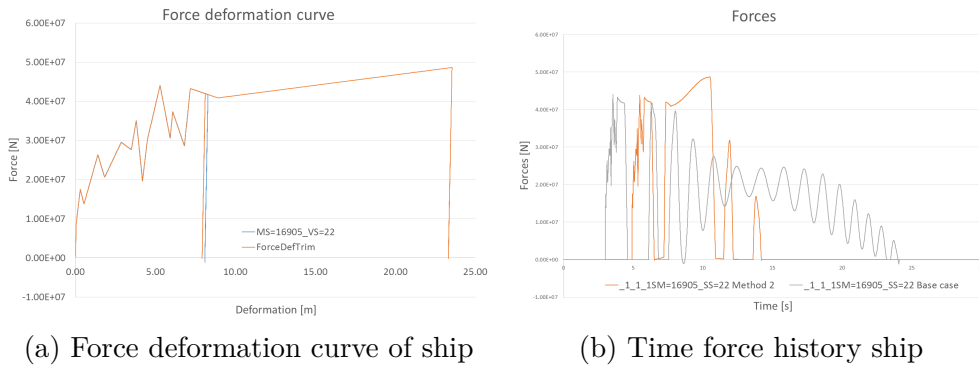
(a) Force deformation curve of ship

(b) Time force history ship

Figure 69: Ship behaviour accounting for trim

5.5.5 Barrier floater collision

As mentioned in section 5.4.5 the barrier can hit the floater due to the lateral displacement. By looking at the barrier motion in section 5.5.1 it is evident that for the largest impact it will indeed collide with the pylon. Accounting for this as outlined in section 5.4.5 gave a barrier displacement as shown in figure 70. By looking at line marked

60

SM=16905_SS=22, which denotes the worst case scenario it is clearly seen that the barrier collides with the pylon, reducing its motion. For the other impacts the barrier does not hit the pylon thus not changing the behaviour.
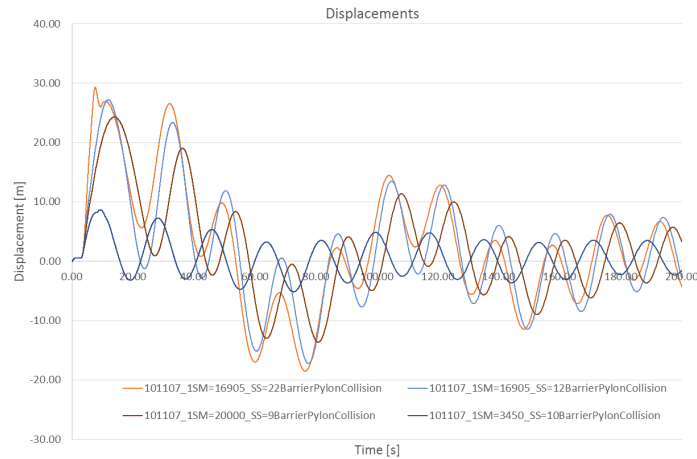
Figure 70: Horizontal motion of the ring

When the barrier collides with the pylon, the collision causes an abrupt change in the motion of the ring. This leads to accelerations of both the ring and pylon. Figure 71 shows the accelerations at the top of the tower for the worst case scenario.
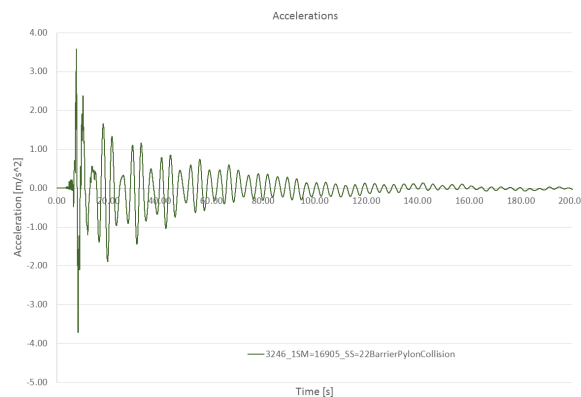
Figure 71: Acceleration of tower with barrier pylon impact

These accelerations are far larger than what the tower experiences both when looking at the barrier without accounting for the floater barrier collision, and when looking at the vessel directly against the floater.

Looking at the force history for the ship, figure 72a, the distinction of two collisions are clearly seen. The first peak represents the initial collision on the barrier, while the third peak represents the collision between the barrier and the pylon.

61

(a) Force time history

(b) Ship force deformation curve
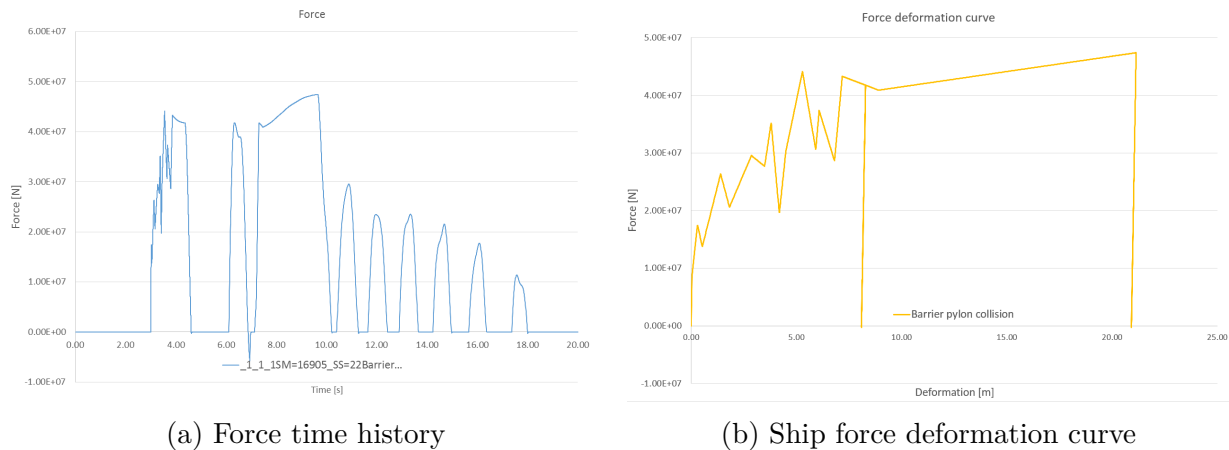
Figure 72: Ship behaviour accounting for barrier pylon impact

The second impact also increases the indent in the ship as shown in figure 72b, the maximum deformation of the ship increases from about 8 metres, for the presented in section 5.5.1, to about 21 metres. This means that more energy is dissipated as strain energy in the ship instead of being transfered to the brige. As a result the maximum displacement of the impacted floater is reduced to16.6 metres, from 20.3 for the base case.

5.5.6   Snapping of tethers

As figure 66 shows the tension force in the tether connecting the barrier to the floater closest to the impact becomes exceedingly large. This means that the tether will fail under the load giving a different response than outlined in section 5.5.4. To remedy this the element was removed after 7.0 seconds. This is the time when the element has reached maximal utilization. The removal leads to the forces being taken up in the two tethers that are presently closest. These also become fully utilized and are removed after 7.5 seconds. The two next tethers are removed at 7.6 seconds, and then two more at 7.72 before the two last are removed at 7.84 seconds. By removing these tethers it is no longer necessary for the ring to submerge in order for it to move horizontally. This means that the barrier will collide into the pylon. The effect this has on the response of the barrier is shown in figure 73.

(a) Horizontal motion

(b) Vertical motion
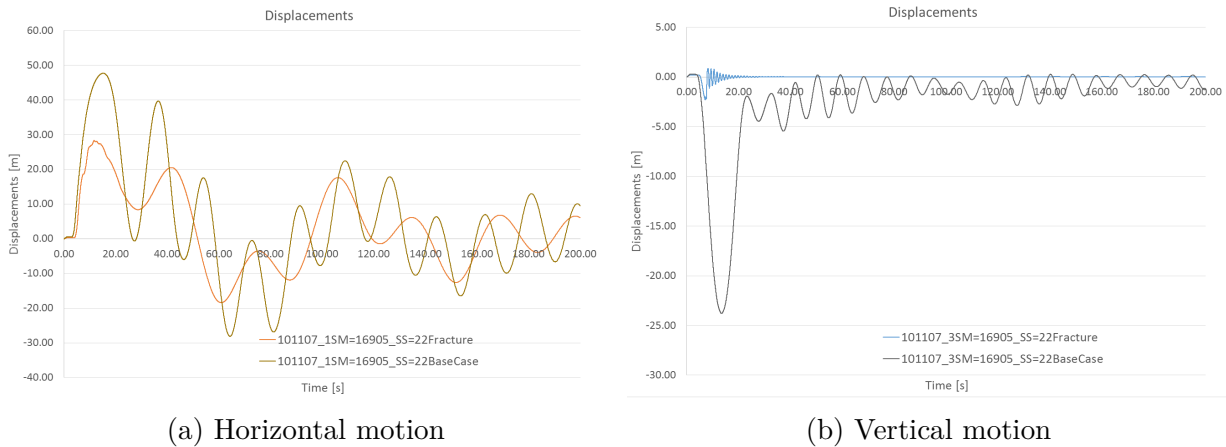
Figure 73: Barrier response with fracture

The snapping of the tethers connecting the barrier to the floater are modelled as an instantaneous loss. This means that the system will experience a shock when the tethers snap. As a result, the acceleration of the floater will see large peaks. Figure 74 shows just that, a very large and oscillating acceleration of the bridge girder when the tethers snap.
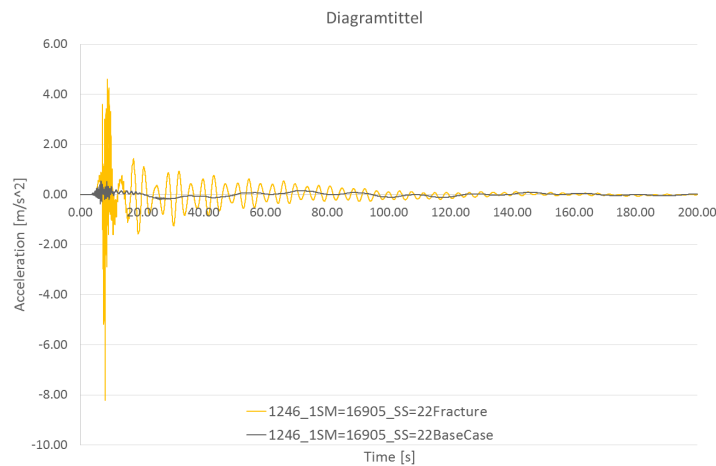
Figure 74: Acceleration of tower with barrier pylon impact

This acceleration in turn affects the tension force in the tethers anchoring the floater. As a result, these get a large transient effect that is shown in figure 75.

In figure 75 it is seen that the tether is in compression for a small period. This is not desirable as it could lead to buckling of the tether. However as noted, the duration is very short and it is unlikely that the tether will have time to buckle.

63
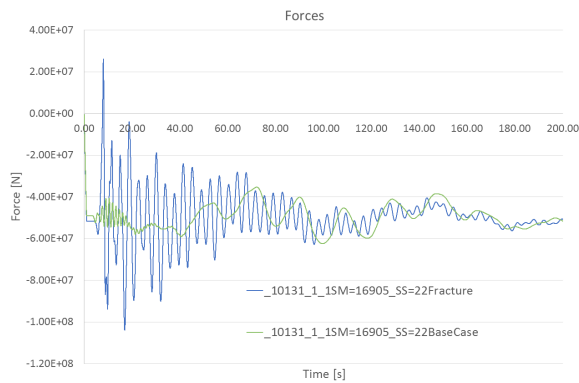
Figure 75: Tether force with barrier pylon impact

5.5.7 Splitting the analyses

As mentioned in section 5.4.6 one strategy that could save computational time is splitting the analyses in two. First looking at the collision against a barrier connected to the ground, and then taking the reaction force as input to the the bridge model. This reduces the need for small time steps for the full bridge model, and thus reduces the computational time. Two approaches were used to study the viability of this approach as described in section 5.4.6. The main difference between the two approaches is the amount of time included in the force history applied to the global model. Where the first approach only includes the first peak, while the second includes the first 50 seconds. Figure 76 shows the horizontal displacement of the impacted floater for the two approaches, when subjected to the worst case scenario. These are labelled "Time history 1" and "Time history 2" respectively. The result for the combined analysis is also included, this is labelled "BaseCase".
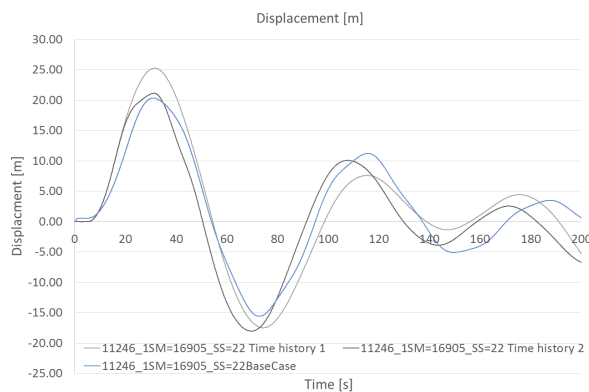
Figure 76: Horizontal motion of impacted floater with a two step analysis

64

Looking at figure 76 shows that the approach where one includes only the initial impulse will overestimate the horizontal displacement of the floater. By including the reaction force for the 50 first seconds reduces the difference of the initial peak. However, both approaches yield an overestimate of the displacement amplitude of the oscillation. It is nonetheless clear that the analyses can be split up, without introducing a significant error to the resulting displacement. A force history covering more than the initial response is however, preferable to get the best representation.

When looking at the acceleration and tether forces, which are shown in figure 77, the differences are larger. By splitting the analyses up,the tether oscillations are changed and will underestimate the maximum tension force

(a) Tether force   (b) Acceleration of impacted floater
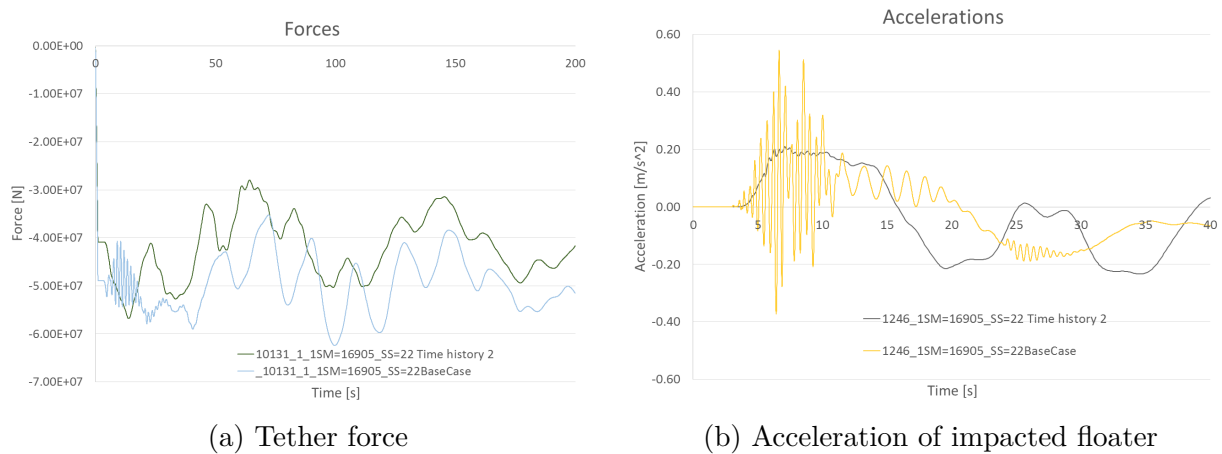
Figure 77: Results with a two step analysis

When comparing the accelerations, shown in figure 77b, the split underestimates the peak accelerations, and instead gives the floater a more constant acceleration. The combined analyses on the other hand, gives an oscillating acceleration with a positive mean level. Furthermore it is seen that the positive acceleration has a longer duration for the combined analysis compared with the two step analyses.

65

6 Environmental loads

The second main goal of this thesis was to investigate the response to extreme environmental loads. This chapter will start by presenting theory for finding extreme environmental conditions and extreme response. Then the methodology and modelling of the environmental loads will be presented before the results will be presented and discussed.

6.1 Theory

6.1.1 Contour method

The contour method was used to establish the 100 year environmental loads. This method has been widely used in the offshore industry and is in the DNV recommended practice, DNV RP-C205 (GL, 2014). It is based on creating a joint environmental probability density function, pdf for the variables of interest for the sea state. The next step is then to establish the combination of parameters that yields an annual exceedance probability of 10^{-2}. A common assumption is that a sea state lasts 3 hours, this means that the probability of exceedance for each sea state is $\frac{1}{29200}$. Figure 78 shows an example of such lines for the Kvitebjørn field.
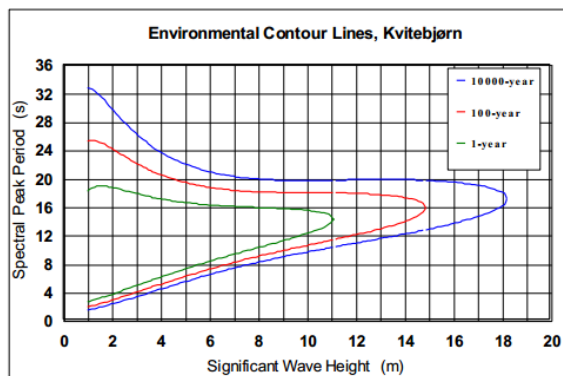
Figure 78: Environmental contour lines for the Kvitebjørn field (Haver, 2011)

An assumption that is introduced by using the contour method is that all sea states are independent. This does not hold true, but it is a conservative assumption (Haver, 2011).

After the contour lines have been established the next step is to run several analyses along the contour lines to find the worst combination. To establish the probability distribution of the response a large number of simulations of the worst sea state with random seeds

have to be carried out.

In order to account for the short term variability it is insufficient to take the mean of the maximum response from these simulations. Instead the maximas for each simulation must be fitted to an extreme value distribution. NORSOK N003 advices to take the 90% percentile from this distribution as the design value.

6.1.2 Extreme value statistics

Using stochastic wind implies that the wind field is simulated, using Monte-Carlo simulation for each time-realization. This means that one realization is not enough to capture the response corresponding to the 100-year maxima. To remedy this 30 one-hour simulations were conducted. The largest response in each simulation, denoted the one hour maxima, was then assumed to follow the Gumbel distribution. This assumption is commonly adopted and yields adequate results (Haver, 2011). The Gumbel distribution assumes that all maximas have the same distribution function, and that they are statistically independent. Assuming that these are fulfilled the Gumbel distribution is defind by equation 32 (Haver, 2011).

$$F_{Y_m}(y) = \exp\{-\exp\{-\frac{y - \alpha}{\beta}\}\} \tag{32}$$

Where Y_m is defined as $Y_m = max(X_1, X_2, ..., X_m)$, and X are independent maximas with equal distributions. α and β in equation are called location and scale parameters. using these parameters the expected value and standard deviation are given by equations 33 and 34.

$$\mu_Y = \alpha + 0.57722\beta \tag{33}$$

$$\sigma_Y = 1.28255\beta \tag{34}$$

To get unbiased estimators for the parameters one can use the moment principle. This gives that the scale parameter can be estimated by equation 35 and the location parameter by equation 36.

$$\hat{\beta} = 0.7797\mathbf{s} \tag{35}$$

$$\hat{\alpha} = \bar{\mathbf{y}} - 0.57722\hat{\beta} \tag{36}$$

In equation 35 and 36, **s** is the sample standard deviation, defined by equation 37 and $\bar{\mathbf{y}}$ is the sample mean, defined by equation 38.

$$S_m = \sqrt{\frac{1}{m-1}\sum_{i=1}^{m}(x_i - \bar{x})^2} \tag{37}$$

$$\bar{x_m} = \frac{1}{m}\sum_{i=1}^{m} x_i \tag{38}$$

Using equation 37 and 38 to calculate the sample mean and standard deviation for the 30 one-hour maxima, it is possible to estimate the parameters for the Gumbel distribution. After the Gumbel distribution has been established the 100 year response can be calculated directly.

6.2   Method

In addition to looking at how the bridge responds to a ship impact, the response to environmental loads was studied. The model used in these analyses was the same used for the ship collision without the collision barrier, as described in section 3. Environmental loads consist of many types of loads including, but not limited to: current, wind and waves. All of these loads are characterized by their fluctuating nature which means that they can induce several of the eigenperiods of the bridge, giving large motions. Response to environmental loads are often used as an ULS design criteria. This means that one looks at the response with a likelihood of exceedance of around 1% for a given year. Or stated more plainly: has a return period of 100 years.

The different contributions where first looked at independently to investigate their impact on the structure. Next several combinations of the loads were analysed to find the most critical combination.

6.2.1   Environmental data

The environmental conditions at the crossing can be found by collecting data at the site, and such measurements are in progress (Statens vegvesen, 2012b). In order to have reliable data, such measurements have to be conducted over several years. This means that the model for the 100 year environmental conditions might still change. As a result, the environmental conditions that are used in these analyses stems from the model for the 100 year conditions with the present knowledge.

The wind conditions were given as presented in table 19 (Statens vegvesen, 2015a)

Table 19: Extreme wind speeds

Return period [years]	1	100	10 000
1 hour mean wind speed at height 10 m [$\mathrm{m\,s^{-1}}$]	21.0	29.0	35.0
Turbulence intensity [%]	12.5	12.5	12.5

This is in accordance with the Eurocode 3 standard, and the national annex which gives that the 1 hour mean wind speed with a 100 year return period in the area is 29 $\mathrm{m\,s^{-1}}$ (Norsk Standard, 2009).

One additional parameter is current. It was assumed that the current was uniformly distributed along the crossing with a depth profile as given in table 20.

Table 20: Extreme current values(Statens vegvesen, 2015a)

Return period [year]	1	100	10 000
Depth [m]	Current speed [$\mathrm{m\,s^{-1}}$]		
0	0.50	0.70	0.82
5	0.50	0.70	0.82
10	0.30	0.40	0.46
20	0.23	0.27	0.30
30	0.23	0.27	0.30
50	0.17	0.25	0.29
100	0.13	0.16	0.18
150	0.13	0.16	0.18

Another parameter that can influence the response of the bridge is the sea level. With a high tide the utilization of the tethers will increase, but the same is true for the stiffness of the system. The sea level at the crossing, compared to the mean level as given in "Multi-span suspension bridge on floating foundations" (Statens vegvesen, 2015a) is shown in table 21.

Table 21: Extreme sea level compared to mean (Statens vegvesen, 2015a)

Return period [year]	1	100	10 000
Maximum sea level [m]	1.9	2.3	2.6
Mean sea level [m]	0.0	0.0	0.0
Minimum sea level [m]	-1.0	-1.3	-1.5

An important parameter for calculating the wave loads on the structure is the sea state. The sea state is used to create a wave spectrum which then completely describes the sea

surface statistically (Pettersen, 2007). At the crossing the sea state is a combination of locally wind-generated waves and swell waves. Table 22 shows the two components.

Table 22: Sea states (Statens vegvesen, 2015a)

Return period [year]			1	100	10 000
Locally wind-generated waves	West- Northwest	Hs [m]	1.80	3.00	3.90
		Tp [s]	4-6	4-6	4-6
	North	Hs [m]	1.20	2.00	2.60
		Tp[s]	4-6	4-6	4-6
Swell	West-Northwest	Hs [m]	0.15	0.39	0.39
		Tp [s]	11-16	11-16	11-16

6.2.2 Waves

As can be seen in section 6.2.1 the 100 year sea state means that the incident waves will be very small. This implies that the effect of linear wave loads will be relatively small. Another point is that the period of oscillation of these loads will be around 4-6 seconds, which is less than 10 % of the relevant eigenperiods. Instead the focus was placed on the second order drift forces which can have an oscillation period from 80 to 100 seconds (Faltinsen, 1990). This is close to the largest eigenperiod, which could lead to larger responses.

The slow drift excitation loads can be calculated by using equation 39.

$$
F_i^{sv} = \sum_{j=1}^{n} \sum_{k=1}^{n} A_j A_k [T_{jk}^{ic} \cos((\omega_k - \omega_j)t + (\epsilon_k - \epsilon_j))
$$
$$
+ T_{jk}^{is} \sin((\omega_k - \omega_j)t + (\epsilon_k - \epsilon_j))] \quad (39)
$$

Here T_{jk}^{ic} and T_{jk}^{is} are the second order transfer functions for difference frequency loads. A_j and A_k are the wave amplitude of wave component j and k, which have frequencies of ω_j and ω_k respectively. ϵ is here a random phase angle. Equation 39 requires one to solve the second-order potential, which is both time consuming and if not done correctly a great source of error.

For slow drift forces the relevant components are the ones where ω_j is very close to ω_k. As a result it is possible to use Newman's approximation, in which one approximate the values of T_{jk}^{ic} and T_{jk}^{is} with their values at the line $\omega_j = \omega_k$. Newman further approximated

the double summation in equation 39 with the square of a single series. This meant that the slow drift loads can be calculated by equation 40.

$$F_i^{sv} = 2(\sum_{j=1}^{n} A_j (T_{jj}^{ic})^{\frac{1}{2}} \cos(\omega_j t + \epsilon_j))^2 \tag{40}$$

In equation 40 the T_{jj}^{ic} is the transfer function for the slow drift forces, but opposed to T_{jk}^{ic} and T_{jk}^{is} it can be calculated using only the linear velocity potential.

T_{jj}^{ic} in equation 40 was calculated using Wadam. Here the floater was modelled as a circular cylinder without the base trusswork. This does not influence the result since the wave force decays exponentially as shown in figure 79.
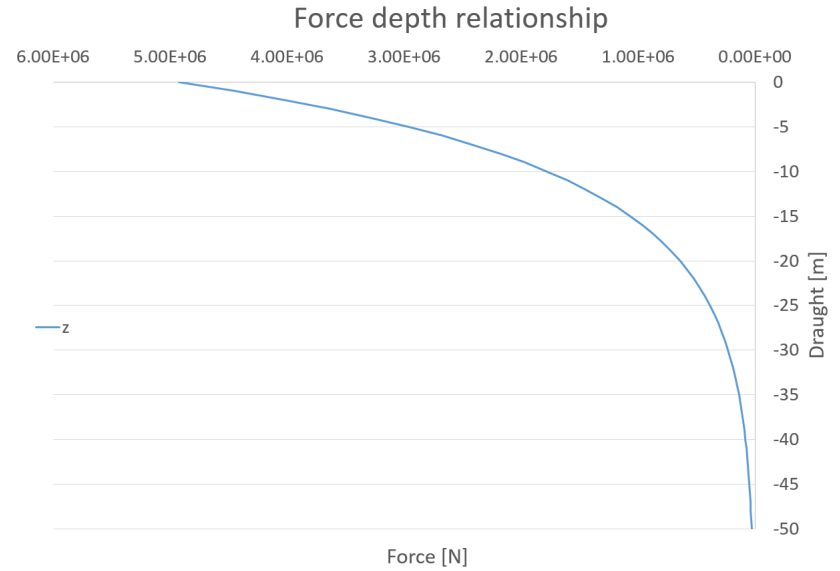
Figure 79: Example of a wave force distribution on cylinder

Given the wave data presented in section 6.2.1 it is clear that the wave loads will be negligible at the base of the floater, and any changes here will have marginal effect on the outcome. The model was built and meshed in GeniE before imported to HydroD, a Wadam preprocessor. Close to the water line a mesh size of about 0.5 metres was used, the rest of the model was meshed with a larger mesh size. In order to calculate the slow drift force at different frequencies both direct integration and far field integration were used. Figure 80 shows the HydroD model of the floater.

Both direct pressure integration and far field integration were used in order to act as a control towards each other. This gave similar results and the resulting transfer function

71
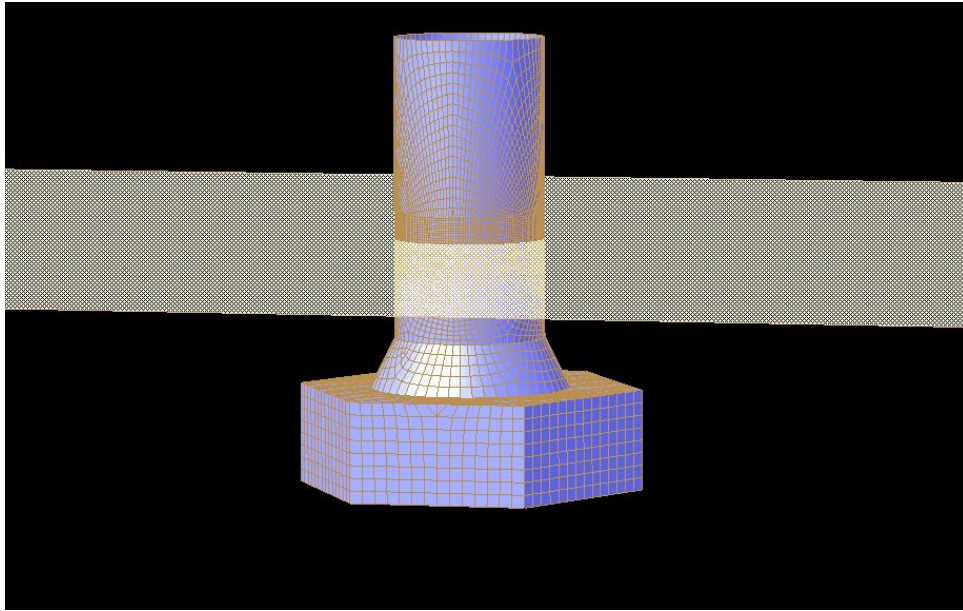
Figure 80: HyrdoD model of the floater

is shown in figure 81.
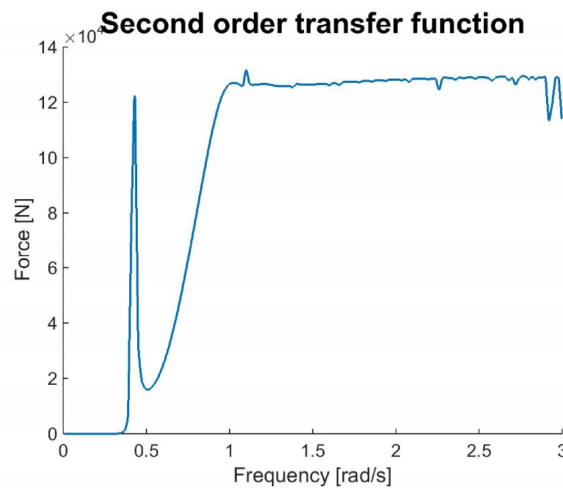
Figure 81: The slow drift force transfer function

One thing to notice about the transfer function in figure 81 is the noise at high frequencies. This is due to numerical errors, and the transfer function is assumed to be constant for frequencies larger than 1.5 $[\text{rad}\,\text{s}^{-1}]$

Another feature is the first peak, this coincides with the eigenfrequency in heave for the floater. This is expected as the drift forces are dependent of the amplitude of the reflected waves, which is dependent on the body motions. Resonance in heave will yield large body

72

motions and thus also large amplitudes of the reflected waves, hence the peak.

Maruos formula can be used to find the average drift load on a structure (Faltinsen, 1990). This is defined by equation 41

$$\bar{F}_1 = \frac{2}{3}\rho g \zeta_a^2 r \cos\beta \tag{41}$$

If it is now assumed that the incoming wave field is parallel with the x-axis such that β is zero, and that the waves are completely reflected. This results in small waves and high wave frequencies. Applying these assumptions one gets:

$$\frac{\bar{F}_1}{\zeta_a^2} = \frac{2}{3}\rho g r \tag{42}$$

Inserting the radius of the bridge pylon one gets:

$$\frac{\bar{F}_1}{\zeta_a^2} = 10.5 \cdot 10^5$$

Which when compared to the high frequency area of figure 81 shows a very good correspondence between the two approaches.

A_j, the wave amplitude, in equation 40 can be defined by equation 43.

$$\frac{1}{2}A_j^2 = S(\omega_j)\Delta\omega \tag{43}$$

Where $S(\omega_j)$ is the value of the wave spectrum for frequency ω_j, and $\Delta\omega$ is the difference between successive frequencies, defined in equation 44.

$$\Delta\omega = \frac{\omega_{max} - \omega_{min}}{N} \tag{44}$$

Here ω_{max} and ω_{min} are the highest and lowest frequencies in the spectrum and N is the number of divisions of the spectrum. This meant that a wave spectrum for the sea state had to be created based on the data given in section 6.2.1. For the wind generated sea a Jonswap spectre with peak period 5 seconds, a significant wave height of 3 metres and a gamma of 3.3 was chosen (Pettersen, 2007). This spectrum is shown in figure 82.

Swell sea was incorparated in a similar way and the spectras were superimposed upon each other to calculate the load.
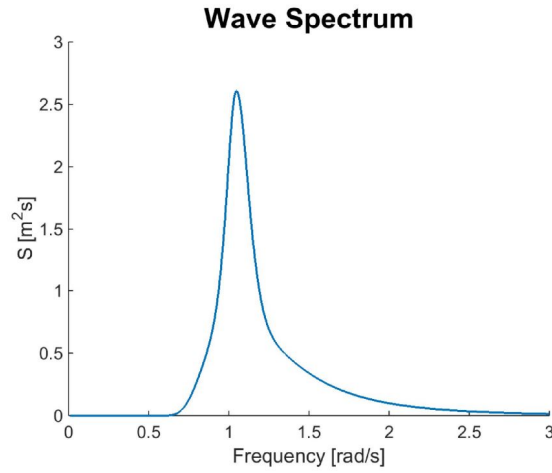
Figure 82: The Jonswap spectrum for the wind generated sea

In order to get a signal that does not repeat itself, N in equation 44 should be chosen such that it fullfills equation 45.

$$\frac{2\pi N}{\omega_{max} - omega_{min}} > t[sec] \tag{45}$$

In equation 45 t, is the time one wants to simulate. A sea state is usually assumed to last for three hours which means that t in this case is 10800 seconds.

Using the sea state and transfer function equation 40 was used to simulate a time history of the drift force. This is shown in figure 83.
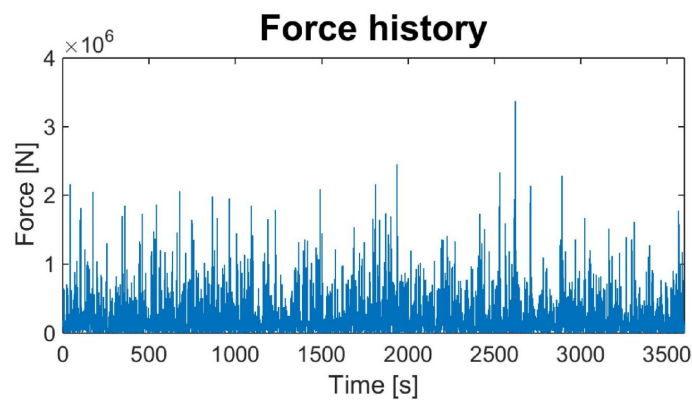
Figure 83: The simulated drift force from equation 40

As can be seen figure 83 is dominated by high frequency noise, which is to be expected, as equation 40 includes non physical high frequency effects (Faltinsen, 1990). Using a

74

band-pass filter removes the noise and the resulting signal is shown in figure 84.
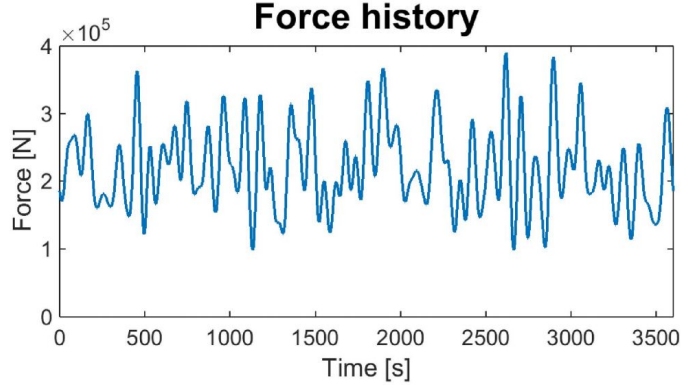
Figure 84: The simulated drift force with filter

Figure 84 shows that the drift force oscillates around a mean value with an oscillation period of approximately 100 seconds.

The distance between the two floaters are over 1300 metres this means that the sea surface at one might not be the same as the sea surface at the other. However, since the crossing is placed in a fjord, and thus that the correlation between the wave conditions at each floater will be significant, the same time history was used on both floaters. An additional advantage of this, is that it represents the most conservative approach.

6.2.3 Wind

The 100 year wind conditions as described in section 6.2.1 was modelled in two ways. As a first step the wind was modelled constant over the length of the bridge, with a distribution over the height of the bridge governed by a power law. Equation 46 shows the governing equation of the power law.

$$U(z) = U_{ref}(\frac{z}{z_{ref}})^{\alpha} \tag{46}$$

This equation yields the wind speed, U, at an altitude, z. Here U_{ref} is the wind speed at a reference height, z_{ref}. α is the power. The parameters used in establishing the wind field are presented in table 23. These have been changed somewhat compared to the data given in 6.2.1 (K. Aas-Jackobsen, Personal communication, May 10TH 2016), and the updated parameters are shown in table 23.

This gave a wind distribution as presented in figure 85.

Table 23: Wind field parameters

Item	Value
U_{ref} [$\mathrm{m\,s^{-1}}$]	31.7
Z_{ref} [m]	10
Z_{Bott} [m]	0
ρ [kg/m^3]	1.293
α [-]	0.128
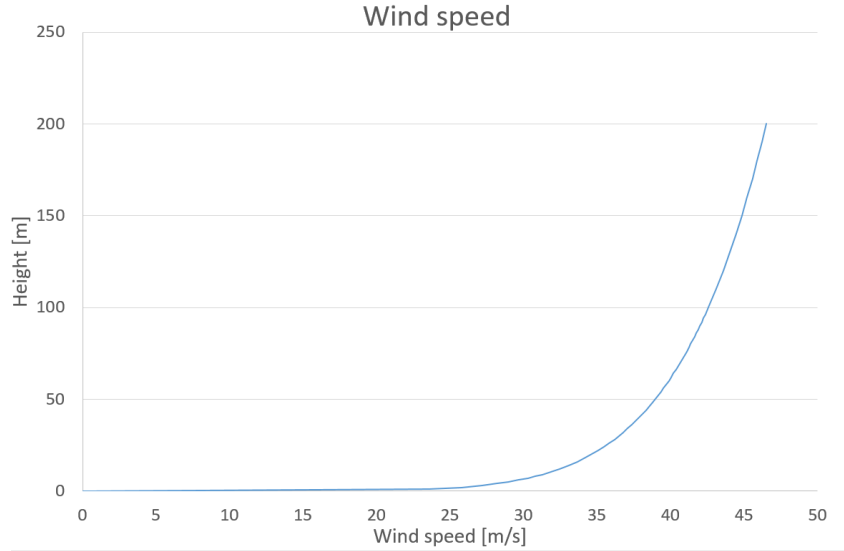
Figure 85: Wind speed profile

The interaction between the wind and the structure are defined by force coefficients. These are divided into three contributions for each element: Lift, drag and moment. Where lift is perpendicular to the wind direction, drag is parallel and moment is around the local length of the elements (Hansen, 2008). These coefficients are made dimensionless in different ways. As an example the definition of the drag coefficient is shown in equation 47. Both the lift coefficient, C_L, and moment coefficient, C_M are defined in a similar manner.

$$C_D = \frac{2F_D}{\rho u^2 A}[-] \tag{47}$$

In equation 47, F_D is the drag force on the element, ρ is the density of air, A is the cross-sectional area and u is the wind speed. The coefficients for the different cross sections are presented in table 24.

76

Table 24: Aerodynamical coefficients

Element	Coefficients	Values
Bridge Girder	C_D	0.529
	C_L	0.133
	C_M	0.048
Main Cable	C_D	0.8
Hangers	C_D	0.8
Floater Superstructure	C_D	0.8
Fixed Superstructure	C_D	1.761

After conducting the static mean wind analysis the next step was to create a stochastic wind field. This was done by simulating a time history of the wind speed at several different points on the bridge. The red rectangle in figure 86 shows the spatial extent of the calculations of stochastic wind on the bridge.
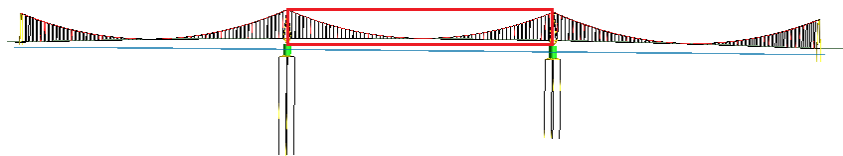
Figure 86: Area with stochastic wind

The area in figure 86 was divided into 70 nodes horizontally and three vertically, and the wind was calculated at each node. As figure 86 shows, stochastic wind is not calculated for the entire bridge. Instead it is only calculated on the midspan of the bridge. Figure 87 shows the wind force across the length of the bridge in a given time instant, while figure 88 shows the force at another time instant. As figures 87 and 88 shows the wind outside the defined grid will also be varying with time. This happens because the wind speed outside the defined grid is equal to the wind speed at the closest border at each time step.
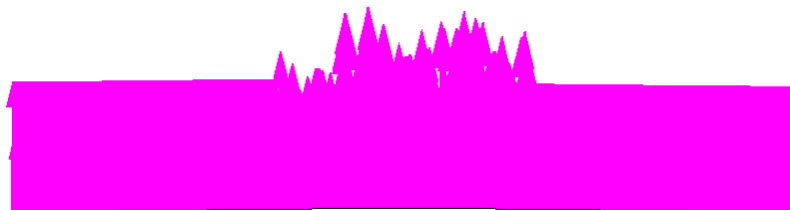
Figure 87: Realization of wind force at time1
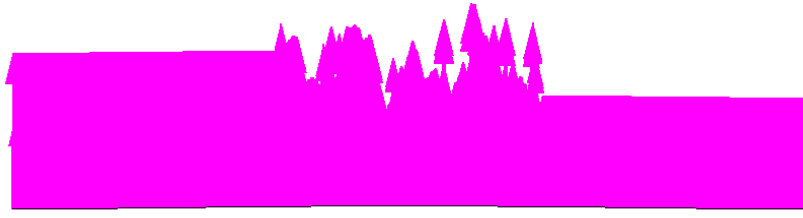
Figure 88: Realization of wind force at time2

Figure 87 and 88 show the area with stochastic wind in the middle of the bridge. More importantly it shows that outside the defined grid, the wind speed is also varying with time, but not over the length of the span.

When looking at the wind force distribution vertically, as presented in figure 89 the effect of the power law is evident. In addition it is clear that the force is uniform around each calculation point, and not interpolated between the points.

(a) Vertical distribution of horizontal force at time1

(b) Vertical distribution of horizontal force at time2

Figure 89: Vertical wind force distribution

The wind spectra for a single point is defined by equation 48 (Aas-Jacobsen, 2008). Where S_{ii} is the spectral value for a given direction in a given point. I_i is the turbulence intensity, which is defined as the ratio of the standard deviation to the mean wind speed(Hau, 2013). U_{10min} is the 10 minute mean wind speed, L_i is the length scale and f is the frequency in Hz.

$$S_{ii}(f) = \frac{I_i^2 U_{10min} L_i}{(1 + 1.5 \frac{fL_i}{U_{10min}})^{5/3}} \qquad (48)$$

78

The spectrum gives the fluctuating component of the wind speed at a given point, as shown in figure 90.
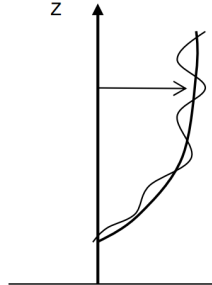
Figure 90: Typical wind profile, with mean wind speed and fluctuating component

By using equation 48 for one of the points within the grid one get the one point spectrum as shown in figure 91. This spectrum shows that the wind speeds have large contributions from the area with several important eigenmodes.
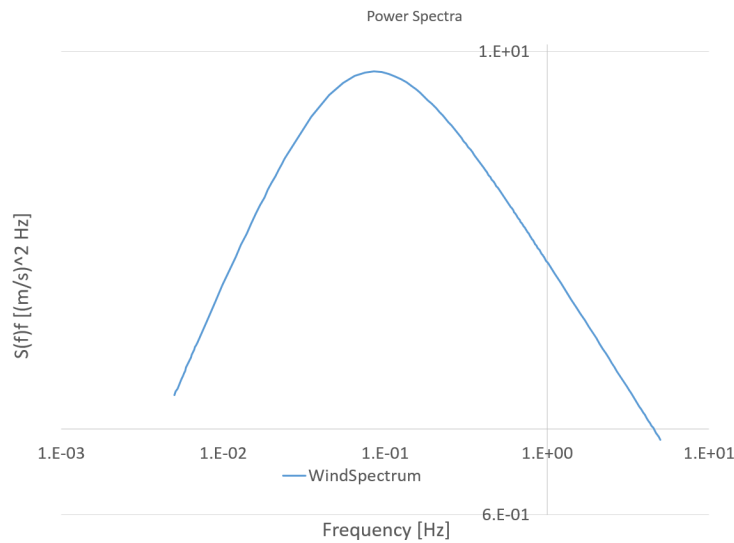
Figure 91: One point wind spectrum

Since the points for which the wind speeds are calculated, are within the same wind field they will depend on each other. This coherence is defined by equation 49.

$$\sqrt{coh(f,s)} = \exp(-\frac{c_i f s}{U_{10min}}) \tag{49}$$

Here c_i is the decay exponent and s is the distance between points, f and U_{10min} are the same as in equation 48.

79

For the calculation of the stochastic wind field the software WINDSIM, created by Ketil Aas Jakobsen was used. The input parameters used in creating the time realisation are shown in table 25. Table 25 starts by defining the grid where the stochastic wind is to be calculated. Then the mean wind speed is defined, with reference to the reference height and the exponent in equation 46. The next step is to define the fluctuating component of the wind speed, before the relevant coherence factors and frequencies is defined.

Table 25: Input for stochastic wind

Grid			
Direction	Min	Max	No
X	0	0	1
Y	1380	2760	56
Z	40	200	3
Mean wind			
Uref [$\mathrm{m\,s^{-1}}$]	31		
Zref[m]	10		
Z_0	0		
alpha	0.128		
boundary height	2000		

Fluctuating					
Comp	Type	Sigma	A	Z0	Zref
u	3	4.20	6.8	0.01	10
v	3	3.67	9.4	0.01	10
w	3	2.75	9.4	0.01	10

Coherence	
Type	Norsk standard 3491-4:2002
Cu	10
Cv	6.5
Cw	6.5

Frequency	
Fmin [Hz]	0.0001
Fmax [Hz]	4.55
nf	14

6.3   Results

As mentioned in section 6.2 the response to environmental loads was investigated by looking at several load cases. First with only one load component in each load case, before the components were combined.

6.3.1 Static Wind

Static wind was initially used to get a feel for how the bridge responds to wind loading. Table 26 shows some key results from static wind. Looking at table 26 it is clear that the displacements due to static wind are significant with both floaters being offset by20 metres. This displacement does not yield any significant increase in the tether force, which in calm water is 33.3 MN per tether.

Table 26: Key results static wind

Floater 1	Displacement Bridge Girder	[m]	22.2
	Displacement Tower	[m]	22.5
Floater 2	Displacement Bridge Girder	[m]	19.9
	Displacement Tower	[m]	20.2
Displacement midspan		[m]	26.3
Cable Force		[MN]	111
Tether Force	Average	[MN]	33.6

Another point in table 26 is that the wind forces makes the top of the floater displace more than the bridge girder, 30 centimetres for both floaters. This induces a small rotation of the bridge towers, which can increase the tension force in some tethers and reduce it in others. Looking at the tether forces for the six equivalent tethers, it is clear that this is exactly what happens. The tether with the lowest tension force has 14 MN, while the highest is54 MN. A difference of 40 MN.

The midspan is the point on the bridge experiencing the largest displacement, 26 metres. That this is reasonable is substantiated by looking at figure 92, which shows the wind loading on the bridge, as represented in USFOS.
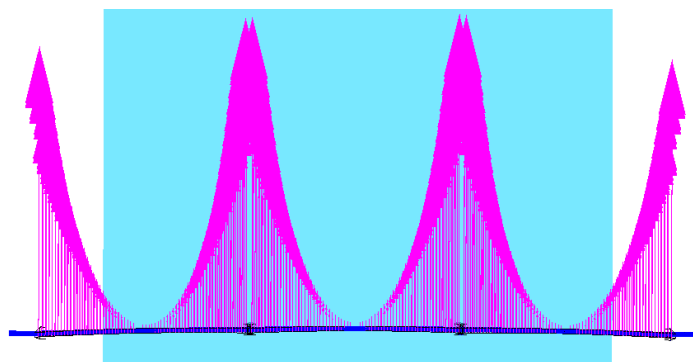
Figure 92: Wind Loads on the bridge

Figure 92 shows that the largest nodal wind forces occur close to the floaters and on the shore supports. This is due to the wind speed, which was seen in figure 85 in section 6.2.3, to increase with increasing height. As the there is a quadratic relationship between the wind speed and the loading the effect increases. In addition it is evident that the hangers in this area are longer, and thus resulting in larger nodal loads.

The resulting deformation shape of the bridge when subjected to static wind loads is presented in figure 93. As this figure shows, the deformation shape corresponds with the modeshape for the largest eigenperiod. This is expected as this is the mode shape with the smallest resistance to bending.
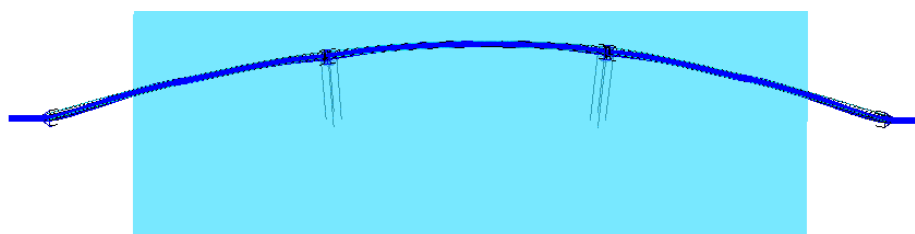
Figure 93: Deformation shape of bridge submitted to static wind loading, scaled by a factor of ten

6.3.2 Drift forces

The next step was to analyse the bridge when it was subjected to wave forces only. How these were calculated is described in section 6.2.2. In USFOS the loads were applied as time varying nodal loads. This is shown in figure 94.
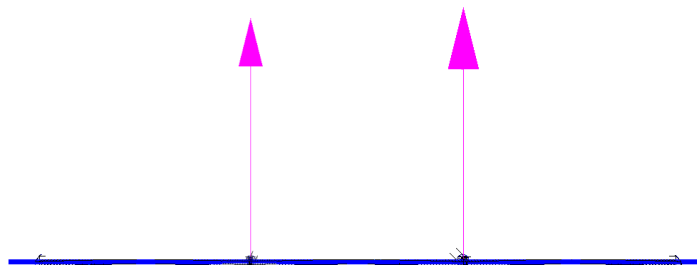
Figure 94: USFOS model of wave loads.

The key results are presented in table 27.

Table 27: Key results drift forces only

Item		Units	Min	Average	Max
	Displacement Bridge Girder	[m]	0.36	0.98	1.54
	Acceleration Bridge Girder	[m s^{-2}]	-0.002	0.0	0.002
Floater 1	Displacement Tower	[m]	0.37	1.0	1.55
	Acceleration Tower	[m s^{-2}]	-0.002	0.0	0.002
	Displacement Bridge Girder	[m]	0.29	1.10	1.89
	Acceleration Bridge Girder	[m]	-0.002	0.0	0.002
Floater 2	Displacement Tower	[m]	0.31	1.11	1.90
	Acceleration Tower	[m s^{-2}]	-0.002	0.0	0.002
Cable force		[MN]	119	119	119
Tether force		[MN]	31.9	33.4	33.7
Displacement midspan		[m]	0.96	1.76	2.51
Accleration midspan		[m s^{-2}]	-0.002	0.0	0.002

As table 27 shows, the drift forces induce both a mean deformation and an oscillating component. The average deflection is 1.8 metres at the midspan, and around one metres for the floaters. The oscillating motion of the bridge girder has an amplitude of 1.5 metres at the midspan and 1.2 for the floaters. This shows that the oscillation is significant compared with the mean drift force. As the total deformation due to drift forces is small compared with e.g wind forces, the forces in the tethers and main cable are not affected much by the waves.

Since the force on the floaters are correlated, the deformation shape of the bridge mimics that of the static wind.

As mentioned in section 4.2 the largest eigenperiod, and the one yielding a correlated motion of the floaters is 104 seconds. If the response due to the drift forces oscillates with periods close to this eigenperiod it can lead to larger deformations. Figure 95a shows the resulting displacement of the midspan for the entire simulated time history. This shows that the oscillation amplitude greatly increases around 2800 seconds. When this area is zoomed into, as shown in figure 95b, it is clear that the period of oscillation is close to the largest eigenperiod, thus leading to larger deformations.
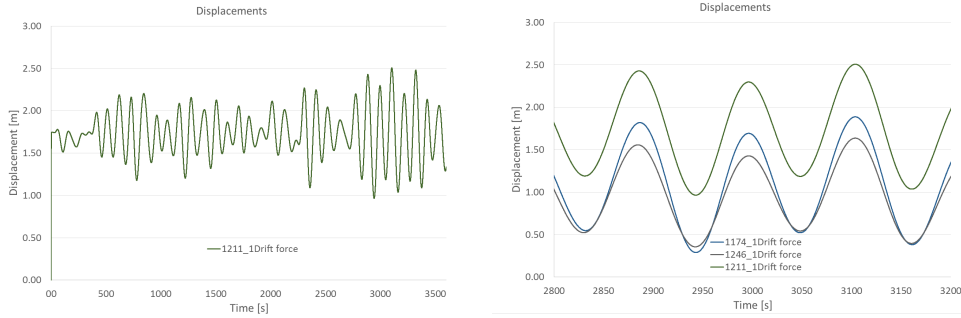
(a) Response of midspan due to drift forces

(b) Response, of floaters and midspan due to drift forces

Figure 95: Response to drift forces

6.3.3 Static Wind and Drift forces

As a next step the second order drift forces were combined with static wind. The key results for this analysis are presented in table 28. If these results are compared with those of the static wind alone it is clear that the addition of the drift forces has a significant impact. The mean average displacement when including drift forces to static wind are increased with approximately 0.4 metres. The drift forces have an oscillating component which increases the maximum displacement additionally. If one looks at the maximum midspan displacement, this is increased with 1.1 metres, compared to the static wind alone.

Table 28: Key results static wind and drift forces

	Item	Units	Min	Average	Max
Floater 1	Displacement Bridge Girder	[m]	19.6	20.2	20.8
	Displacement Tower	[m]	19.9	20.5	21.1
Floater 2	Displacement Bridge Girder	[m]	21.8	22.6	23.3
	Displacement Tower	[m]	22.1	22.9	23.6
	Cable force	[MN]	112	112	112
	Tether force	[MN]	18.9	33.3	48.9
	Displacement midspan	[m]	25.9	26.6	27.3

Another thing that is evident in table 28 is that the addition of the static wind does not have a great influence on the oscillation amplitude of the drift forces. Reducing it by approximately 10 centimetres

Figure 96 shows the response of the bridge girder at each floater and at the midspan. For comparison the static wind displacement of the midspan is also included. This substan-

tiated the findings in table 28, namely that the static wind dominates the response, but with some additional oscillations due to the drift forces.

Figure 96: Response to mean wind and drift forces

6.3.4 Stochastic wind

When running stochastic wind several simulations with different realizations of the wind speed history were conducted. The key results for one of these runs are presented in table 29.

Table 29: Key results stochastic wind

	Item	Units	Min	Average	Max
	Displacement Bridge Girder	[m]	7.9	17.9	27.3
	Displacement Tower	[m]	8.1	18.2	27.6
Floater 2	Accelerations Bridge Girder	[m s^{-2}]	-0.20	0.0	0.19
	Accelerations Tower	[m s^{-2}]	-0.48	0.0	0.42
	Displacement Bridge Girder	[m]	6.4	20.0	35.0
	Displacement Tower	[m]	6.8	20.3	35.1
Floater 2	Accelerations Bridge Girder	[m s^{-2}]	-0.20	0.0	0.19
	Accelerations Tower	[m s^{-2}]	-0.48	0.0	0.45
	Cable force	[MN]	103	112	120
	Tether force	[MN]	-13.3	33.3	74.8
	Displacement midspan	[m]	11.5	24.0	37.4
	Acceleration midspan	[m s^{-2}]	-0.73	0.00	0.69

As table 29 shows, the maximum displacements are considerably larger than for the static

wind case. The stochastic wind gives an increase of the midspan displacement by 10.1 metres, compared to the static wind case. The average deflection is however reduced with 2.6 metres compared with the static wind field. Another observation that is evident from table 29, is that the top of the superstructure has an average displacement of 0.3 metres more than the bridge girder. This reflects a rotation of the bridge tower.
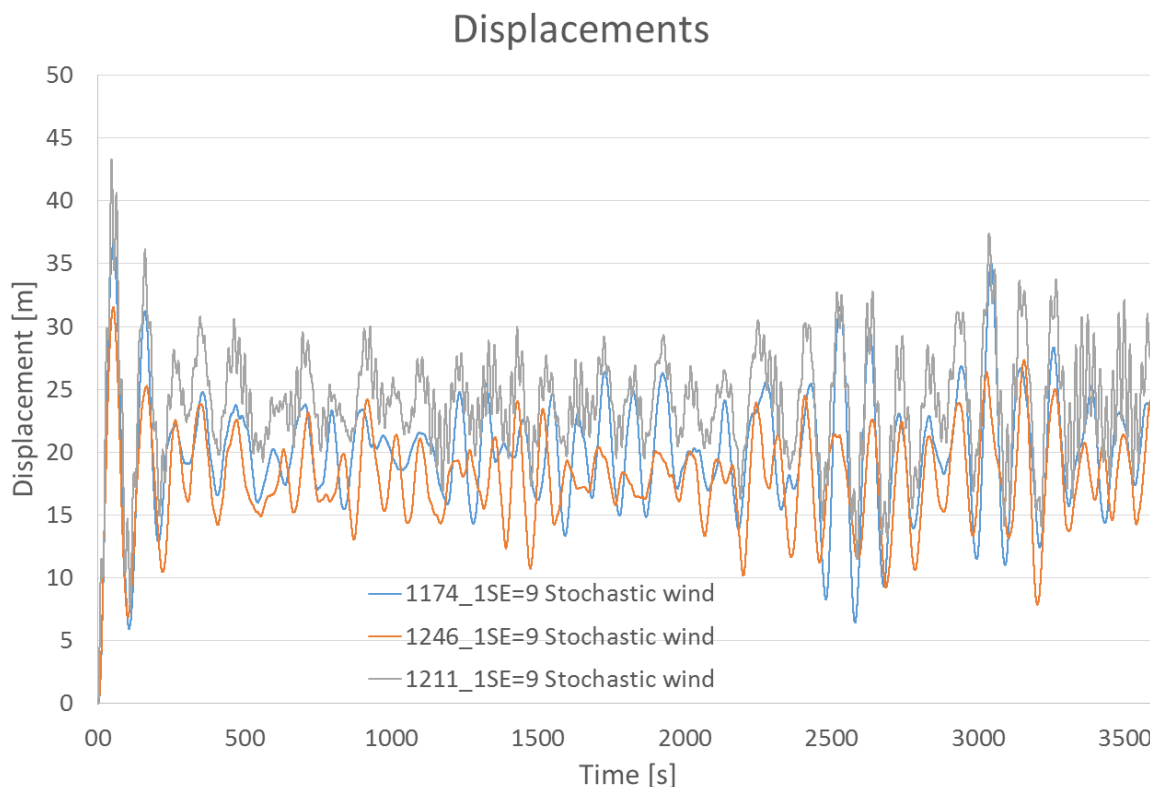
Figure 97: MidSpan deflection due to stochastic wind

Figure 97 shows the midspan deflection due to the stochastic wind forces. Here it is visible that the oscillation period of the bridge with stochastic loading is not far from the eigenperiod of the bridge. The blue and orange line in figure 97 displays the motion of the bridge girder at the floaters. These show that the floaters move independently, and that when their motion is in phase the displacement of the midspan increases. If one looks closer at the area with the largest oscillation amplitude, as shown in figure 98, it is seen that this occurs with the bridge oscillating at around 100 seconds. This is close to the largest eigenperiod.

In addition the response at the midspan have higher frequency contributions. Comparing this to the response of the two floaters, the orange and blue line, it is clear that the

86
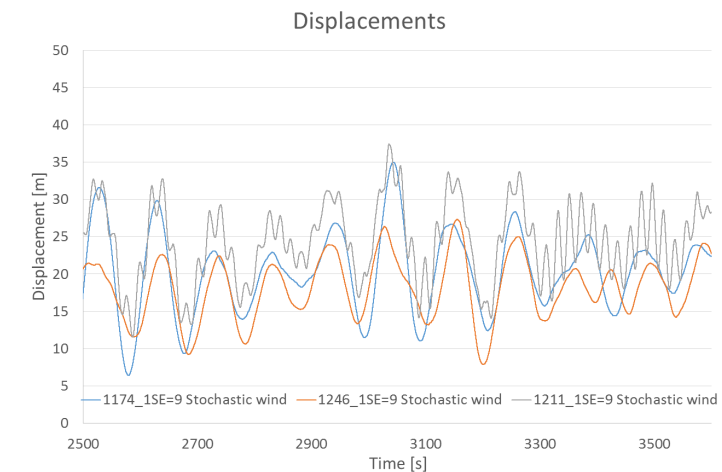
Figure 98: Midspan deflection due to stochastic wind

floaters are dominated by low frequency oscillations. These findings are substantiated by looking at figure 99.
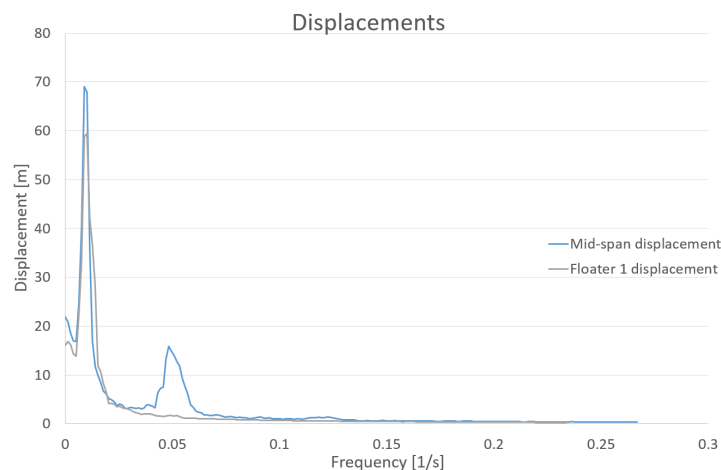
Figure 99: Frequency plot of displacements

Figure 99 shows that the displacements for both midspan and floaters have a peak at 0.0097 Hz. This corresponds with the largest eigenperiod of the system which is 104 seconds. In addition to this the midspan has a second peak at 0.043 Hz which corresponds to the third eigenperiod of 23.6 seconds. This eigenperiod corresponds to a bending of the bridge girder, with one half-wave over the span. Since this eigenmode only consists of local bending of the bridge girder, it has no influence on the floaters. It is however clear from figure 99 that the response is dominated by the largest eigenperiod, which also is evident from figure 97.

Due to the layout of the equivalent tethers, the slight rotation of the floater has a significant impact on the tethers. The tilt makes the distance from the floater tether connection to the tether ground connection shorter for the tether labelled 10132 This means that the tension force in the tether is reduced.
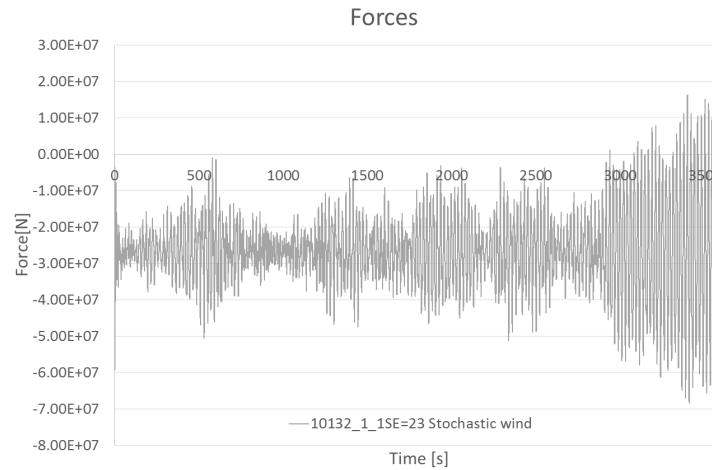
Figure 100: Tether force due to Stochastic wind

As figure 100 shows the tension force does become negative, i.e. the tether comes into compression. The effect of this will be discussed further in chapter 7.5.3. Another point to take away from figure 100 is that the tension force oscillates with a higher frequency than the floater displacements. This can also be seen in figure 101 which shows the frequency plot of the tension force in the tether 10132.
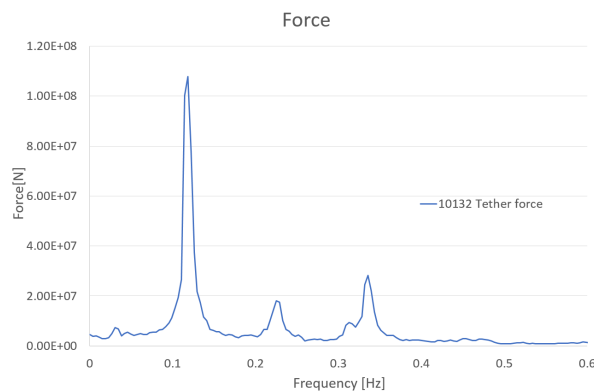
Figure 101: Frequency plot of the force in tether 10132

From figure 101 it is clear that the single largest contribution to tension force in tether has a frequency of 0.13 [Hz] which corresponds with the 17th eigenmode, see appendix C. Figure 101 shows, that it in addition is a contribution from the 12th eigenmode as well

as some higher modes. One thing to notice is that the response of the other tethers is not dominated in the same way by the 17th eigenmode. This is shown in figure 102, which shows a frequency plot for the tether 10131 from the same simulation as figure 101.
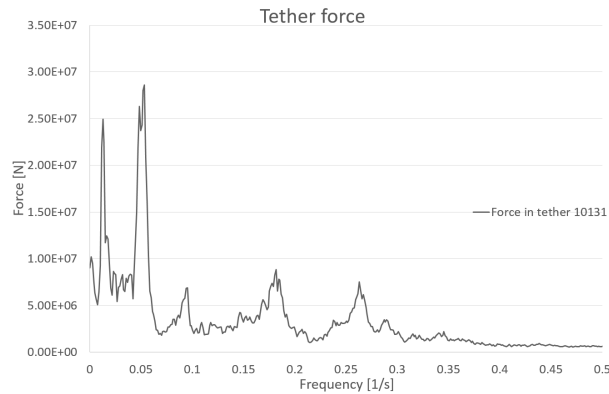
Figure 102: Frequency plot of the force in tether 10131

By studying figure 102 it is clear that for the tether 10131, the response is dominated by lower frequencies than for the tether 10132. The response for this tether is dominated by the first, third and fourth eigenmode.

When accelerations are plotted in the frequency plane,as shown in figure 103, it is seen that the midspan accelerations are dominated by lower eigenperiods. Especially the frequency 0.048 gives large accelerations. This frequency which also had a contribution to the midspan displacements, dominates the responding accelerations. The frequency dominating displacements only has a minor contribution on the acceleration.
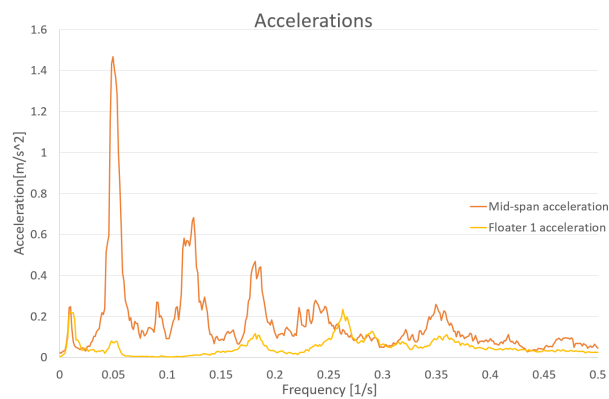
Figure 103: Frequency plot of Accelerations

The acceleration at the midspan also have significant contributions from higher frequencies such as 0.12 and 0.17 Hz.

The accelerations for one of the floaters is included in figure 103. This response is dominated by the two largest eigenperiods, with little influence from the bending modes of the bridge girder.

Another thing worth studying is the heave motion of the floaters and at the midspan. This was looked at in only one of the simulations due to time restrictions. Figure 104a shows the heave motion of the midspan, whereas figure 104b shows the heave motion for the floaters. Both figures have been zoomed in to the most critical region, where the motions are largest.

(a) midspan

(b) Floaters
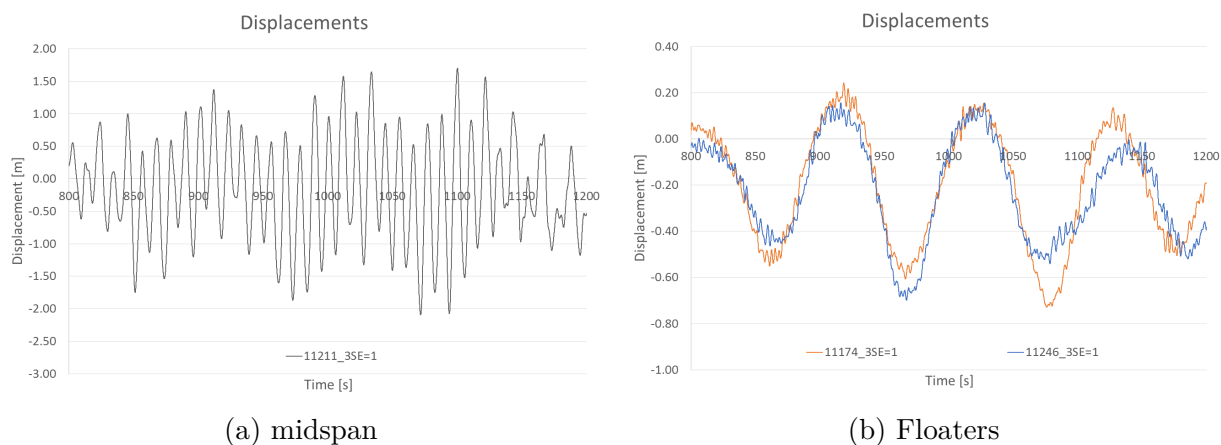
Figure 104: Heave motions

As can be seen in figure 104a the midspan has an oscilalting motion with amplitudes in excess of 3.5 metres. In addition to the amplitudes being large, the oscillations also have a small period, which means fast motions. This can e.g. be seen at the 1100 second mark where the midspan travels 3.8 metres in the course of 6 seconds. This rapid change causes large accelerations which was found to be ranging between -0.8 and 0.8 $[\mathrm{m\,s^{-2}}]$.

As figure 104b shows, the floaters too experiences heave oscillations, albeit smaller than for the midspan. For the floaters the oscillations have amplitudes of just under one meter. These oscillations have a large slowly oscillating component, as well as a smaller component with a higher frequency.

The findings in figure 104 can be substantiated by looking at figure 105, which shows the frequency plot of the heave motions.

(a) midspan
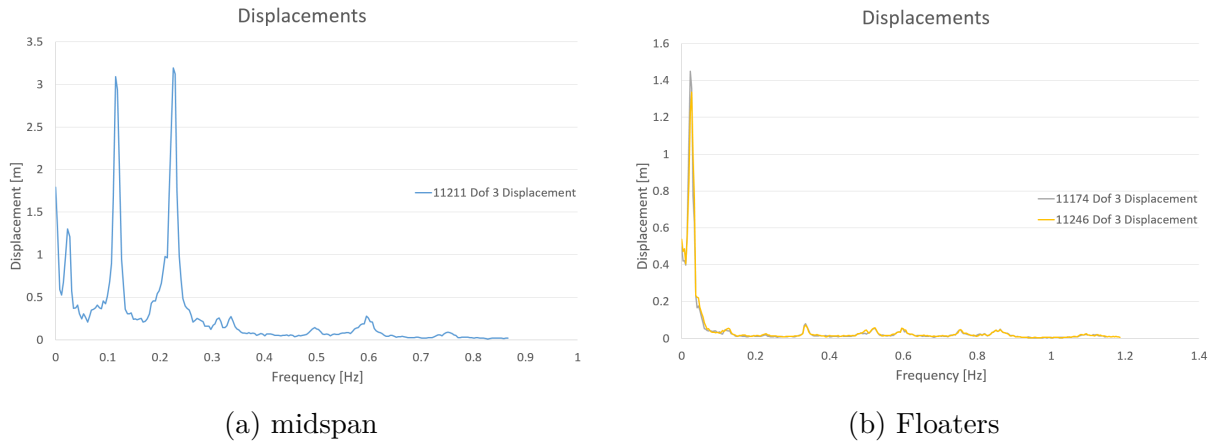
(b) Floaters

Figure 105: Heave motions

By looking at figure 105a it is seen that the two largest contributions have frequencies of 0.11 and 0.23 [Hz]. For the floaters the largest contribution has a frequency of 0.022. In addition to this there are also smaller contributions from higher frequencies such as 0.35 and 0.6 [Hz].

The next step was to create a sample of the largest maximas from the simulations. This was done by selecting the largest maxima in each category in table 29 for every simulation. For all samples a mean and standard deviation was found. These were then used to estimate parameters for the Gumbel distribution, which was used to find the 90 % percentile. The sample means, standard deviations and the 90 % percentile are presented in table 30

Table 30: Stochastic wind maxima

Item		Units	Mean	σ	F(x)=0.9
Floater 1	Displacement Bridge Girder	[m]	27.5	1.5	29.5
	Acceleration Bridge Girder	[m s^{-2}]	0.2	0.02	0.22
	Acceleration Tower	[m s^{-2}]	0.49	0.05	0.55
Floater 2	Displacement Bridge Girder	[m]	30.1	1.8	32.4
	Acceleration Bridge Girder	[m s^{-2}]	0.19	0.01	0.21
	Acceleration Tower	[m s^{-2}]	0.49	0.05	0.55
Midspan	Displacement	[m]	35.2	1.1	36.7
Midspan	Acceleration	[m s^{-2}]	0.72	0.07	0.81
Tether force	Maximum tension	[MN]	69.6	4.95	76.1
Tether force	Minimum tension	[MN]	4.94	4.92	11.4

Some key takeaways to note in table 30 is that in a hundred year storm it is seen that

some tethers will get a compression load. However the compression loads are small, which means that the only issue is buckling. This will be discussed in section 7.5.3.

Another observation in table 30 is that the maximum tension force is quite moderate. A maximum force of 76.1 MN yields a stress of 206 MPa, which is well below yield strength. In addition it is seen that a midspan displacement of 36.7 metres is more than twice the displacement from the worst case scenario ship collision.

For results from all simulations see appendix E.

7 Discussion

7.1 Eigenvalue analysis

As mentioned in section 4 the eigenvalue analysis was used to study the behaviour of the bridge. Parallel with the work done on this thesis a collaboration lead by Statens vegvesen has revised and updated the design. This means that the behaviour and eigenvalues of the bridge has changed as well. Furthermore this work is not finished as of June 2016 and it is thus difficult to compare the results from this thesis to other current work. As of May 2016 no eigenvalues for the updated bridge design over the Bjørnafjorden have been published. However, for the four legged design considered in phase one, eigenvalues are available. Table 31 shows the four largest eigenvalues found in this thesis, compared with the eigenvalues of the four legged design.(Statens vegvesen, 2012b).

Table 31: Eigenvalue comparisons

Eigenmode	This thesis	Four legged	Difference
1	104.4	91.8	12%
2	81.5	61.8	24%
3	23.6	29.3	-24%
5	22.2	18.0	19%

As table 31 shows, all eigenvalues have changed considerably with the difference being almost 25%. It is expected that the difference is large, as the the two designs are very different. The largest difference occurs for the third eigenvalue, which involves vertical displacement of the bridge girder and a rotation of the floaters. This stiffness has two main contributions, namely that from the tethers, and the resistance against roll motion. The latter is dependent on the centre of gravity, which is lower for the new design than for the four legged structure causing the large difference.

7.2 Added Mass

In the analyses presented in this thesis the added mass was assumed to be constant. This assumption was made because the floaters were assumed to be oscillating slowly, i.e. with a large period. For slowly moving structures the added mass is not frequency dependent, as is seen in figure 28 in section 4.1. When studying the frequency plot of the motion of the floaters in section 6.3.4 it was seen that the motion was dominated by low frequencies.

This is further substantiated by the eigenperiods, which for the floaters are 104 and 81.5 seconds, and thus well within the area with constant added mass.

7.3 Saddle modelling

The saddles, the contact point between the superstructure and the main cables, were in these analyses modelled as fixed, as stated in section 3. In reality these are not fixed, but held in place by friction forces. Figure 106 shows the force difference in the main cable on each side of a superstructure, with environmental loads. This shows that the difference in force between the two sides of the saddle is maximum 10 [MN] which is within the design load (Statens vegvesen, 2012b).
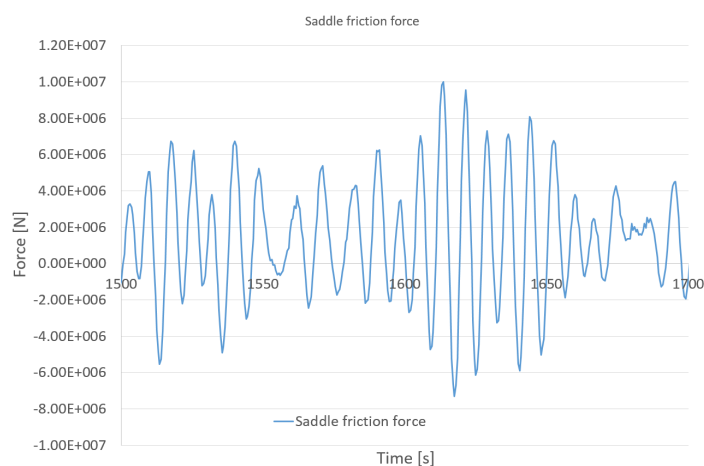
Figure 106: Friction force in the saddles

7.4 Ship Collisions

7.4.1 Effect of assumptions

One assumption that is introduced in these analyses is the model of the ship, which is a nodal mass given an initial velocy, and connected to the structure with a series of springs. This is a simplification, and in order to get reliable results the spring has to accurately represent the force deformation characteristic of the ship. The reason for this is that the force deformation characteristic determines the strain energy dissipated by the ship, the duration of the impulse, and the peak force on the structure. Figure 107 shows the force deformation curve from non-linear finite element analysis in LS-DYNA, which was used

as input to the spring in USFOS and the resulting force deformation characteristic of the USFOS spring.

(a) With barrier
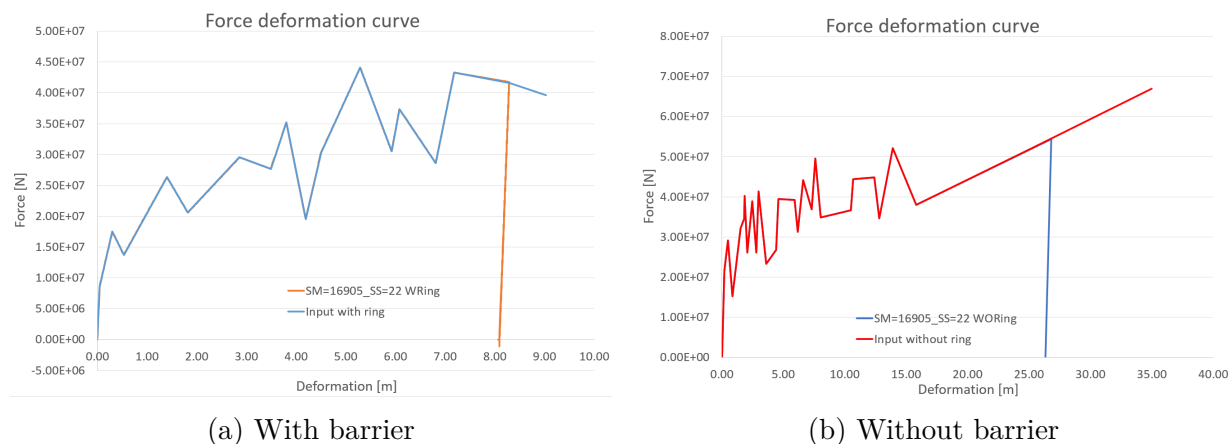
(b) Without barrier

Figure 107: Response with and without the barrier

As both figure 107a and 107b shows, the force deformation characteristic of the spring in USFSOS follows the force deformation characteristic used as input. Meaning that the model yields a good representation of the ship behaviour.

Using the force deformation characteristic for a horizontal impact does not introduce any errors for the collision directly on the floater. For the collision against the barrier, the assumption will cause some uncertainties. The reason for this is that the ship barrier interaction is uncertain. As a result, how the barrier will deform the vessel is not given, which can change the force deformation characteristic.

Another assumption in the analyses is the strength design principle. This means that nearly all strain energy is dissipated in the ship and none in the floater or barrier. The bridge will be an important part of vital infrastructure and will thus have strong demands to reliability and safety. Hence, it is reasonable to expect the floater to be constructed such that it is able to crush the bow of the striking vessel. There will however always be some strain energy taken up in the impacted structure, which is not accounted for here. This will not yield any large errors for the global response, but means that local analyses has to be conducted to further investigate the barrier and floater design.

As mentioned in section 3 the floater and barrier was modelled as pipe elements with equivalent thickness's and densities. This does not give a correct representation of the local behaviour, but for the global behaviour the errors will not be significant.

Furthermore the direction and position of impact is an obvious assumption, as all impacts

studied are head on collisions with the barrier or floater. In a real world collision this would not necessarily be the case and would result in a different response from the floater. In addition if the the impact is oblique instead of perpendicular the interaction between the vessel and the floater or barrier will change. This in turn will lead to a new force deformation curve of the vessel, and make it erroneous to split the collision into external and internal mechanisms. Instead a coupled approach might be necessary to capture the interaction and thus also the force history between the ship and floater. A coupled approach means that both the global and local response of the ship is updated at each time step. The global response of the ship is then governed by manoeuvring formulas. For more on this see e.g. Yu and Amdahl (2016) and Yu, Amdahl, and Storheim (2016).

7.4.2   Viability of barrier

When looking at the results in sections 5.5.1 and 5.5.2 it is clear that the collision barrier increases the global response of the bridge when subjected to ship impacts. Figure 108 shows the response of the impacted floater both with and without the barrier.
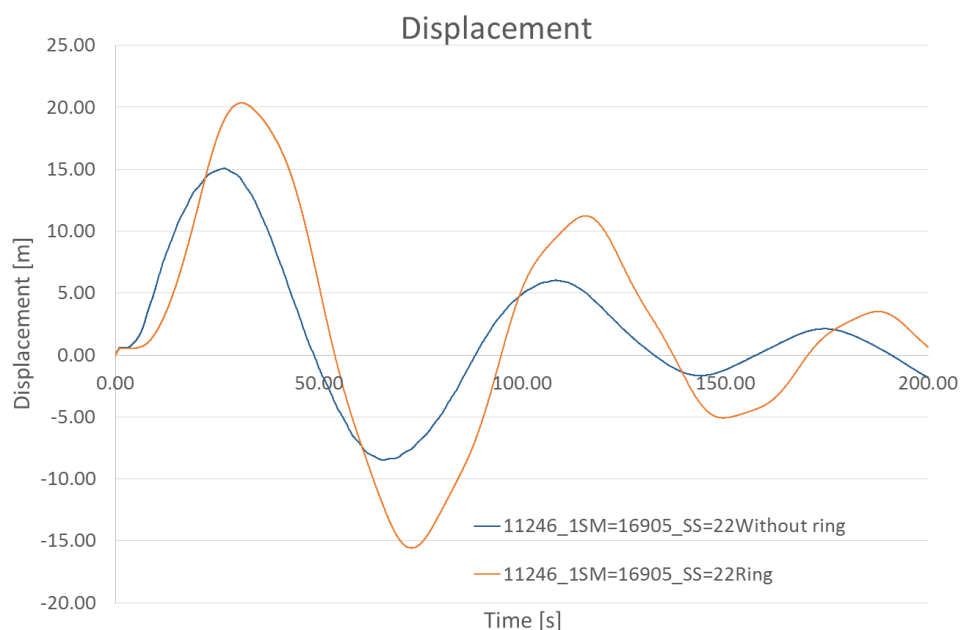
Figure 108: Displacements of the impacted floater with and without ring

This shows that the response actually increases with almost 50 % with the barrier compared to without it. A similar increase is seen for displacements of the second floater, figure 109a. For the accelerations, seen in figure 109b, the barrier has a positive impact, reducing the maximum accelerations.

(a) Displacement of second floater

(b) Accelerations of impacted floater
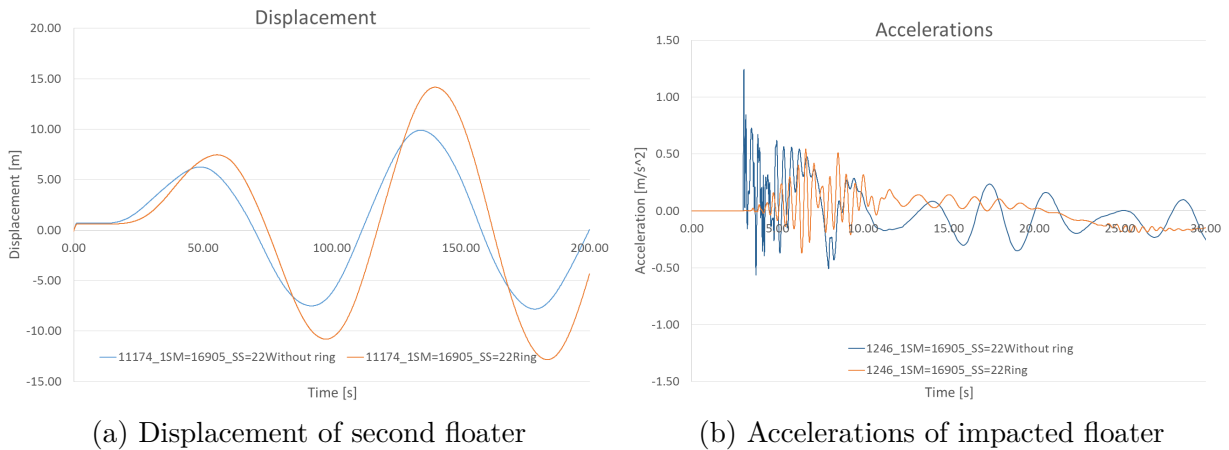
Figure 109: Response with and without the barrier

When looking at figure 109b it is clear that the maximum acceleration of the bridge girder at the impacted floater is larger without the collision barrier. 1.3 $[\mathrm{m\,s^{-2}}]$ without the barrier compared to 0.53 with the barrier.

The acceleration of the floater with the barrier is delayed compared to the scenario without it, which is expected as the maximum force on the pylon is largest when the barrier has started to move. It is also seen that the barrier creates strongly oscillating accelerations that occurs after the initial impact. These accelerations stem from the oscillation of the barrier.

One of the reasons for the changed response can be seen in figure 110.
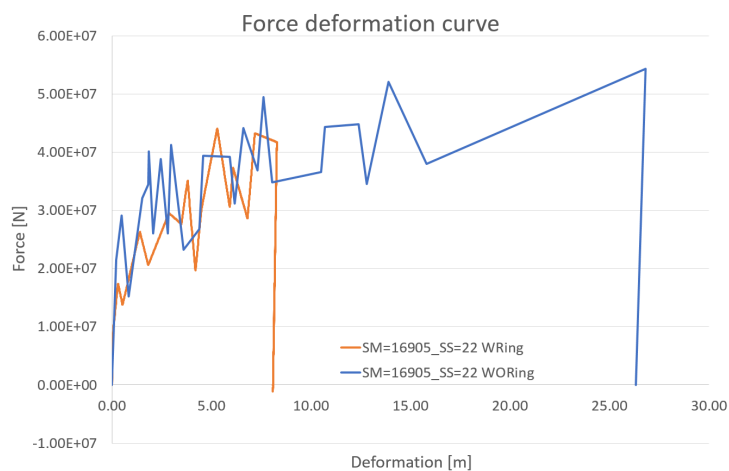
Figure 110: Force deformation of ship with and without barrier

Figure 110 shows the force deformation characteristics of the ship, both with and without

the barrier. It is clear from figure 110 that the strain energy absorbed in the ship when it collides directly against pylon is far larger than when it collides against the barrier. This means that the amount of energy added to the bridge is less when the impact is directly against the pylon.

The increase in strain energy occurs because the mass that the impacting vessel is far larger without the barrier. When the impact is against the barrier, the vessel only needs to accelerate the mass of the barrier. Without the barrier, the entire floater has to be accelerated. As the ship indentation increases, the force required to deform the ship further is increased. This leads to the larger peak force.

The increase in acceleration is expected when considering the peak force on the bridge by the ship. Even though the peak acceleration is much larger without the barrier, the duration is shorter. The peak only lasts for a fraction of a second, and the floater only has a positive acceleration for 5 seconds. As opposed to with the barrier which gives the floater a positive accelerations for 20 seconds. This is explained by looking at figure 111, which shows the force time history for the ship.
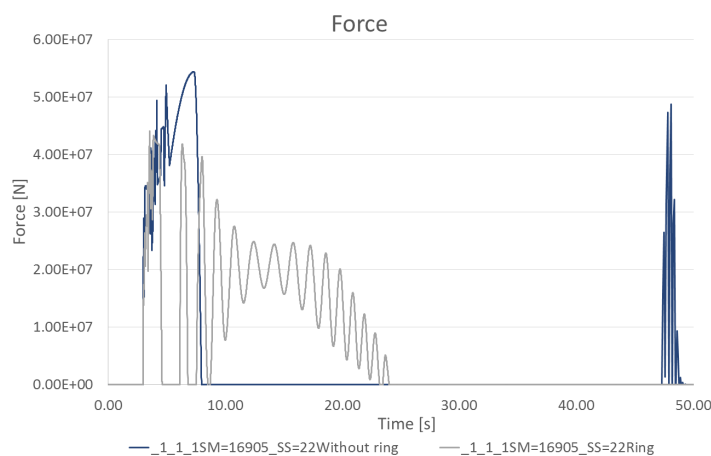
Figure 111: Force time history of ship with and without barrier

By looking at the force history both with and without the barrier it is clear that the duration of the impulse with the barrier is 4 times longer than without it. This explains the increased acceleration duration of the floater with the barrier. In addition, the difference in peak forces gives an explanation for the difference in the peak accelerations.

Figure 111 also shows another reason for the difference in displacements of the impacted floater, namely the difference in impulse duration. Compared to the eigenperiods involving floater displacements, the duration of the impulse is short both with and without

98

the barrier. However, even when both impulses have a short duration, the difference can influence the response. This is best exemplified by looking at a single degree of freedom system Figure 112 shows the dynamic amplification factor for some common impulse shapes for a single degree of freedom system.
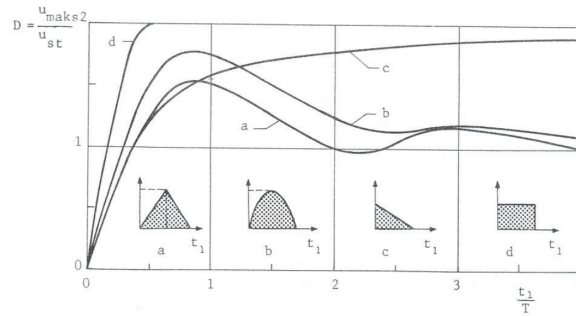
Figure 112: Dynamic amplification factor (Haver, 2011)

In figure 112 it is seen that with the durations that the impulses both with and without the barrier is, the dynamic amplification factor will be less than one. However, regardless of the shape of the impulse, it is seen that even a small difference in duration can greatly influence the result. The bridge is naturally not a single degree of freedom system, but figure 112 shows how important the duration of the impulse is for the response.

When examining the impact of the barrier, the effect on the cable and tether forces are of significance. This is shown in figure 113a, and 113b respectively.
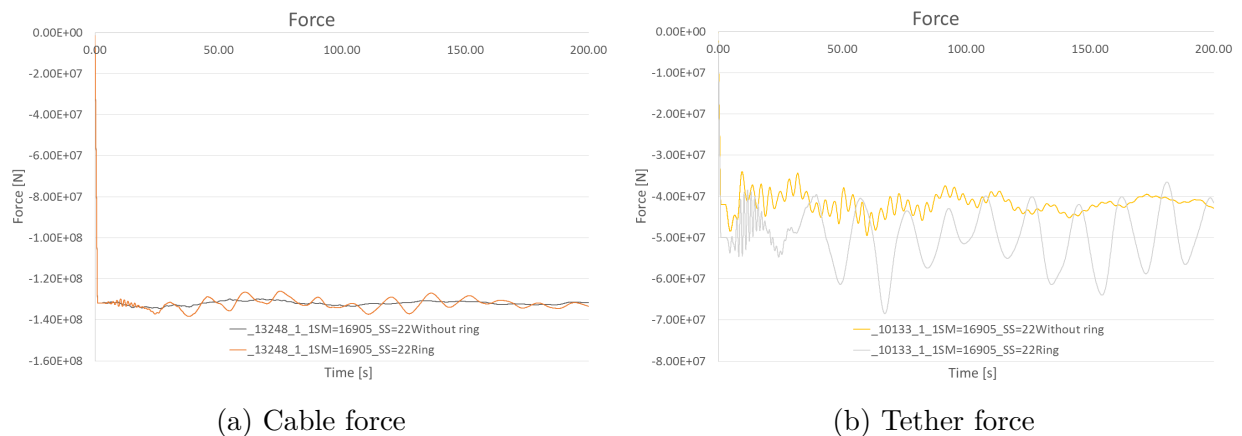
(a) Cable force

(b) Tether force

Figure 113: Effect of the barrier

One effect the barrier has on the tether force is to increase the tension in the tethers. This happens due to the added net buoyancy from the barrier. However, the barrier increases the responding oscillations in the tethers, as seen in figure 113b.

99

The effect of the cable force is not large, but again the barrier increases the oscillations somewhat.

By looking at the strict comparison between the floater with and without the barrier, it is seen that the barrier has some beneficial effects on the response. It reduces the maximum accelerations and the ship deformation. Furthermore the increased displacement from 15 to 20 metres is not significant when compared to the displacement from environmental loads.

There are however several sources of concern for this concept. First of all accounting for the trimming moment removes many of the advantages with the barrier. Figure 114 shows the acceleration and tether force with the barrier accounting for trim and without the barrier.

(a) Tether force (b) Acceleration
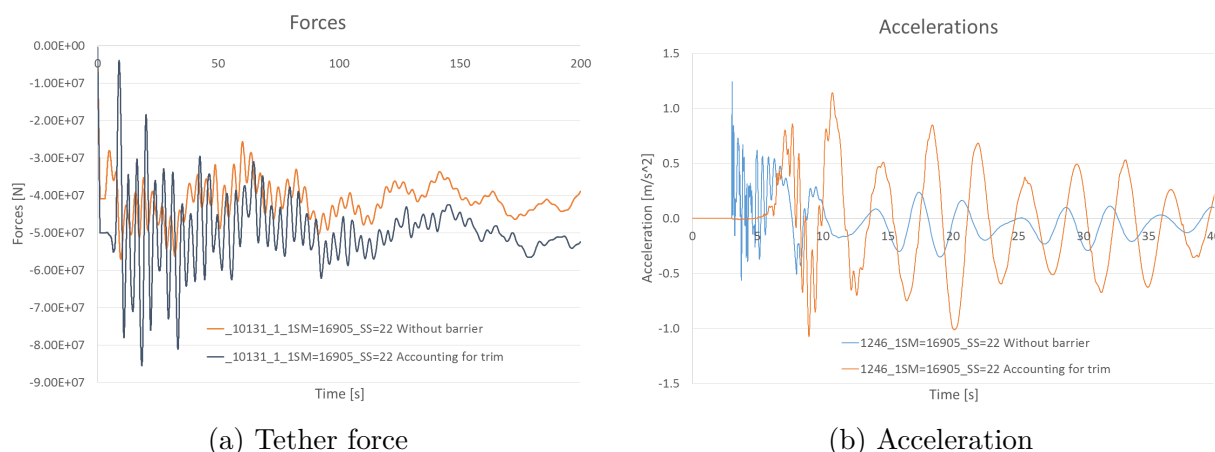
Figure 114: With trim and without the barrier

Accounting for trim with the barrier gives much larger oscillations in the tether force than the case without the barrier, as figure 114a shows. Not only is the oscillations larger with the barrier, but the maximum tension force is also larger. In addition, figure 114b shows that another positive trait of the barrier vanishes when trim is included, namely the lowered accelerations. Albeit the peak acceleration is lower with the barrier accounting for trim, the subsequent oscillating accelerations are larger.

Forcing the vessel to trim also leads to large forces in the tethers as described in section 5.5.4. This could lead to fracture of the tethers supporting the barrier.

In addition to the weakness of the barrier it is also evident that the global response to ship impact will not be critical for the survival of the bridge. Even for the worst case

scenario the response is modest. If the bridge is further designed against impact energies of 200 [MJ] or even 50 [MJ] the response will be negligible. If the steel design is chosen the local response should not be a problem either. This means that the bridge barrier will be redundant.

If the concrete design is chosen the barrier could have more merits. This is because of the resistance to penetration for concrete is less than for steel. The proposed concrete design is also heavier, meaning that even more energy will be taken up as strain energy in a direct collision.

The barrier can in addition have a negative effect on the fatigue of the structure. In section 4 it was seen that the barrier had an eigenperiod of 12 seconds. This means that it can be excited by linear wave forces, and thus increase the load on the structure in smaller sea states. As a result, a barrier with properties as outlined in this thesis is not viable.

7.4.3 Effect of speed restrictions

As mentioned in section 5.2 there has been talk about imposing a speed restrictions of 12 knots under the crossing. This will reduce the maximum displacement significantly, both with the barrier and without it, as can be seen in figure 115.
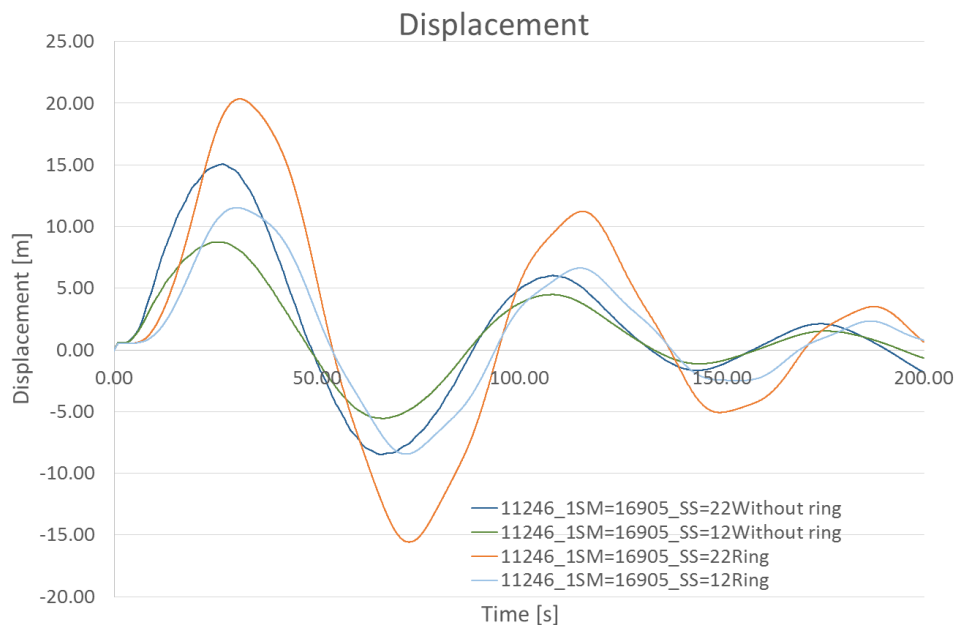
Figure 115: Displacement of impacted floater with and without speed restriction

As figure 115 shows, the maximum displacement of floater is reduced by 43% with the speed restrictions. This is true both with the barrier and without it.

Without the barrier the acceleration of the impacted floater and the tether forces are not as affected by the speed restriction as shown in figure 116a, and 116b.

(a) Acceleration
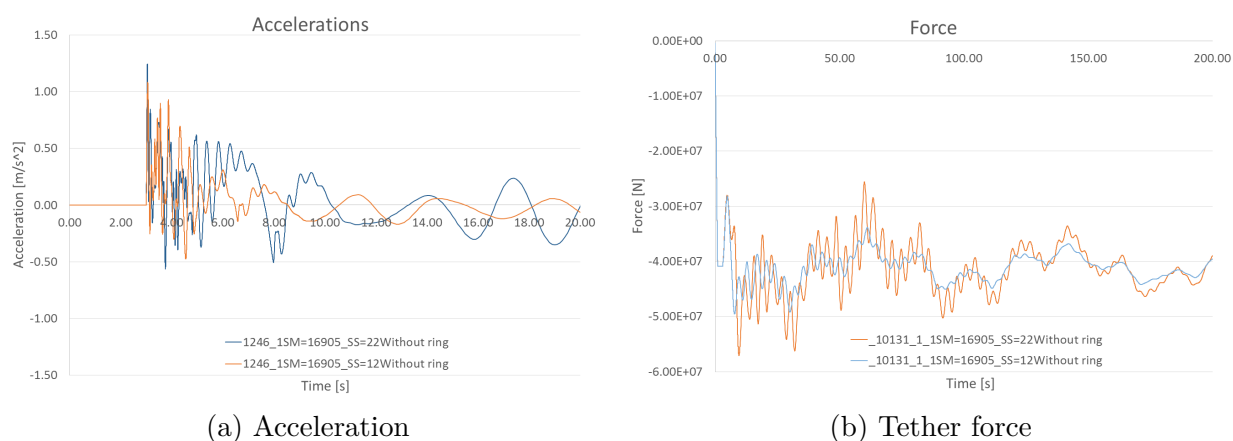
(b) Tether force

Figure 116: Effect of the speed restriction

By looking at figure 116a it is seen that the inital acceleration spike is almost the same for the two cases. It is this spike that leads to the strongly oscillating tether forces as shown in figure 116b. After the inital spike, the acceleration from the scenario with speed restriction dampens out much faster than without. This also has an effect on the tether forces that have a reduced oscillation amplitude compared with the full speed impact.

If the barrier is installed it is seen in figure 117b and 117a that the effect of the speed restriction is noticeable also for these parameters.

(a) Acceleration

(b) Tether force
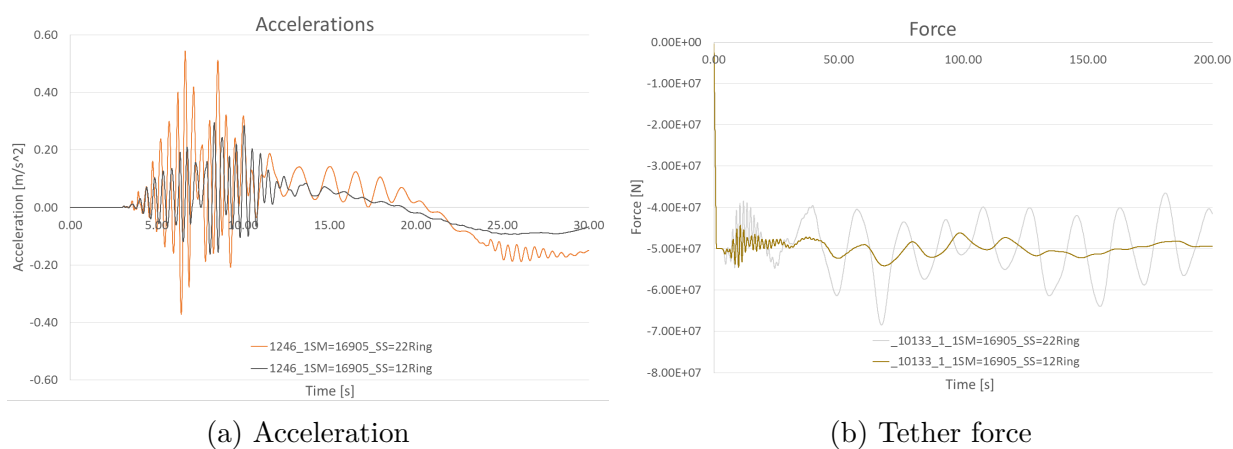
Figure 117: Effect of the speed restriction with barrier

This is due to the fact that the acceleration of the floater is reliant upon the speed the barrier achieves, and this is lower with the speed restrictions. Both with and without the barrier the speed restriction yields lower peak force and indentation of the ship.

7.4.4 Design ship considerations

In section 5.2 it is described that the design energy for ship impacts on the bridge is not yet determined. Throughout this thesis four vessels have been used with energies ranging from 50 [MJ] to 1200 [MJ]. It is clear that if the speed restrictions are put in place the worst case scenario is ruled out as a potential candidate. However the container vessel with a speed of 12 knots yields a significantly larger response than that of the proposed 50 and 200 [MJ] design impacts. Given that the container vessel sails under the crossing twice a week it is clear that there is a possibility of collision, albeit a small one. As a result this should be used as the design basis both for the local and global response.

7.4.5 Snapping of tethers

As noted in section 5.5.6 the snapping of tethers were modelled dependent on time. Furthermore they were modelled as snapping instantaneously. This means that they go from full load carrying ability in one time step to carrying no load in the next. As a result the shock to the system is large. This shock has large consequences for the response of the system as outlined in section 5.5.6. However, a fracture and snapping would be more gradual than the method used in this thesis. As a first step the material would yield, with strain hardening this could lead to a higher load carrying ability, but the yielding can also lead to load shedding. The result of this is that the other tethers will carry some of the load carried by the yielding tether. If this occurs, the shock to the system will be reduced. To further verify the barrier this behaviour would have to be studied in more detail.

7.4.6 Splitting up the analyses

Splitting the analyses into two parts when looking at an impact to the barrier is viable if only the displacements are of interest. Furthermore this method reduces the computational time considerably. However as section 5.5.7 shows, splitting the analyses up will lead to errors for the tether forces and accelerations.

As a result splitting the analyses up to save time is a viable option if the critical response is the displacement of the impacted floater. If it is accelerations or tether forces then

the combined analysis should be used. A further point is that the two step analysis gives a wrong local response on the floater. In addition it will be difficult to account for snapping of tethers, or collision between the barrier and pylon. Both of these can significantly change the response of the bridge.

7.4.7 Effect of updated model

As mentioned in section 3.4 the design of the monopile has changed during the work on this thesis. Table 32 shows the key results for the old monopile design when it was subjected to the worst case scenario.

Table 32: Original monopile desing worst case scenario without barrier

Item		Units	Min	Average	Max
Floater 1	Displacement Bridge Girder	[m]	-11.9	0	19.6
	Acceleration Bridge Girder	$\mathrm{m\,s^{-2}}$]	-0.24	0.0	0.71
	Displacement Tower	[m]	-11.9	0.0	19.5
	Acceleration Tower	$[\mathrm{m\,s^{-2}}]$	-0.59	0.0	0.74
Floater 2	Displacement Bridge Girder	[m]	-10.5	0.0	10.9
	Acceleration Bridge Girder	$[\mathrm{m\,s^{-2}}]$	-0.07	0.0	0.09
	Displacement Tower	[m]	-10.5	0.0	10.9
	Acceleration Tower	$[\mathrm{m\,s^{-2}}]$	-0.17	0.0	0.18
Cable Force		[MN]	85	87	90
Tether Force		[MN]	36.0	49.1	61.3

By comparing table 32 with the results for the new design, table 16 it is clear that the new design reduces the response. The largest contributor to this reduction is the increased weight, as it increases the amount of energy being dissipated as strain energy. In addition the new design has larger eigenperiods, which reduces the ratio of the impulse duration to the eigenperiod. The result of this is, as was discussed in section 7.4.2, a reduced dynamic response.

7.5 Environmental loads

7.5.1 Importance of stochastic wind

By comparing the results from the static mean wind, and the stochastic wind it is evident that just looking at the 100 year static mean wind is insufficient. The mid-span displacement increases by 9 metres when accounting for wind fluctuations. The difference in response between the static mean wind speed and stochastic wind is shown in figure

118. This shows that the mid span has a mean displacement below that of the static mean wind, but significantly larger maximas.
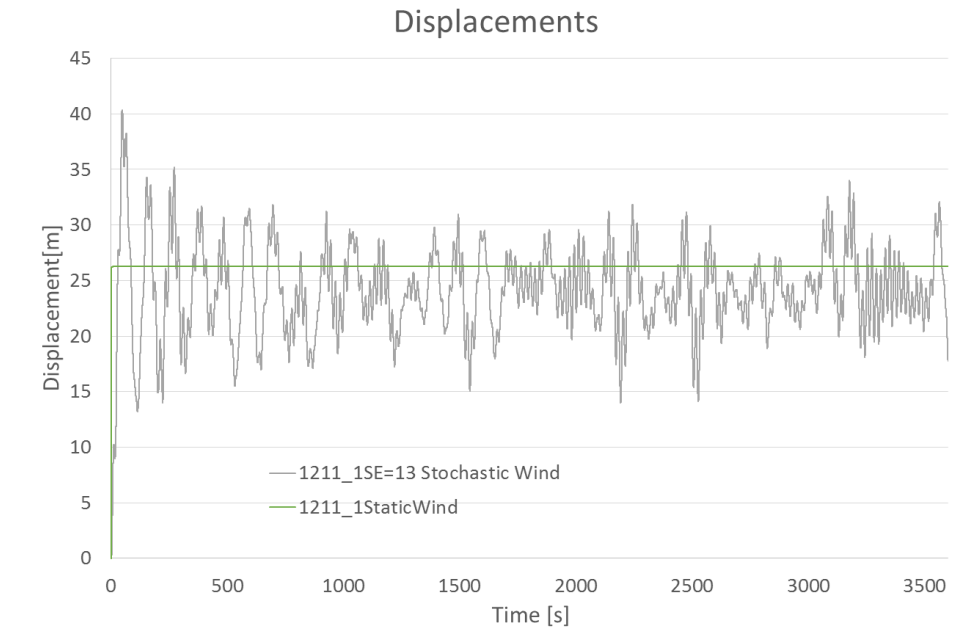
Figure 118: Stochastic vs. mean wind

Furthermore, introducing stochastic wind yields some additional parameters to consider. This includes both accelerations and the oscillating tether forces.

7.5.2 Number of simulations

7.5.3 Buckling of tethers

As mentioned in section 6.3.4, the tethers can experience a compressive load during the one hundred year storm. It was also evident that the loading posed no problem in regards to yielding or plastic utilization. Therefore, the only potential problem is buckling of the tether. The Euler buckling load for a beam is defined by equation 50

$$P = \frac{\pi^2 EI}{L^2} \tag{50}$$

Inserting the parameters for the tethers, the buckling load is calculated to 112 kN, or 0.1 MN. This is far below the estimated load level. However, since the tether is so long, it needs time to buckle. As a result the tether can take compressive loads as long as the

duration is short enough. Figure 119 shows the duration of one example of compression loads in a tether.
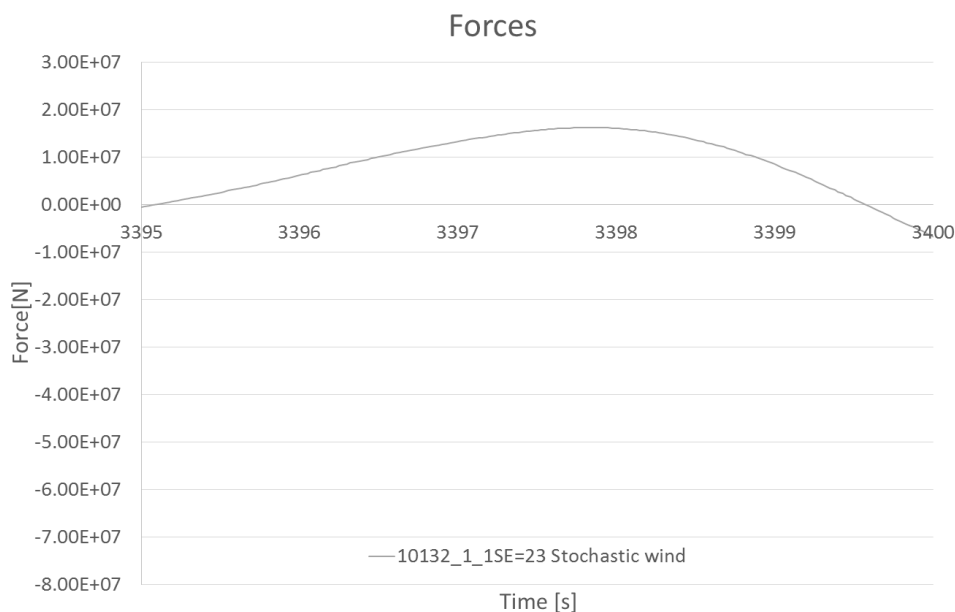
Figure 119: Tether force compression

As figure 119 shows that the compression loads lasts for 5 seconds. This is too short for the tether to buckle. Something that was evident in the analyses where no buckling took place. However if this will be allowed by the governing authorities is another matter.

7.5.4   Effect of wind grid selection

How the wind grid for the stochastic wind is selected can influence the results. This is due to several things. First all wind outside of the grid is 100 % correlated and at every time step equal to the closest border of the wind grid. Furthermore, within the defined grid the wind is not interpolated between the nodes. Instead it divides the grid into blocks, where the wind speed is uniform in each block. As a result how the grid is defined vertically will influence the wind speed.

To check the effect of correlated wind over the bridge two analyses were conducted. In the first the wind grid was selected such that the wind was 100 % correlated over the entire bridge. This meant using only one point in the wind grid. The wind grid in the second analysis was selected such that it gave stochastic wind over the entire bridge. In this analysis the grid had one node vertically and 168 nodes along the length of the

106

bridge. Figure 120 shows the midspan displacement for the two cases, marked OnePoint and FullBridge respectively.
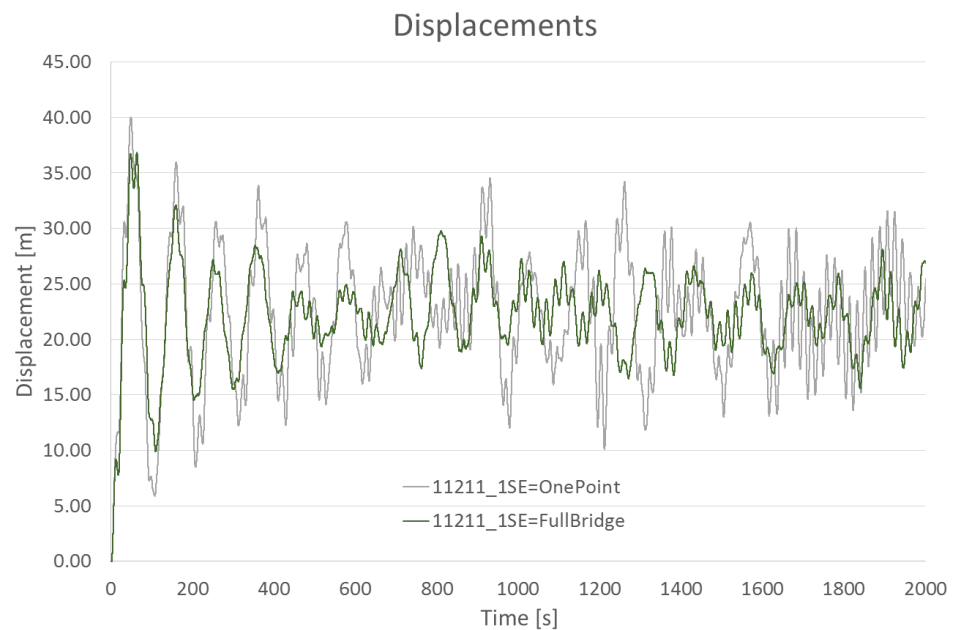
Figure 120: Midspan displacement with different wind grids

As can be seen in figure 120 fully correlated wind yields larger midspan displacements than fully stocahstic wind. If one look at the floater response, figure 121a and 121b, it is seen that their displacement increases when the wind is fully correlated. Another thing that is evident in figure 121 is that with fully correlated wind the motion of the floaters also are fully correlated.
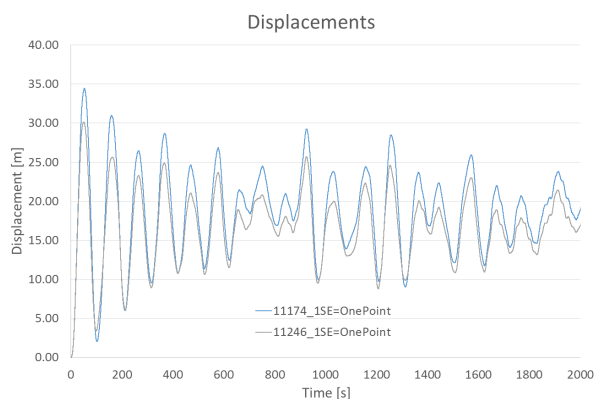
(a) Fully correlated wind
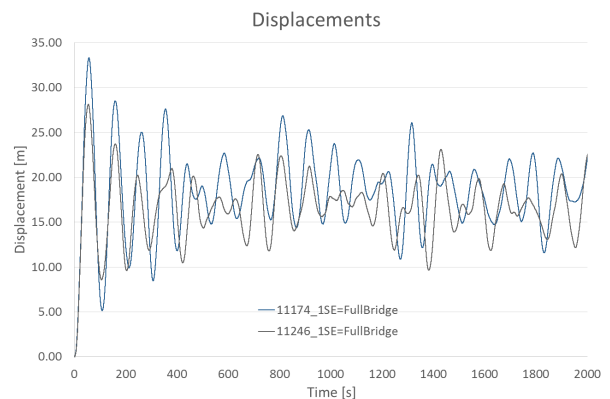
(b) Fully stochastic wind

Figure 121: Displacement of floaters

107

7.5.5 Comparison

As stated in section 1 a lot of work has been done on the proposed design parallel to the work done in this thesis. This means that the there is not a lot of results to compare the analyses with environmental loads conducted herein to. However, for the four legged design such analyses have been conducted. In addition to comparing with the response of the four legged floater, the response is also compared to a simplified model. This simplified model is based on static wind, but adjusting the loading to include gusts by equation 51, (Larsen, 2016).

$$F_q(z) = [1 + 7 \cdot I_u(z)] \cdot F_m(z) \tag{51}$$

In equation 51 $F_q(z)$ is the wind force accounting for gust, $I_u(z)$ is the turbulence intensity and $F_m(z)$ is the mean wind force. The simplified model only yields displacements and forces and not accelerations. Both of the results outlined above, as well as the results from the stochastic analyses conducted are presented in table 33.

Table 33: Environmental loads comparisons

Item		Units	Four Legged	Simplified	Stochastic wind
Floater 1	Acceleration BG	$[\mathrm{m\,s^{-2}}]$	0.22	N/A	0.22
Floater 2	Acceleration BG	$[\mathrm{m\,s^{-2}}]$	0.21	N/A	0.21
Midspan	Displacement	$[\mathrm{m}]$	38.3	38.8	36.7
Midspan	Acceleration	$[\mathrm{m\,s^{-2}}]$	0.75	N/A	0.81
Tether force	Maximum tension	$[\mathrm{MN}]$	26.2	40.3	76.1
Tether force	Minimum tension	$[\mathrm{MN}]$	5.7	30.2	-11.4

By comparing the results presented in table 33 it is seen that the accelerations calculated from the stochastic wind for the monopile is similar to those obtained for the four legged model. Midspan displacement gives a very good correlation between the four legged model and the simplified load model. However, both of these yields a larger displacement than the stochastic wind analyses in this thesis. The differences are not large, i.e. less than 10%, and some discrepancies are to be expected. It is also expected that the four legged model yields a larger displacement , as it has lower tension forces than the monopile. For the simplified model the reason can be conservatism in the factors used. However, to get the same result for all models is not a goal and there will be differences in the results from the different models.

7.6 Design criteria

This thesis has investigated the global response of the bridge against two types of loads. The first one is ship collisions which represents an ALS load. This means that it is assumed to have an annual probability of occurrence of 10^{-4}. Furthermore, being an ALS load, means that the structure is allowed to sustain some damage as long as it retains structural integrity. The second load studied in this thesis is the environmental loads. This is a ULS type loading, which means that the annual probability is 10^{-2}. In addition the structure is not allowed to sustain damage from ULS loading.

By comparing the two types of loading studied it is evident that the ULS environmental loads will govern the global respons of the design, both for the displacement of the floaters, the midspan, and the tether forces. The ALS design will govern the local design of the floaters.

However, the ship collision might give some restrictions on the global design. This is because the bridge will be closed down ahead of a hundred year storm. As a result there will not be any traffic on the bridge at that time. This is not the case for a ship collision, as it is difficult to predict when a ship might collide, and thus evacuate and close the bridge ahead of the impact. The effect of this can be that the tolerances for accelerations and displacements are lower in this case.

Two limit states have not been addressed in this thesis, both of which can influence the design. These are the serviceability limit state, SLS, and the fatigue limit state, FLS. A serviceability limit state gives requirements on how often the bridge can be closed, maximum accelerations and displacements with traffic on the bridge and so on. The fatigue limit state on the other hand, gives restrictions to how long different components have to last, how easily accessible they are for inspection and so on. As the bridge will be essential infrastructure the regulations for when it is allowed to close will be strict. In addition to this the bridge will be expected to have a long lifespan, which will give large demands for lifetime of components and accessibility of critical connections. The result of the demands for serviceability and fatigue is that both SLS and FLS design criteria will play an important part in the design of the bridge.

8 Further work

If the barrier is to be studied further, it requires a more detailed design. This is important to establish the basic behaviour of the barrier, as both the weight and the diameter has a significant impact on the barrier response. In addition the interaction between the barrier and the impacting vessel has to be modelled better. This means modelling the interaction in a non-linear FEM software, and adding the ship behaviour based on global ship motions. Furthermore, the fracture of the tethers connecting the barrier to the floater must be modelled more physically, as a sudden snap at a given time step introduces some uncertainties.

Regardless of if the barrier is looked at further, some key issues needs to be addressed. Firstly, collisions with different point of impacts and different directions have to be looked at. A potential issue can be an oblique impact that can lead to a rotation of the tower, this can be especially critical with the barrier as the torsional moment increases. Another thing that needs further studies is the environmental conditions at time of impact. The likelihood of a 100 year storm and a ship impact occurring simultaneously is small, but it is equally unlikely that the bridge is subjected to no environmental loading at the time of impact. This addition can change the response of the bridge.

For ship impacts, the largest omission in this thesis is the local response. The local response is the most important response for design against ship collisions and thus has to be studied further.

In regards to the environmental loads, the most important thing to add is a stochastic wind field spanning the entire bridge. Doing this will increase the reliability of the results as one avoids fully correlated wind at the sidespans. Furthermore, the response of the side spans should be included, in addition to the heave motion of both the floaters and midspans.

In addition, one should also apply the 100-year environmental conditions on the bridge in a damaged state. These analyses should include a wide range of damage states, including, but not limited to loss of a tether and flooding of a compartment.

9 Conclusion

From the results presented in this thesis, it is clear that the addition of the barrier increases the global response of the bridge. With the barrier, the displacement of the impacted floater is increased by 5.3 metres for the worst-case scenario. In addition the barrier is seen to increase the oscillations of the tether forces. The barrier does nonetheless have its merits, as it reduces the accelerations of the floater from 1.24 to 0.54 $[\mathrm{m\,s^{-2}}]$. However, the largest advantage of the barrier is the reduction in strain energy, which for the worst case scenario the ship indentation is reduced by 70 %

An additional conclusion that can be drawn from the results in this thesis, is that the vessel barrier and barrier floater interaction will have a significant impact on the response. Since the barrier in addition can increase the fatigue load on the floaters, a barrier with the configuration looked at here is not viable.

It is seen that the response of the bridge is dependent on the impact energy, both with and without a barrier. This is especially true for the displacement of the impacted floater, which was without the barrier 15.1 metres for the largest energy and 2.4 metres for the 50 [MJ] impact. The acceleration of the impacted floater was not as affected by the impact energy as the difference between the largest and smallest impact energy is only 20%.

From the analyses it is also concluded that the ship model yields a good representation of ship impacts for the global response. The reason for this is that the total energy, strain energy and the peak force is well represented by the model.

When studying environmental loads accounting for stochastic wind is important in order to get a correct representation of the response. In addition, the wind load is the largest load component of the environmental loads, and thus dominates the response of the bridge. It is also seen that it is important to run several simulations in order to obtain the correct estimate for the response, as the maxima varies greatly from simulation to simulation. This method, the contour method, which is common in the offshore industry, proved to give a good estimate for the response of floating bridges.

The environmental analysis also showed that the tethers will come into compression for extreme environmental conditions, but that the duration is too short to get buckling. Even though buckling is avoided it is unlikely that this is acceptable for ULS design.

For design, environmental loading will govern the global response, whereas the local design of the floaters is governed by ship impacts. The analyses conducted herein show

that the bridge is able to withstand both ship impacts and extreme environmental loads. This shows that the TLP supported floating bridge gives a viable alternative to cross the Bjørnafjorden.

References

Aas-Jacobsen, K. (2008, May). *Swaysim verification: appendix-06 windsim*. SwaySim.

Amdahl, J., Endahl, A., Hultgreen, L. R., Minsaas, K., Rasmussen, M., Sillerud, B., . . . Valland, H. (2011). *Tmr4100 - marin teknikk intro, tmr4105 - marin teknikk 1*. Trondheim: Studieprogram for Marin teknikk.

Amdahl, J. & Sha, Y. (n.d.). *Design of floating bridge pontoon subjected to ship collision load*. Submitted for publication Proceedings of the ICCGS 2015 , 15-18 June, 2016.

Braker, J. (2011, November). Maersk flensburg kiel canal. Retrieved October 25, 2015, from http://www.marinetraffic.com/en/photos/of/ships/shipid:123015/#forward

Eidem, M. E. (2015, October). Kryssing av e39 bjørnafjorden med hengebru på flytende fundament. Retrieved December 16, 2015, from https://www.doffin.no/Notice/Details/2015-113742

Faltinsen, O. (1990). *Sea loads on ships and offshore structure*. Cambridge: Cambridge University Press.

Forsman, N. (2015, June). *Fergefri e39 ship collision risk analysis of the bjørnafjorden crossing*. SSPA.

GL, D. (2014, April). *Recommended practice dnv-rp-c205 envrionmental conditions and environmental loads*. DNV GL.

Google Maps. (2015, November). Map of bjørnafjorden. Retrieved October 20, 2015, from https://goo.gl/maps/HbEWpgQTkW52

Hansen, M. O. (2008). *Aerodynamics of wind turbines* (2nd edition). London: Earthscan.

Hau, E. (2013). *Wind turbines: fundamentals, technologies, application, economics* (3rd edition). Munich: Springer.

Haver, S. (2011, September). *Prediction of characteristic response for design purposes*. Statoil ASA.

Ivar Langen, R. S. (1978). *Dynamisk analyse av konstruksjoner*. Trondheim: Tapir forlag.

Larsen, P. N. (2016, February). *Curved bridge - navigation channel in south*. Aas-Jacobsen, COWI, Johs. Holt, Global Maritime.

Leira, B. J. (2014). *Tmr4170 marine structures basic course*. Trondheim: Akademika forlag.

Marintek. (2001, June). *Usfos getting started*. SINTEF GROUP.

Negrut, D., Ottarsson, G., Rampalli, R., & Sajdak, A. (2005). On the use of the hht method in the context of index 3 differential algebraic equations of multibody dynamics. In *Proceedings of idetc/msndc 200*.

Norsk Standard. (2009, October). *Nasjonalt tillegg na eurokode 1: laster på konstruk-sjoner, del 1-4: allmenne laster, vindlaster.* Norsk Standard.

Norsk standard. (2004, October). *Norsok standard n-004 design of steel structures, annex a design agains accidental actions.* Standards Norway.

Petersen, M. J. (1982). Dynamics of ship collisions. *Ocean Engineering, 9*(4), 295–329.

Pettersen, B. (2007). *Marin teknikk 3 hydrodynamikk.* Trondheim: Institutt for marin teknikk.

Roadtraffic-Technology. (2015). Akashi kaikyo bridge, akashi strait, japan. Retrieved November 25, 2015, from http://www.roadtraffic-technology.com/projects/akashi-kaikyo-bridge-strait-japan/

Sekse, J. H. (2015, September). Coastal highway route e39. Retrieved October 25, 2015, from http://www.vegvesen.no/Vegprosjekter/ferjefriE39/Konferanse/teknologidagene2015/_attachment / 1023746 ? _ts = 14ff49775f8 & fast_title = 09+ - +Coastal + Highway + Route+E39+-+R%C3%B8rbru+-+Jorunn+Sekse.pdf

Statens vegvesen. (2012a, December). Delprosjekt fjordkryssing ferjefri e39. Retrieved October 25, 2015, from http://www.vegvesen.no/_attachment/415285/binary/711216?fast_title=Hovedrapport+Ferjefri+E39%2C+desember+2012.pdf

Statens vegvesen. (2012b). Hovedrapport ferjefri e39. Retrieved October 25, 2015, from http://www.vegvesen.no/_attachment/415285/binary/711216?fast_title=Hovedrapport+Ferjefri+E39%2C+desember+2012.pdf

Statens vegvesen. (2015a, September). *Multi-span suspension bridge on floating founda-tions.* Statens vegvesen.

Statens vegvesen. (2015b). Statusrapport ferjefri e39. Retrieved October 25, 2015, from http : / / www . vegvesen . no / _attachment / 926185 / binary / 1041502 ? fast_title = Statusrapport+Ferjefri+E39+mai+2015.pdf

Storheim, M. (2016, January). *Structural response in ship-platform and ship-ice collisions* (Doctoral dissertation, NTNU).

Teknisk Data AS. (2014, October). *Bjørnafjorden TLP Supported Suspension Bridge, Meeting on Hydrodynamics and Acceptance Criteria.* Teknisk Data AS.

Veie, J. (2015, September). Suspension bridge on floating foundations - when is the technology ready? Retrieved October 25, 2015, from http://www.vegvesen.no/Vegprosjekter/ferjefriE39/Konferanse/teknologidagene2015/_attachment/1023556?_ts = 14ff54620d0 & fast_title = 11+ - +Johannes + Veie + +Presentation + of + TLP-concept+Teknologidagene.pdf

Villoria, B. (2015, September). Floating bridge - when is the technology ready? Retrieved October 25, 2015, from http://www.vegvesen.no/Vegprosjekter/ferjefriE39/Konferanse/teknologidagene2015/_attachment/1023747?_ts=14ff497c800&fast_title=10+Coastal+Highway+Route+E39+-+floating+bridge+-+Bruno+Villoria+NPRA.pdf

Warn, G. P. & Ryan, K. L. (2012). A review of seismic isolation for buildings: historical development and research needs. *Buildings*, *2*(3).

Wikimedia - Commons. (2015, September). Aidaluna picture. Retrieved October 25, 2015, from https://upload.wikimedia.org/wikipedia/commons/e/e6/AIDAluna_40_01-2-2.jpg

Yu, Z. & Amdahl, J. (2016). Full six degrees of freedom coupled dynamic simulation of ship collision and grounding accidents. *Marine Structures*, *47*, 1–22. doi:http://dx.doi.org/10.1016/j.marstruc.2016.03.001

Yu, Z., Amdahl, J., & Storheim, M. (2016). A new approach for coupling external dynamics and internal mechanics in ship collisions. *Marine Structures*, *45*, 110–132. doi:http://dx.doi.org/10.1016/j.marstruc.2015.11.001

A   Theoretical background MATLAB script

To calculate the behaviour of the barrier in MATLAB several assumptions were made. Firstly it was assumed that the floater itself will not move during collision, secondly it was assumed that the ring will displace as a rigid body following a circular path, finally that the motion and forces can be decomposed into one contribution in the x-direction and on in the z-direction. This means that the ring itself will behave as a TLP meaning that its motions are described by equations 1 to 5.

It is also assumed that the ring is made up of circular tubes, this means that the mass of the ring can be calculated from:

$$m_r = \frac{\pi^2 D}{4}(d^2 - (d-t)^2)\rho \tag{52}$$

This makes it possible to use equation 20 and 22 to calculate the amount of strain and kinetic energy. In the algorithm it is assumed that the kinetic energy of the system will be dissipated by displacing the ring leading to work due to drag, buoyancy , and stiffness forces.

The algorithm is based upon calculating the speed at timestep $i+1$ by using the principle of conservation of energy. The speed is then given by solving equation 53 for $V_{t_{i+1}}$

$$\frac{1}{2}mV_{t_i}^2 = \frac{1}{2}mV_{t_{i+1}}^2 + W_{drag} + W_{Bouyancy} + W_{stiffness} \tag{53}$$

Where W_{drag} is found from splitting the drag force up into two contributions. One contribution in the z-direction, given as

$$Fd_z = \rho Cd_z d\pi Dw|w| + \dot{w}\rho Cm_z D\pi(\frac{d}{2})^2\pi A \tag{54}$$

and one in the x-direction. Where it is calculated from the component normal to the ring at every point by equation 54, where the x-component of speed and acceleration replaces the z-component and integrating over the circle, such that.

$$Fd_x = \int_0^{2\pi} Cd_x d\pi Du|u||\sin(\theta)| + \dot{u}\rho Cm_x D\pi(\frac{d}{2})^2\pi A|\sin(\theta)|d\theta \tag{55}$$

Which for numerical calculations where approximated by.

$$Fd_x = \sum_{\theta=0}^{2\pi} Cd_x d\pi Du|u||\sin(\theta)| + \dot{u}\rho Cm_x D\pi(\frac{d}{2})^2 \pi A|\sin(\theta)|)\Delta\theta \tag{56}$$

When calculating the drag-force C_D was chosen to be 0.7 for both in z- and x-direction. While C_m where chosen to be 1 in both directions, as this is a common, and in this case conservative assumption regarding tubular members in steady flow. Since the motion is inversely proportional with the drag force, this means that a larger C_D will result in a smaller motion. Faltinsen, 1990 Meanwhile $W_{buoyancy}$ is calculated from

$$W_{bouyancy} = (B - G)z \tag{57}$$

The acceleration is assumed to be constant over one time step Ivar Langen, 1978. This will underestimate the motion, but by selecting a short time step the error should be negligible. When the speed is calculated for time step $i + 1$ the x- and z-component is calculated from

$$u_{t_{i+1}} = V_{t_{i+1}}\cos(\theta), w_{t_{i+1}} = V_{t_{i+1}}\sin(\theta) \tag{58}$$

thus making it possible to calculate the displacements

$$x_{t_{i+1}} = x_{t_i} + u_{t_i}\Delta t, z_{t_{i+1}} = z_{t_i} + w_{t_i}\Delta t \tag{59}$$

Using these equations for each time step it is possible to track the motion, and find where the speed will be zero, and hence how much the ring will displace.

B Matlab script

B.1 Main script

Defining of input variables and running the calculations.

Clear Memory

```
clc
clear all
```

Ring dimensions

```
%Outer diameter
Dmin=80; %m
Dmax=80;
Dstep= 10;
%Cross sectional diameter
dmin=6000;%mm
dmax=6000;
dstep=1000;
%Wall thickness
tmin=125; %mm
tmax=125;
tstep= 10;
%Density
rhomin=7850; %kg/m
rhomax=7850;
rhostep=100;
%Length of tethers
lmin= 40; % m
lmax= 40;
lstep=10;
%Creating vectors based on input
D=CreateInput(Dmin,Dmax,Dstep);
d=CreateInput(dmin,dmax,dstep);
t=CreateInput(tmin,tmax,tstep);
rho=CreateInput(rhomin,rhomax,rhostep);
l=CreateInput(lmin,lmax,lstep);
```

Task related

```
DeltaT=0.01;     % timestep
Cdx = 0.7;       % Drag coefficient i x
Cdz = 0.7;       % Drag coefficient i z
Rbridge = 25;    % Radius of bridge leg
```

```
global rhow g
g=9.81;
rhow=1025;
```

Ship dimensions and calculations

```
Free msmin=2000; \%tonnes
msmax=28300;
msstep=2000;

vsmin=10 ; \%knots
vsmax=10;
vsstep=0.5;
ms=CreateInput(msmin,msmax,msstep);
vs=CreateInput(vsmin,vsmax,vsstep);
fout='Output/Output.txt';
wout='Output/Work.txt';
Calculation(D,d,t,rho,l,ms,vs,DeltaT,Cdx,Cdz,Rbridge,fout,wout)
```

Container 140 – 160

```
ms=16905;
vs=22;
fout='Output/OutputCont.txt';
wout='Output/WorkCont.txt';
Calculation(D,d,t,rho,l,ms,vs,DeltaT,Cdx,Cdz,Rbridge,fout,wout)
%
```

B.2 Calculating the dispersion of energy for several different cases

```
function [] = Calculation(D,d,t,rho,l,ms,vs,DeltaT,Cdx,Cdz,Rbridge,fout,wout)
```

Defining variables

```
var1=0;
Davg=Average(D);
davg=Average(d);
```

```matlab
tavg=Average(t);
rhoavg=Average(rho);
lavg=Average(l);
if isvector(ms)==1 && isvector(vs)==1
    msavg=Average(ms);
    vsavg=Average(vs);
end

Work=fopen(wout,'w');
j=1;
```

Calculating with a varying D

```matlab
var='D';
CreateHeader(Davg,davg,tavg,rhoavg,lavg,msavg,vsavg,var,fout)
s=length(D);
for i=1:s
    [Es, Estrain, xmax, zmax,Vint,Ebridge] = Energiberegning(D(i),davg,...
        tavg,rhoavg,lavg,msavg,vsavg,Work,DeltaT,Cdx,Cdz,Rbridge,j);
    var1=D(i);
    CreateOutput(var1,Es,Estrain,Vint,xmax,zmax,var,Ebridge,j,fout);
    j=j+1;
end
```

Varying the cross-sectional diameter d

```matlab
var='d';
CreateHeader(Davg,davg,tavg,rhoavg,lavg,msavg,vsavg,var,fout)
s=length(d);
for i=1:s
    [Es, Estrain, xmax, zmax,Vint,Ebridge] = Energiberegning(Davg,d(i),...
        tavg,rhoavg,lavg,msavg,vsavg,Work,DeltaT,Cdx,Cdz,Rbridge,j);
    var1=d(i);
    CreateOutput(var1,Es,Estrain,Vint,xmax,zmax,var,Ebridge,j,fout);
     j=j+1;
end
```

V

Varying the thickness t

```
var='t';
CreateHeader(Davg,davg,tavg,rhoavg,lavg,msavg,vsavg,var,fout)
s=length(t);
for i=1:s
    [Es, Estrain, xmax, zmax,Vint,Ebridge] = Energiberegning(Davg,davg,...
        t(i),rhoavg,lavg,msavg,vsavg,Work,DeltaT,Cdx,Cdz,Rbridge,j);
    var1=t(i);
    CreateOutput(var1,Es,Estrain,Vint,xmax,zmax,var,Ebridge,j,fout)
     j=j+1;
end
```

Varying the material density rho

```
var='rho';
CreateHeader(Davg,davg,tavg,rhoavg,lavg,msavg,vsavg,var,fout)
s=length(rho);
for i=1:s
    [Es, Estrain, xmax, zmax,Vint,Ebridge] = Energiberegning(Davg,davg,...
        tavg,rho(i),lavg,msavg,vsavg,Work,DeltaT,Cdx,Cdz,Rbridge,j);
    var1=rho(i);
    CreateOutput(var1,Es,Estrain,Vint,xmax,zmax,var,Ebridge,j,fout)
     j=j+1;
end
```

Varying the length of the tethers

```
var='l';
CreateHeader(Davg,davg,tavg,rhoavg,lavg,msavg,vsavg,var,fout)
s=length(l);
for i=1:s
    [Es, Estrain, xmax, zmax,Vint,Ebridge] = Energiberegning(Davg,davg,...
        tavg,rhoavg,l(i),msavg,vsavg,Work,DeltaT,Cdx,Cdz,Rbridge,j);
    var1=l(i);
    CreateOutput(var1,Es,Estrain,Vint,xmax,zmax,var,Ebridge,j,fout)
     j=j+1;
```

```
end


```
Varying the ship mass ms

```
if isvector(ms)==1
var='ms';
CreateHeader(Davg,davg,tavg,rhoavg,lavg,msavg,vsavg,var,fout)
s=length(ms);
for i=1:s
    [Es, Estrain, xmax, zmax,Vint,Ebridge] = Energiberegning(Davg,davg,...
        tavg,rhoavg,lavg,ms(i),vsavg,Work,DeltaT,Cdx,Cdz,Rbridge,j);
    var1=ms(i);
    CreateOutput(var1,Es,Estrain,Vint,xmax,zmax,var,Ebridge,j,fout)
     j=j+1;
end
end


```
varying the ship speed vs

```
if isvector(vs)==1
var='vs';
CreateHeader(Davg,davg,tavg,rhoavg,lavg,msavg,vsavg,var,fout)
s=length(vs);
for i=1:s
    [Es, Estrain, xmax, zmax,Vint,Ebridge] = Energiberegning(Davg,davg,...
        tavg,rhoavg,lavg,msavg,vs(i),Work,DeltaT,Cdx,Cdz,Rbridge,j);
    var1=vs(i);
    CreateOutput(var1,Es,Estrain,Vint,xmax,zmax,var,Ebridge,j,fout)
     j=j+1;
end
end
fclose(Work);


end
```

B.3 Function for calculating energy dissipation of a ship collision

```
function[Es, Estrain, xmax, zmax,Vinitial, Ebridge] = Energiberegning(D,d,t,...
rho,l,ms,vs,Work,DeltaT,Cdx,Cdz,Rbridge,j)
```

Defining parameters

```
theta=0; %Angle
time(1)=0; %the time
u=0; % speed in x-direction
w=0; % speed in z-direction
global rhow g
x=0;
z=l;
xcoor(1)=x;
zcoor(1)=z;
d=d/1000;
t=t/1000;
ms=ms*1000;
vs=vs*0.5144;
A=0.1;%Added mass
DragForceX=0;
DragForceZ=0;
Bouyancy=0;
Xr= D/2-Rbridge; % how much the ring can move
Ebridge=0; %How much energy that is transfered to the bridge
i=1;
```

Calculating the properties of the ring and ship

```
mr=pi*D*pi/4*(d^2-(d-t)^2)*rho;%Mass of the ring
Vr=pi^2*D*d^2/4; %Volume of the ring
Es= 1/2*(1+A)*ms*vs^2;%Impact energy
m=mr+ms;
```

Calculating the amount of strain energy

```
V(i)=(ms*vs)/(m); % speed after collision
Vinitial=V;
E2= 1/2*(m)*V^2; %Kinetic energy after collision
Estrain=Es-E2; %Amount of strain energy
PreTension=1.14*10^6;
```

Calculating the response of the ring

```
while V(i)>0 && x<Xr && z>0

    %Calculating the speed and acceleration components
    u=V(i)*cos(theta);
    w=V(i)*sin(theta);
    if i==1
        acc=0;
        accu=0;
        accw=0;
    else
        acc=(V(i)-V(i-1))/DeltaT;
        accu=acc*cos(theta);
        accw=acc*sin(theta);
    end
    x=x+u*DeltaT;
    z=sqrt(l^2-x^2);
    theta=acos(z/l);
    %Calculationg the resulting forces
    Fb=BuoyancyForce(D,d,l,z,mr);
    Wb=Fb*w*DeltaT;
    FK=KForce(l,z,d);
    k=x/l*PreTension*FK;
    Wk=k*x*u*DeltaT;
    [Fdx,Fdz,Anew] = DragForce(u,w,D,d,rhow,Cdx,Cdz,accu,accw,l,z);
    WFdx=Fdx*DeltaT*u;
    WFdz=Fdz*DeltaT*w;
```

```
    %Calculating the speed for the next step
    V(i+1)=sqrt((V(i)^2-(2/((m+Anew)))*(Wb+WFdx+WFdz+Wk)));
    %Creating output
    DragForceX=DragForceX+WFdx/1000000;
    DragForceZ=DragForceZ+WFdz/1000000;
    Bouyancy=Bouyancy+Wb/1000000;
    Ebridge=1/2*m*V(i)^2;
    i=i+1;
    xcoor(i)=-x;
    zcoor(i)=z-l;
    time(i)=time(i-1)+DeltaT;
end
```

Preparing the output

```
xmax=x;
zmax=z-l;
Estrain=Estrain/1000000;
Es=Es/1000000;
Ebridge=Ebridge/1000000;
formatSpec='%d  B=%4.2f  Fdx=%4.2f, Fdz=%5.2f\n';
fprintf(Work,formatSpec,j,Bouyancy, DragForceX,DragForceZ);
limitsx=[0 9 -30 0];
limitsz=[0 9 -12 0];
figure
plot(time,xcoor)
title('Displacement of ring in x')
xlabel('time')
ylabel('Displacement [m]')
axis(limitsx)
figure
plot(time,zcoor)
axis(limitsz)
title('Displacement of ring in z')
xlabel('time')
ylabel('Displacement [m]')
```

```
end
```

B.4 DragForce

Calculating the drag force on a ring with 2D speed

```
function [Fdx, Fdz,AddedMass]=DragForce(u,w,D,d,rhow,Cdx,Cdz,accu,accw,L,z)
```

Determining variables

```
Fdx=0;
dtheta=0.1;
theta=0;
Cirkel=2*pi;
Cmx=1;
Cmz=1;
Ax=0;
%Calculating the submerged area of the cross section
ZetaMax=L-z;
if ZetaMax<d/2
    DeltaZeta=0.001;
    Zeta=0;
    A=pi*d^2/8;
    if ZetaMax~=0
        while Zeta<ZetaMax
            Theta=asin(Zeta/(d/2));
            A=A+DeltaZeta*(d/2)*cos(Theta);
            Zeta=Zeta+DeltaZeta;
        end
        ACirkel=(d/2)^2*pi;
        A=A/ACirkel;
    end
else
    A=1;
end
```

Calculating the drag force in x and z

```
Az=rhow*Cmz*D*pi*(d/2)^2*pi*A;
Fdz= rhow*Cdz*d*pi*D*w*abs(w)*A+accw*Az;
%Dividing the ring into elements and summing the contributions together
while theta<Cirkel
    Fdx=Fdx+rhow*Cdx*d*u*abs(u)*abs(sin(theta))*(D/2)*dtheta*A;
    DeltaAx=rhow*Cmx*(d/2)^2*pi*(D/2)*dtheta*A*abs(sin(theta));
    Ax=Ax+DeltaAx;
    Fmx=DeltaAx*accu;
    Fdx=Fdx+Fmx;
    theta=theta+dtheta;
end


AddedMass=sqrt(Az^2+Ax^2);

end
```

B.5 Function for calculating the buoyancy force

```
function [Fb]=BuoyancyForce(D,d,L,z,m)
global rhow g
%Calculating the submerged area of the  cross section
ZetaMax=L-z;
if ZetaMax<d/2
    DeltaZeta=0.001;
    Zeta=0;
    A=pi*d^2/8;
    if ZetaMax~=0
        while Zeta<ZetaMax
            Theta=asin(Zeta/(d/2));
            A=A+DeltaZeta*(d/2)*cos(Theta);
            Zeta=Zeta+DeltaZeta;
        end
    end
    % calculating the buoyancy force
```

```
    Vb=A*D*pi;
    Fb=Vb*rhow*g-m*g;
else
    Vb=pi*d^2*pi*D/4;
    Fb=Vb*rhow*g-m*g;
end


end
```

B.6   Calculating the submerged area to find pretension

```
function [Fk]=KForce(L,z,d)
global rhow g
%Calculating the submerged area
ZetaMax=L-z;
if ZetaMax<d/2
    DeltaZeta=0.001;
    Zeta=0;
    A=pi*d^2/8;
    if ZetaMax~=0
        while Zeta<ZetaMax
            Theta=asin(Zeta/(d/2));
            A=A+DeltaZeta*(d/2)*cos(Theta);
            Zeta=Zeta+DeltaZeta;
        end
    end
    Factor=A/(pi*d^2/8);
else
    Factor=2;
end
Fk=Factor;
end
```

B.7 A function for writing the results to a file

```
function [] = CreateOutput(var1,Es,Estrain,Vint,xmax,zmax,var,Ebridge,j,fout)
```

Writing the result to file

```
Output=fopen(fout,'a');
formatSpec='%d   %s=%3.0f  Es=%4.2f, Estrain=%5.2f, Vint=%4.2f, xmax=%5.2f, ...
zmax=%5.2f, Ebridge=%5.2f\n';
fprintf(Output,formatSpec,j, var,var1,Es,Estrain,Vint,xmax,zmax,Ebridge);
fclose(Output);
```

B.8 Creating a header for the outputfile

```
function[] = CreateHeader(D,d,t,rho,l,ms,vs,var,fout)
if var=='D'
    Outputfile=fopen(fout,'w');
    formatSpec='d=%3.0f mm, t=%3.0f mm, rho=%4.0f kg/m^3, l=%2.0f m, ms=%6.0f ton,...
     vs=%2.0f knots\n';
    fprintf(Outputfile,'The varying parameter is %c, while the others are set...
     to:\n',var);
    fprintf(Outputfile,formatSpec, d,t,rho,l,ms,vs);
    fclose(Outputfile);


elseif var=='d'
    Outputfile=fopen(fout,'a');
    formatSpec='D=%2.0f m, t=%3.0f mm, rho=%4.0f kg/m^3, l=%2.0f m, ms=%6.0f ton,...
     vs=%2.0f knots\n';
    fprintf(Outputfile,'\nThe varying parameter is %c, while the others are set...
     to:\n',var);
    fprintf(Outputfile,formatSpec, D,t,rho,l,ms,vs);
    fclose(Outputfile);

elseif var=='t'
    Outputfile=fopen(fout,'a');
```

```matlab
        formatSpec='D=%2.0f m, d=%3.0f mm, rho=%4.0f kg/m^3, l=%2.0f m, ms=%6.0f ton,...
         vs=%2.0f knots\n';
        fprintf(Outputfile,'\nThe varying parameter is %c, while the others are set...
         to:\n',var);
        fprintf(Outputfile,formatSpec, D,d,rho,l,ms,vs);
        fclose(Outputfile);

elseif strcmp(var,'rho')==1
        Outputfile=fopen(fout,'a');
        formatSpec='D=%2.0f m, d=%3.0f mm, t=%3.0f mm, l=%2.0f m, ms=%6.0f ton,...
         vs=%2.0f knots\n';
        fprintf(Outputfile,'\nThe varying parameter is %s, while the others are set...
         to:\n',var);
        fprintf(Outputfile,formatSpec, D,d,t,l,ms,vs);
        fclose(Outputfile);

elseif var=='l'
        Outputfile=fopen(fout,'a');
        formatSpec='D=%2.0f m, d=%3.0f mm, t=%3.0f mm,rho=%4.0f kg/m^3, ms=%6.0f ton,...
         vs=%2.0f knots\n';
        fprintf(Outputfile,'\nThe varying parameter is %c, while the others are set...
         to:\n',var);
        fprintf(Outputfile,formatSpec, D,d,t,rho,ms,vs);
        fclose(Outputfile);

elseif strcmp(var,'ms')==1
        Outputfile=fopen(fout,'a');
        formatSpec='D=%2.0f m, d=%3.0f mm, t=%3.0f mm,rho=%4.0f kg/m^3,  l=%2.0f m,...
         vs=%2.0f knots\n';
        fprintf(Outputfile,'\nThe varying parameter is %s, while the others are set...
         to:\n',var);
        fprintf(Outputfile,formatSpec, D,d,t,rho,l,vs);
        fclose(Outputfile);

elseif strcmp(var,'vs')==1
```
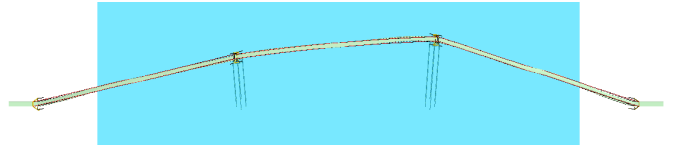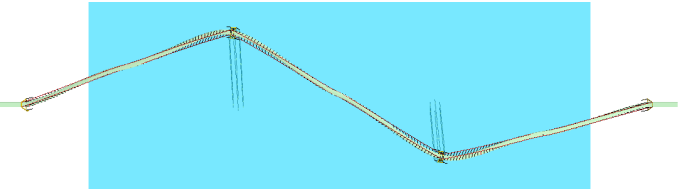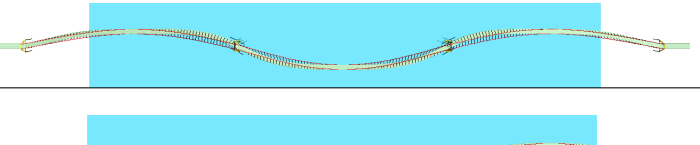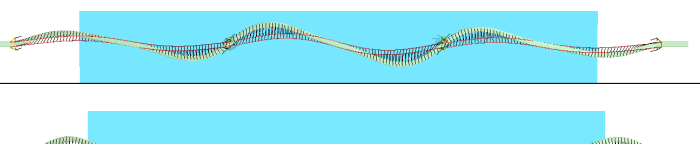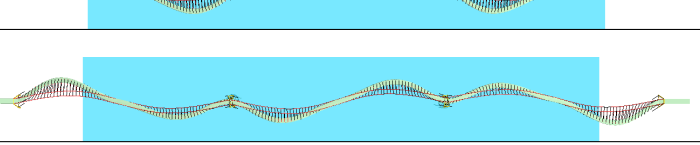
```
    Outputfile=fopen(fout,'a');
    formatSpec='D=%2.0f m, d=%3.0f mm, t=%3.0f mm,rho=%4.0f kg/m^3,  l=%2.0f m,...
     ms=%6.0f ton\n';
    fprintf(Outputfile,'\nThe varying parameter is %s, while the others are set...
     to:\n',var);
    fprintf(Outputfile,formatSpec, D,d,t,rho,l,ms);
    fclose(Outputfile);

else
    error('Wrong variable');
end
end
```
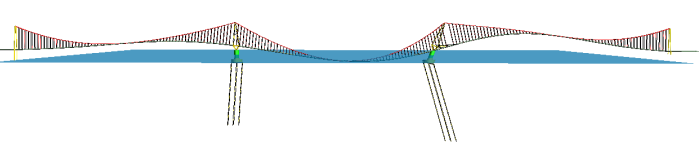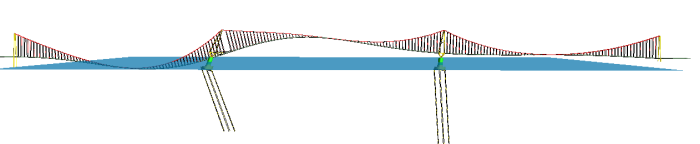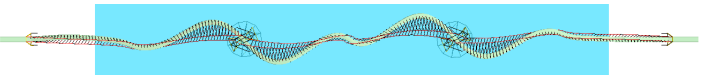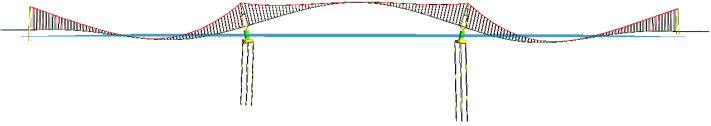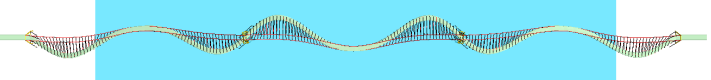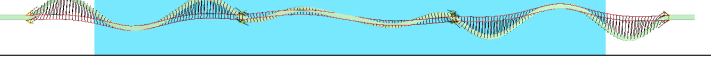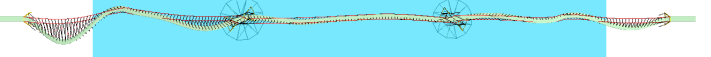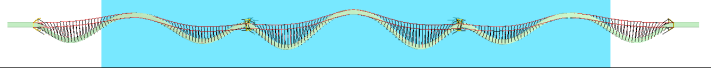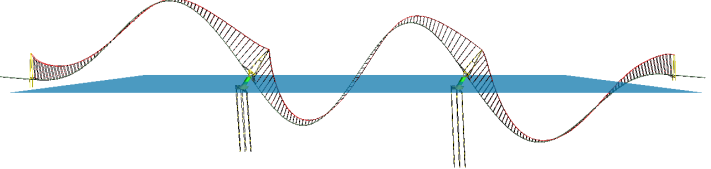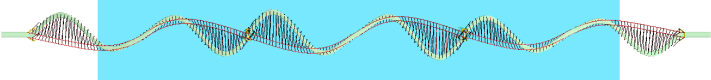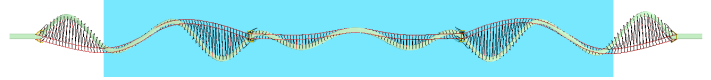
C   Eigenvalues
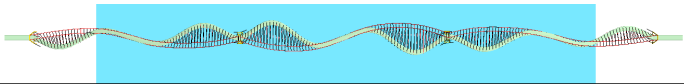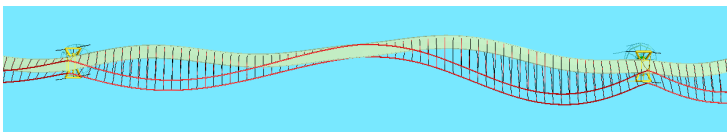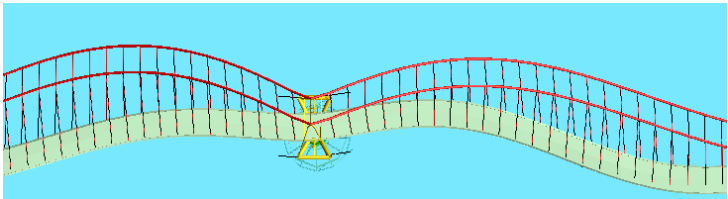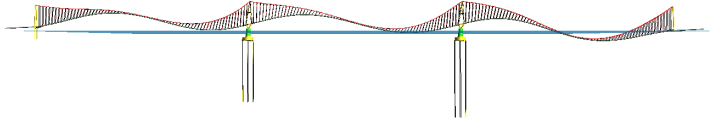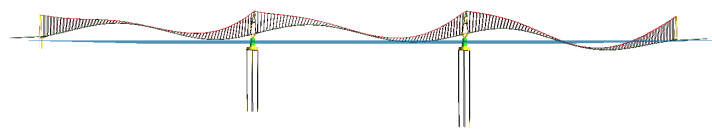
Eigenperiods and eigenmodes

Mode number	Eigenperiod [s]	Eigenmode
1	104.4	
2	81.5	
3	23.6	
4	22.2	
5	22.1	
6	21.4	
7	20.7	
8	13.3	
9	12.3	
10	11.4	

Eigenperiods and eigenmodes

Mode number	Eigenperiod [s]	Eigenmode
11	11.1	
12	10.8	
13	9.7	
14	9.0	
15	8.8	
16	8.3	
17	7.5	
18	6.7	
19	6.3	

Eigenperiods and eigenmodes

Mode number	Eigenperiod [s]	Eigenmode
20	6.0	
21	5.5	
22	5.3	
23	5.2	
24	5.0	

D Additional results ship collisions

D.1 With barrier

D.1.1 Key results

Key results 50 [MJ] impact

Item		Units	Min	Average	Max
	Displacement Bridge Girder	[m]	-0.9	0	2.2
	Acceleration Bridge Girder	[m s^{-2}]	-0.18	0.0	0.23
Floater 1	Displacement Tower	[m]	-0.8	0.0	2.2
	Acceleration Tower	[m s^{-2}]	-0.12	0.0	0.15
	Displacement Bridge Girder	[m]	-0.5	0.0	1.8
	Acceleration Bridge Girder	[m s^{-2}]	-0.01	0.0	0.01
Floater 2	Displacement Tower	[m]	-0.5	0.0	1.8
	Acceleration Tower	[m s^{-2}]	-0.01	0.0	0.01
Cable force		[MN]	131	131	132
Tether force		[MN]	46.4	49.6	52.8
Barrier dof 1		[m]	-4.9	0	8.7
Barrier dof 3		[m]	0	0	0.4
Ship indentation		[m]	0	0	1.4
Peak force		[MN]	0	0	26.4

Key results 200 [MJ] impact

Item		Units	Min	Average	Max
	Displacement Bridge Girder	[m]	-7.4	0	10.3
	Acceleration Bridge Girder	[m s^{-2}]	-0.10	0.0	0.22
Floater 1	Displacement Tower	[m]	-7.3	0.0	10.3
	Acceleration Tower	[m s^{-2}]	-0.15	0.0	0.15
	Displacement Bridge Girder	[m]	-5.9	0.0	7.2
	Acceleration Bridge Girder	[m s^{-2}]	-0.04	0.0	0.03
Floater 2	Displacement Tower	[m]	-5.8	0.0	7.2
	Acceleration Tower	[m s^{-2}]	-0.03	0.0	0.03
Cable force		[MN]	130	131	133
Tether force		[MN]	42.0	49.7	57.1
Barrier dof 1		[m]	-13.3	0	24.3
Barrier dof 3		[m]	0	0	4.8
Ship indentation		[m]	0	0	2.2
Peak force		[MN]	0	0	26.4

Key results 350 [MJ] impact

Item		Units	Min	Average	Max
Floater 1	Displacement Bridge Girder	[m]	-8.5	0	11.5
	Acceleration Bridge Girder	[m s^{-2}]	-0.16	0.0	0.30
	Displacement Tower	[m]	-8.3	0.0	11.5
	Acceleration Tower	[m s^{-2}]	-0.22	0.0	0.25
Floater 2	Displacement Bridge Girder	[m]	-6.8	0.0	8.1
	Acceleration Bridge Girder	[m s^{-2}]	-0.04	0.0	0.04
	Displacement Tower	[m]	-6.7	0.0	8.0
	Acceleration Tower	[m s^{-2}]	-0.04	0.0	0.04
Cable force		[MN]	130	131	133
Tether force		[MN]	40.2	49.7	58.7
Barrier dof 1		[m]	-16.5	0	28.9
Barrier dof 3		[m]	0	0	7.3
Ship indentation		[m]	0	0	3.2
Peak force		[MN]	0	0	29.5

Key results 1 200 [MJ] impact

Item		Units	Min	Average	Max
Floater 1	Displacement Bridge Girder	[m]	-15.6	0	20.4
	Acceleration Bridge Girder	[m s^{-2}]	-0.37	0.0	0.54
	Displacement Tower	[m]	-15.3	0.0	20.3
	Acceleration Tower	[m s^{-2}]	-0.57	0.0	0.69
Floater 2	Displacement Bridge Girder	[m]	-12.8	0.0	14.2
	Acceleration Bridge Girder	[m s^{-2}]	-0.08	0.0	0.08
	Displacement Tower	[m]	-12.6	0.0	14.0
	Acceleration Tower	[m s^{-2}]	-0.08	0.0	0.09
Cable force		[MN]	124	132	139
Tether force		[MN]	31.6	49.9	68.4
Barrier dof 1		[m]	-28.1	0	47.8
Barrier dof 3		[m]	0	0	23.8
Ship indentation		[m]	0	0	8.1
Peak force		[MN]	0	0	44.1

D.1.2 Figures
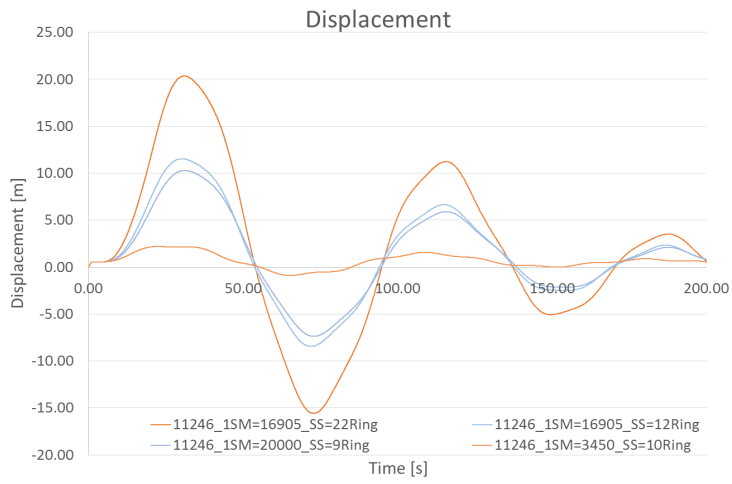
Displacement of impacted floater with barrier
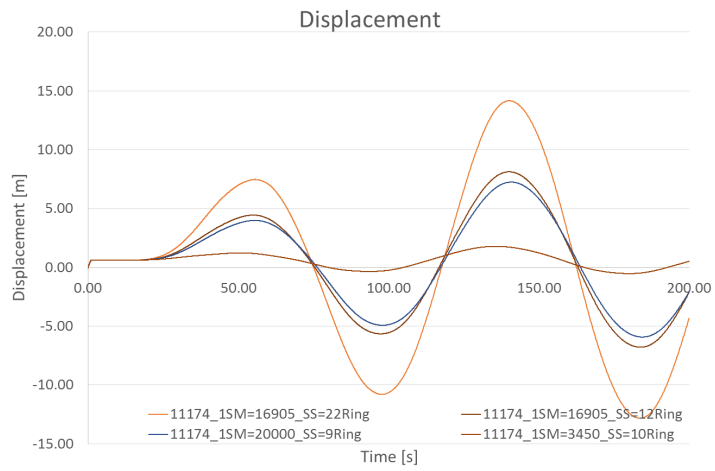
Displacement of second floater with barrier

Displacement of superstructure on impacted floater with barrier

XXII
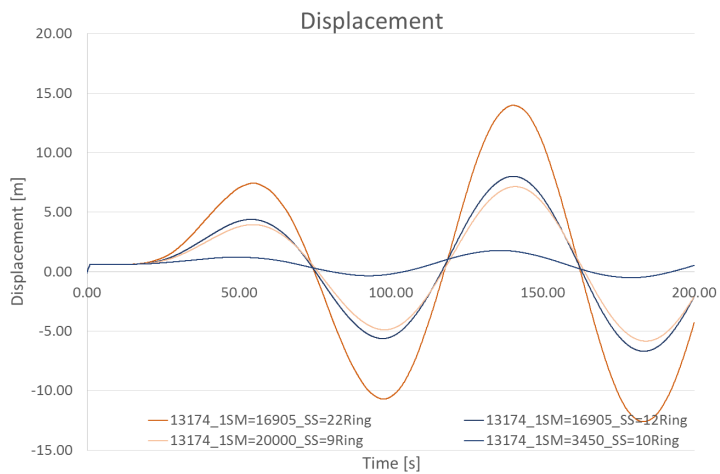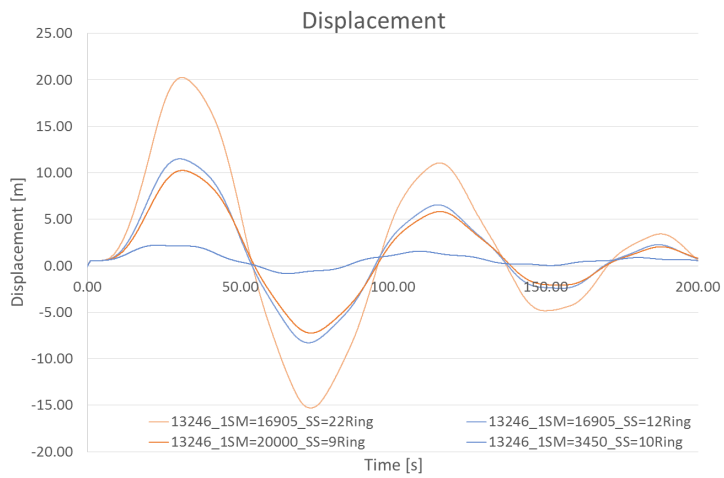
Displacement of superstructure on second floater with barrier
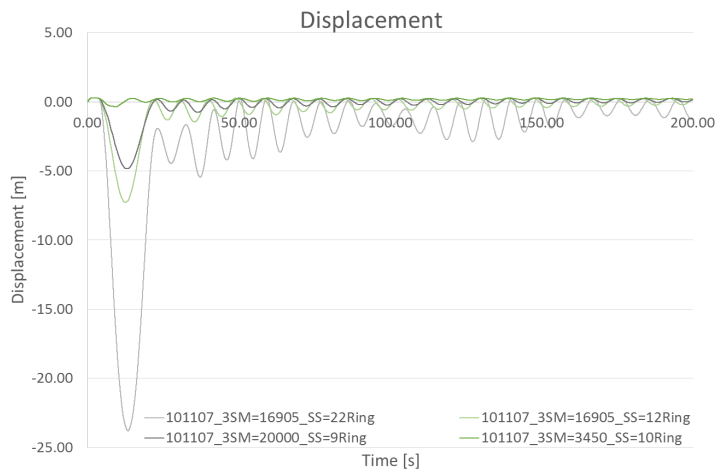
Vertical displacement of barrier
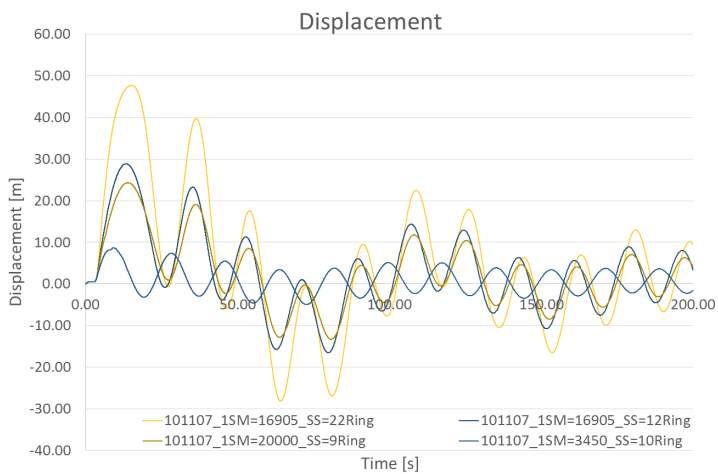
Horizontal displacement of barrier
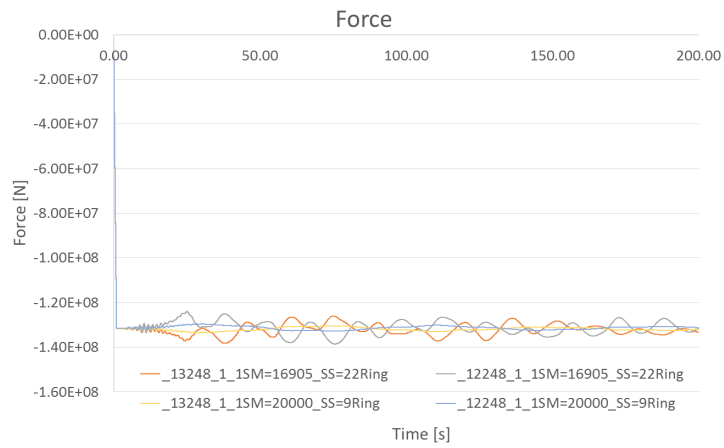
Cable force with barrier

Cable force with barrier

Force in tether 10131 barrier

XXIV
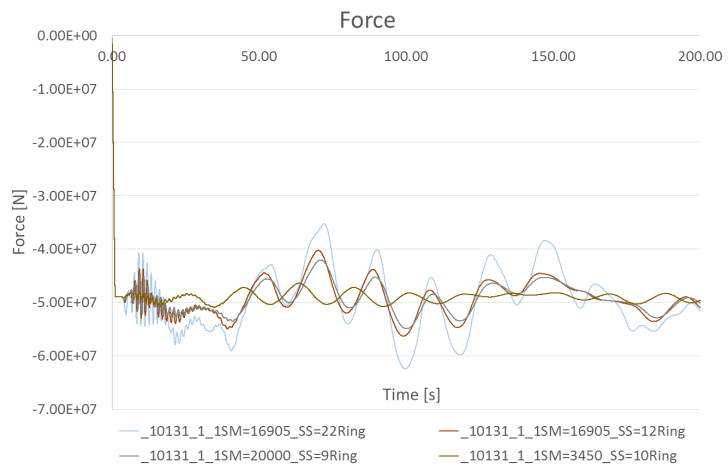
Force in tether 10132 barrier

Force in tether 10133 barrier

Force in tether 10134 barrier
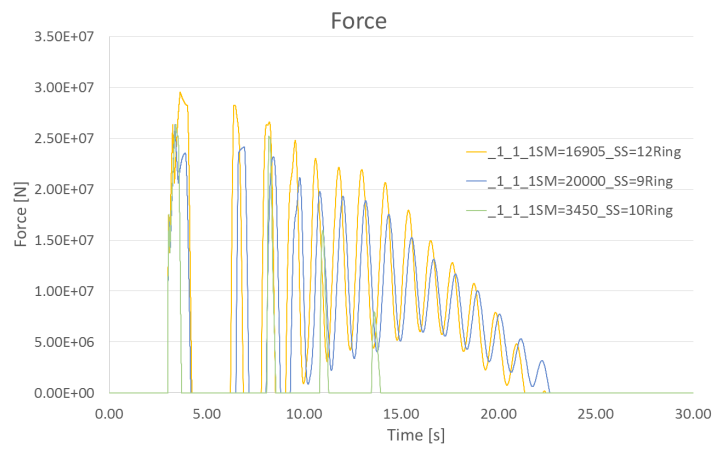
Force in tether 10133 barrier

D.2   Without barrier

D.2.1   Key results

Key results 50 [MJ] impact

Item		Units	Min	Average	Max
Floater 1	Displacement Bridge Girder	[m]	-0.8	0	2.4
	Acceleration Bridge Girder	[m s^{-2}]	-0.47	0.0	1.01
	Displacement Tower	[m]	-0.7	0.0	2.5
	Acceleration Tower	[m s^{-2}]	-0.99	0.0	0.95
Floater 2	Displacement Bridge Girder	[m]	-0.5	0.0	2.0
	Acceleration Bridge Girder	[m s^{-2}]	-0.03	0.0	0.04
	Displacement Tower	[m]	-0.5	0.0	2.0
	Acceleration Tower	[m s^{-2}]	-0.09	0.0	0.09
Cable force		[MN]	130	131	132
Tether force		[MN]	33.6	41.6	49.5
Ship indentation		[m]	0	0	1.9
Peak force		[MN]	0	0	34.6

Key results 200 [MJ] impact

Item		Units	Min	Average	Max
Floater 1	Displacement Bridge Girder	[m]	-5.0	0	8.0
	Acceleration Bridge Girder	[m s^{-2}]	-0.32	0.0	0.99
	Displacement Tower	[m]	-5.0	0.0	8.0
	Acceleration Tower	[m s^{-2}]	-0.61	0.0	1.01
Floater 2	Displacement Bridge Girder	[m]	-4.3	0.0	6.0
	Acceleration Bridge Girder	[m s^{-2}]	-0.03	0.0	0.04
	Displacement Tower	[m]	-4.3	0.0	5.9
	Acceleration Tower	[m s^{-2}]	-0.06	0.0	0.08
Cable force		[MN]	130	131	133
Tether force		[MN]	29.9	44.5	53.2
Ship indentation		[m]	0	0	6.7
Peak force		[MN]	0	0	41.3

Key results 350 [MJ] impact

Item		Units	Min	Average	Max
Floater 1	Displacement Bridge Girder	[m]	-5.6	0	8.7
	Acceleration Bridge Girder	[m s^{-2}]	-0.48	0.0	1.08
	Displacement Tower	[m]	-5.5	0.0	8.7
	Acceleration Tower	[m s^{-2}]	-0.62	0.0	1.06
Floater 2	Displacement Bridge Girder	[m]	-4.9	0.0	6.5
	Acceleration Bridge Girder	[m s^{-2}]	-0.03	0.0	0.03
	Displacement Tower	[m]	-4.8	0.0	6.5
	Acceleration Tower	[m s^{-2}]	-0.06	0.0	0.07
Cable force		[MN]	130	132	133
Tether force		[MN]	28.1	41.6	55.1
Ship indentation		[m]	0	0	9.4
Peak force		[MN]	0	0	49.5

Key results 1 200 [MJ] impact

| Item		Units	Min	Average	Max
Floater 1	Displacement Bridge Girder	[m]	-8.5	0	15.1
	Acceleration Bridge Girder	[m s^{-2}]	-1.11	0.0	1.24
	Displacement Tower	[m]	-8.4	0.0	15.0
	Acceleration Tower	[m s^{-2}]	-1.35	0.0	1.31
Floater 2	Displacement Bridge Girder	[m]	-7.8	0.0	9.9
	Acceleration Bridge Girder	[m s^{-2}]	-0.06	0.0	0.07
	Displacement Tower	[m]	-7.7	0.0	9.8
	Acceleration Tower	[m s^{-2}]	-0.13	0.0	0.14
Cable force		[MN]	130	132	135
Tether force		[MN]	25.6	41.6	57.7
Ship indentation		[m]	0	0	26.8
Peak force		[MN] [MN]	0	0	54.4

D.2.2 Figures
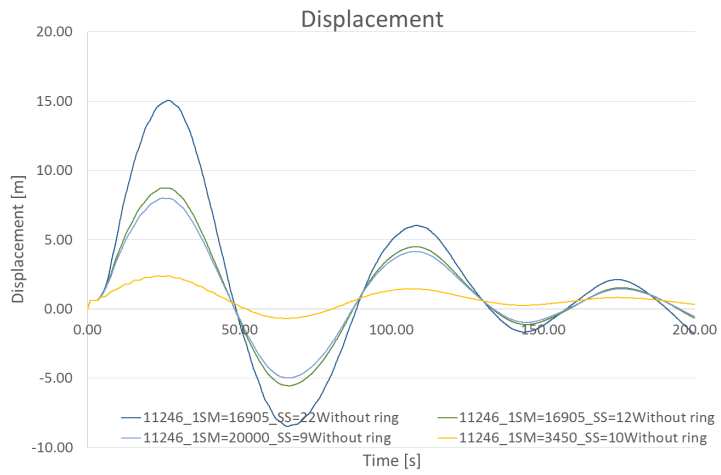
Displacement of impacted floater with barrier
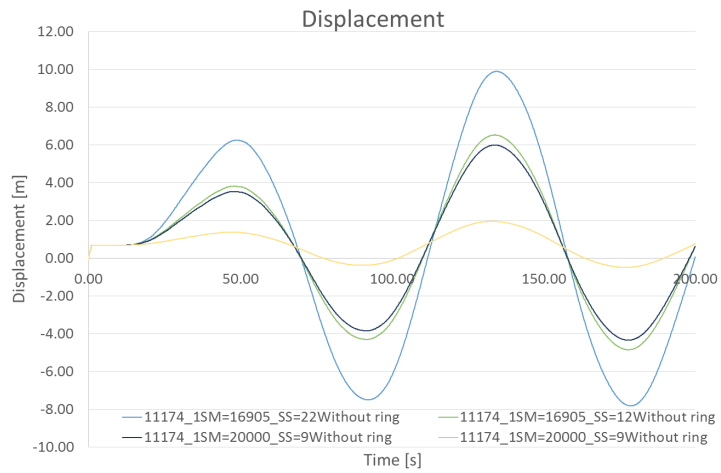

Displacement of second floater with barrier

Displacement of superstructure on impacted floater with barrier

XXIX
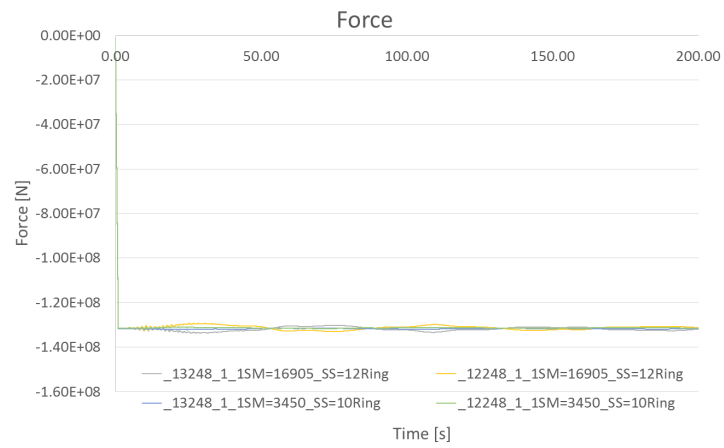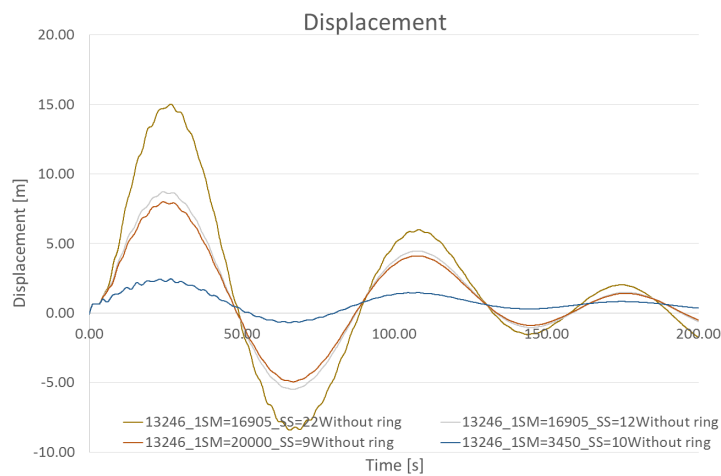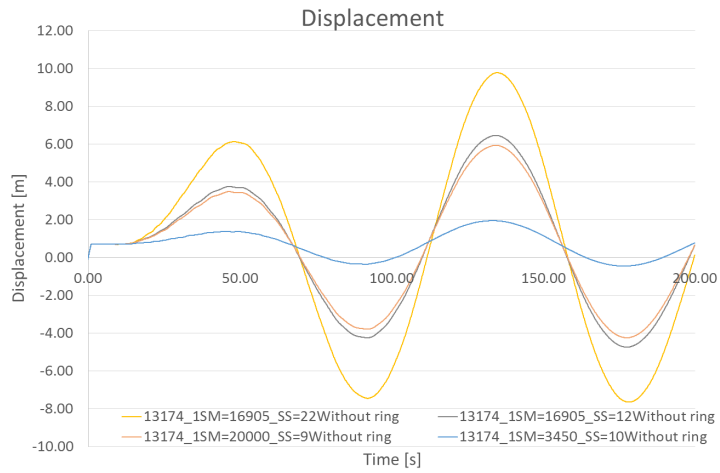
Displacement of superstructure on second floater with barrier
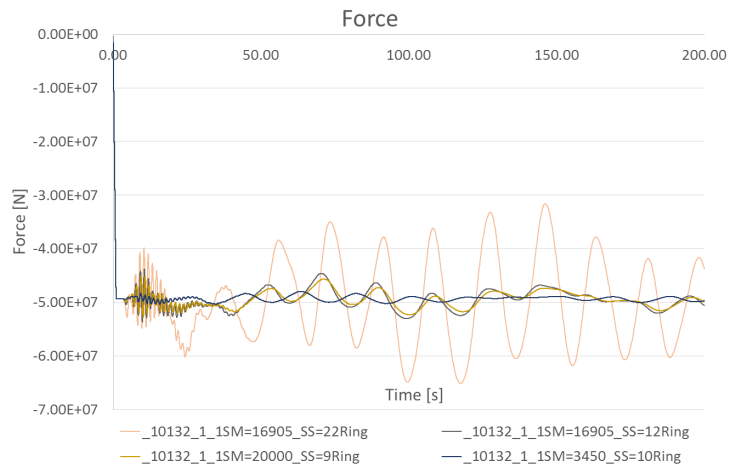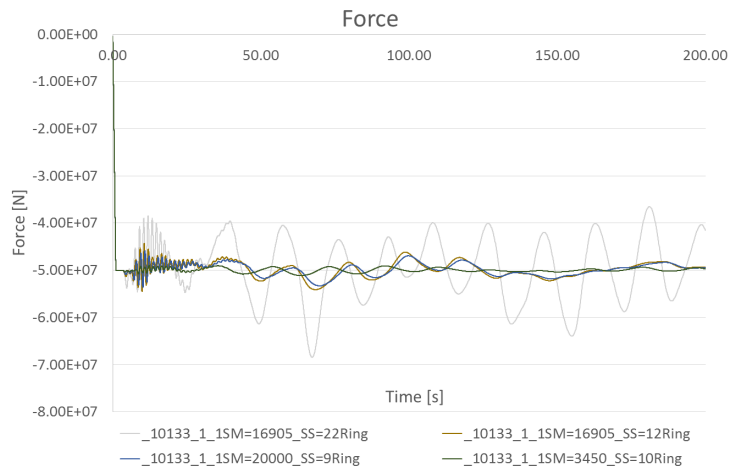

Cable force with barrier
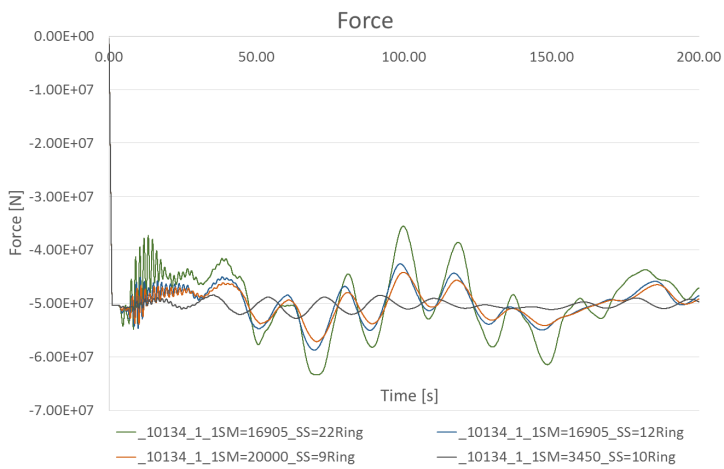

Cable force with barrier

XXX
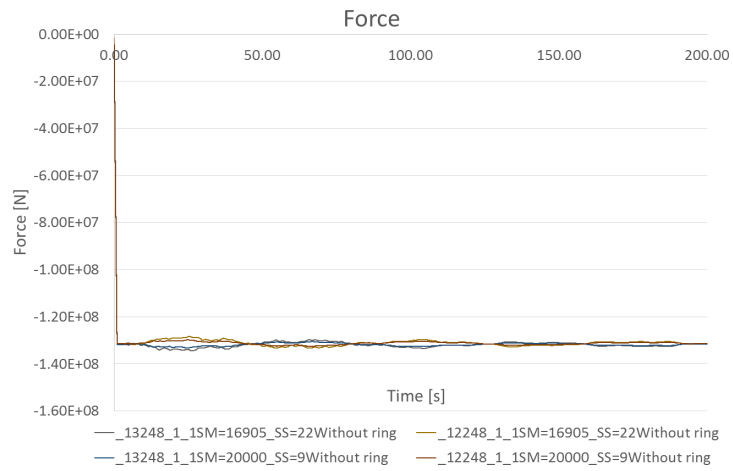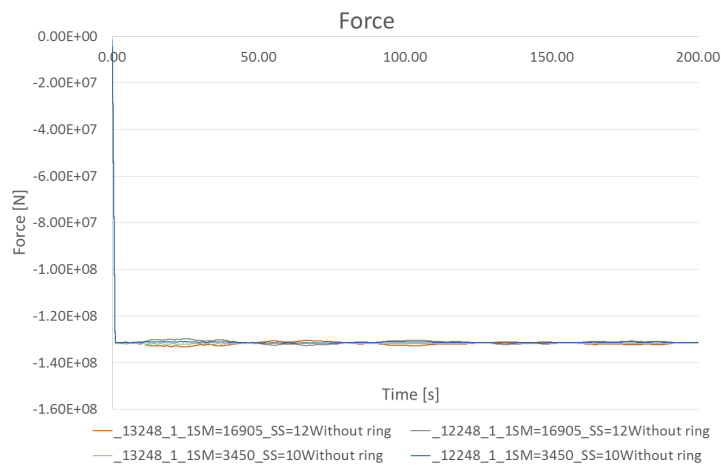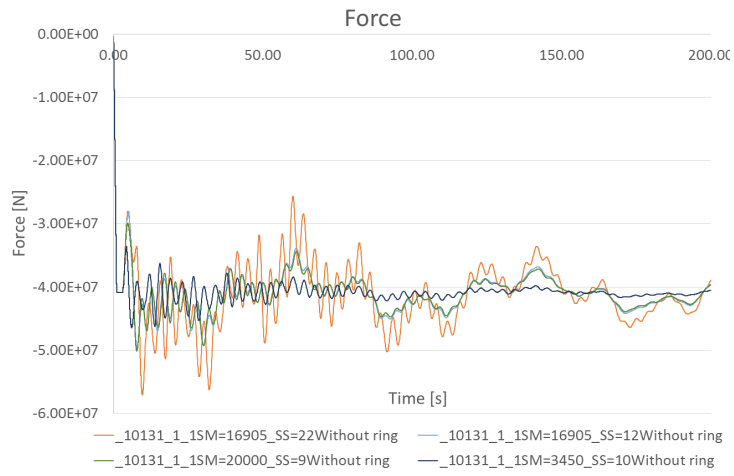
Force in tether 10131 barrier

Force in tether 10132 barrier
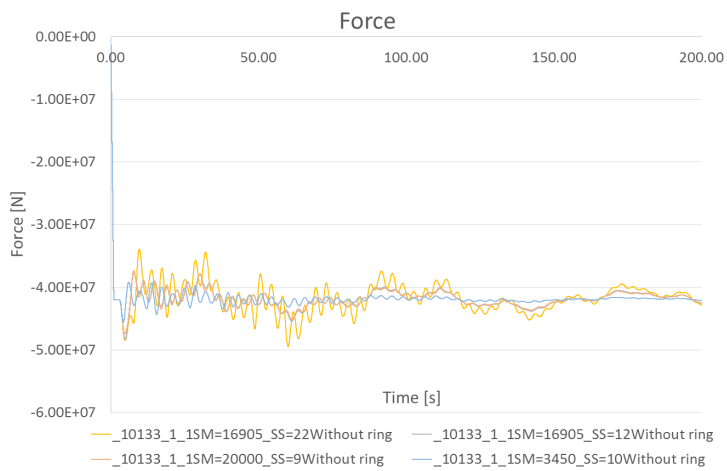
Force in tether 10133 barrier

XXXI

Force in tether 10134 barrier

Force in tether 10133 barrier

XXXII
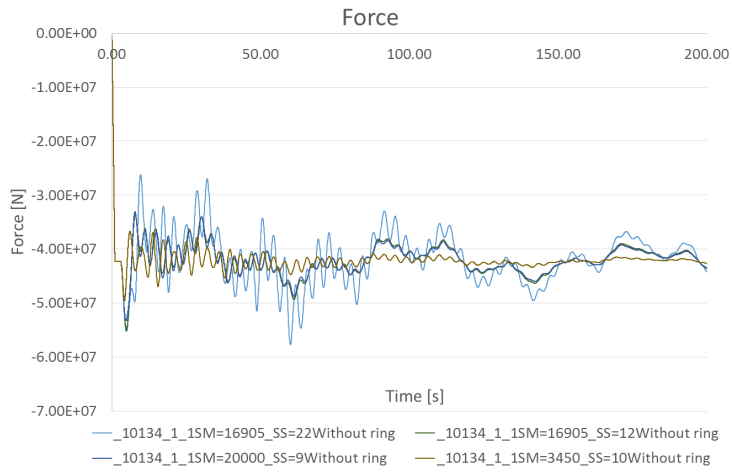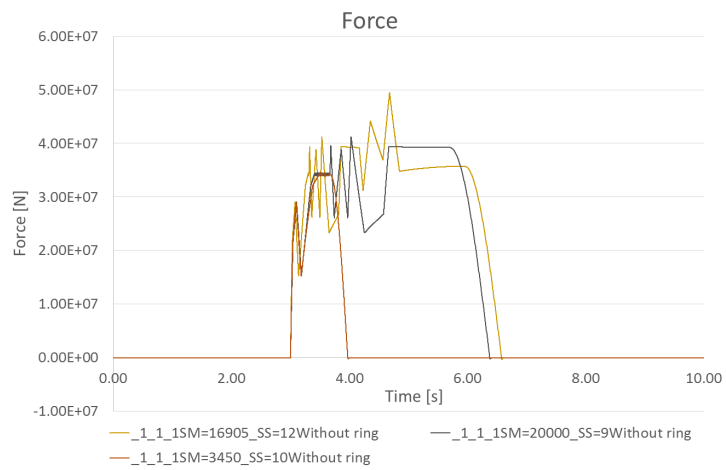
D.3   Parameter study

Key results Diameter=4[m] and thickness=25 [mm]

Item		Units	Min	Average	Max
Floater 1	Displacement Bridge Girder	[m]	-19.0	0	15.2
	Acceleration Bridge Girder	[m s^{-2}]	-0.49	0.0	0.36
	Displacement Tower	[m]	-18.9	0.0	15.1
	Acceleration Tower	[m s^{-2}]	-1.04	0.0	1.06
Floater 2	Displacement Bridge Girder	[m]	-14.3	0.0	15.2
	Acceleration Bridge Girder	[m s^{-2}]	-0.16	0.0	0.13
	Displacement Tower	[m]	-14.2	0.0	15.0
	Acceleration Tower	[m s^{-2}]	-0.31	0.0	0.25
Cable force		[MN]	110	131	151
Tether force		[MN]	5.0	41.4	84.3
Barrier dof 1		[m]	-33.6	0	48.7
Barrier dof 3		[m]	0	0	27.4
Ship indentation		[m]	0	0	4.6
Peak force		[MN]	0	0	35.2

Key results Diameter=4[m] and thickness=50 [mm]

Item		Units	Min	Average	Max
Floater 1	Displacement Bridge Girder	[m]	-15.7	0	16.5
	Acceleration Bridge Girder	[m s^{-2}]	-0.39	0.0	0.54
	Displacement Tower	[m]	-15.5	0.0	16.2
	Acceleration Tower	[m s^{-2}]	-0.77	0.0	0.60
Floater 2	Displacement Bridge Girder	[m]	-12.4	0.0	13.9
	Acceleration Bridge Girder	[m s^{-2}]	-0.11	0.0	0.12
	Displacement Tower	[m]	-12.2	0.0	13.8
	Acceleration Tower	[m s^{-2}]	-0.22	0.0	0.24
Cable force		[MN]	110	131	151
Tether force		[MN]	-1.4	39.8	81.0
Barrier dof 1		[m]	-33.9	0	51.3
Barrier dof 3		[m]	0	0	31.0
Ship indentation		[m]	0	0	5.2
Peak force		[MN]	0	0	42.9

Key results Diameter=4[m] and thickness=75 [mm]

Item		Units	Min	Average	Max
Floater 1	Displacement Bridge Girder	[m]	-14.7	0	19.0
	Acceleration Bridge Girder	[m s^{-2}]	-0.35	0.0	0.41
	Displacement Tower	[m]	-14.5	0.0	18.8
	Acceleration Tower	[m s^{-2}]	-0.97	0.0	0.71
Floater 2	Displacement Bridge Girder	[m]	-12.0	0.0	14.2
	Acceleration Bridge Girder	[m s^{-2}]	-0.10	0.0	0.09
	Displacement Tower	[m]	-11.8	0.0	14.1
	Acceleration Tower	[m s^{-2}]	-0.21	0.0	0.18
Cable force		[MN]	120	131	145
Tether force		[MN]	8.5	39.6	85.4
Barrier dof 1		[m]	-32.7	0	53.4
Barrier dof 3		[m]	0	0	36.0
Ship indentation		[m]	0	0	10.0
Peak force		[MN]	0	0	44.1

Key results Diameter=6[m] and thickness=25 [mm]

Item		Units	Min	Average	Max
Floater 1	Displacement Bridge Girder	[m]	-14.0	0	18.8
	Acceleration Bridge Girder	[m s^{-2}]	-0.45	0.0	0.37
	Displacement Tower	[m]	-14.0	0.0	18.6
	Acceleration Tower	[m s^{-2}]	-0.72	0.0	0.5
Floater 2	Displacement Bridge Girder	[m]	-12.1	0.0	13.6
	Acceleration Bridge Girder	[m s^{-2}]	-0.09	0.0	0.10
	Displacement Tower	[m]	-11.9	0.0	13.5
	Acceleration Tower	[m s^{-2}]	-0.19	0.0	0.20
Cable force		[MN]	120	131	145
Tether force		[MN]	20.2	45.1	66.8
Barrier dof 1		[m]	-25.0	0	45.9
Barrier dof 3		[m]	0	0	17.3
Ship indentation		[m]	0	0	6.4
Peak force		[MN]	0	0	44.1

Key results Diameter=6[m] and thickness=50 [mm]

Item		Units	Min	Average	Max
Floater 1	Displacement Bridge Girder	[m]	-14.4	0	19.8
	Acceleration Bridge Girder	[m s^{-2}]	-0.74	0.0	0.73
	Displacement Tower	[m]	-14.3	0.0	19.8
	Acceleration Tower	[m s^{-2}]	-0.80	0.0	0.49
Floater 2	Displacement Bridge Girder	[m]	-12.2	0.0	14.2
	Acceleration Bridge Girder	[m s^{-2}]	-0.07	0.0	0.07
	Displacement Tower	[m]	-12.0	0.0	14.1
	Acceleration Tower	[m s^{-2}]	-0.10	0.0	0.10
Cable force		[MN]	120	131	141
Tether force		[MN]	15.8	43.3	66.8
Barrier dof 1		[m]	-28.2	0	45.6
Barrier dof 3		[m]	0	0	19.9
Ship indentation		[m]	0	0	7.4
Peak force		[MN]	0	0	44.1

Key results Diameter=6[m] and thickness=75 [mm]

Item		Units	Min	Average	Max
Floater 1	Displacement Bridge Girder	[m]	-15.2	0	21.1
	Acceleration Bridge Girder	[m s^{-2}]	-0.36	0.0	0.52
	Displacement Tower	[m]	-15.0	0.0	21.0
	Acceleration Tower	[m s^{-2}]	-0.55	0.0	0.67
Floater 2	Displacement Bridge Girder	[m]	-13.2	0.0	15.3
	Acceleration Bridge Girder	[m s^{-2}]	-0.07	0.0	0.07
	Displacement Tower	[m]	-13.0	0.0	15.2
	Acceleration Tower	[m s^{-2}]	-0.08	0.0	0.07
Cable force		[MN]	126	131	138
Tether force		[MN]	24.9	41.9	58.8
Barrier dof 1		[m]	-29.4	0	47.8
Barrier dof 3		[m]	0	0	23.8
Ship indentation		[m]	0	0	8.3
Peak force		[MN]	0	0	44.1

Key results Diameter=8[m] and thickness=25 [mm]

Item		Units	Min	Average	Max
Floater 1	Displacement Bridge Girder	[m]	-15.3	0	21.0
	Acceleration Bridge Girder	[m s^{-2}]	-0.31	0.0	0.72
	Displacement Tower	[m]	-15.2	0.0	20.8
	Acceleration Tower	[m s^{-2}]	-0.35	0.0	0.57
Floater 2	Displacement Bridge Girder	[m]	-13.2	0.0	15.3
	Acceleration Bridge Girder	[m s^{-2}]	-0.07	0.0	0.09
	Displacement Tower	[m]	-12.9	0.0	14.3
	Acceleration Tower	[m s^{-2}]	-0.13	0.0	0.14
Cable force		[MN]	130	132	137
Tether force		[MN]	33.2	48.9	65.6
Barrier dof 1		[m]	-25.1	0	34.1
Barrier dof 3		[m]	0	0	10.6
Ship indentation		[m]	0	0	8.3
Peak force		[MN]	0	0	44.1

Key results Diameter=8[m] and thickness=50 [mm]

Item		Units	Min	Average	Max
Floater 1	Displacement Bridge Girder	[m]	-15.1	0	20.4
	Acceleration Bridge Girder	[m s^{-2}]	-0.22	0.0	0.53
	Displacement Tower	[m]	-15.0	0.0	20.2
	Acceleration Tower	[m s^{-2}]	-0.25	0.0	0.42
Floater 2	Displacement Bridge Girder	[m]	-12.7	0.0	14.3
	Acceleration Bridge Girder	[m s^{-2}]	-0.07	0.0	0.07
	Displacement Tower	[m]	-12.5	0.0	14.2
	Acceleration Tower	[m s^{-2}]	-0.07	0.0	0.07
Cable force		[MN]	130	132	137
Tether force		[MN]	32.9	47.0	60.5
Barrier dof 1		[m]	-26.7	0	36.0
Barrier dof 3		[m]	0	0	11.9
Ship indentation		[m]	0	0	9.5
Peak force		[MN]	0	0	44.1

Key results Diameter=8[m] and thickness=75 [mm]

Item		Units	Min	Average	Max
Floater 1	Displacement Bridge Girder	[m]	-15.1	0	19.6
	Acceleration Bridge Girder	[m s^{-2}]	-0.19	0.0	0.45
	Displacement Tower	[m]	-13.8	0.0	19.5
	Acceleration Tower	[m s^{-2}]	-0.33	0.0	0.39
Floater 2	Displacement Bridge Girder	[m]	-12.5	0.0	14.2
	Acceleration Bridge Girder	[m s^{-2}]	-0.07	0.0	0.07
	Displacement Tower	[m]	-12.3	0.0	14.1
	Acceleration Tower	[m s^{-2}]	-0.08	0.0	0.08
Cable force		[MN]	130	132	135
Tether force		[MN]	26.0	45.0	61.1
Barrier dof 1		[m]	-29.2	0	38.7
Barrier dof 3		[m]	0	0	13.8
Ship indentation		[m]	0	0	10.5
Peak force		[MN]	0	0	44.1

Key results Diameter=10[m] and thickness=25 [mm]

Item		Units	Min	Average	Max
Floater 1	Displacement Bridge Girder	[m]	-14.6	0	19.5
	Acceleration Bridge Girder	[m s^{-2}]	-0.29	0.0	0.57
	Displacement Tower	[m]	-14.5	0.0	19.5
	Acceleration Tower	[m s^{-2}]	-0.40	0.0	0.46
Floater 2	Displacement Bridge Girder	[m]	-11.8	0.0	12.9
	Acceleration Bridge Girder	[m s^{-2}]	-0.08	0.0	0.10
	Displacement Tower	[m]	-11.8	0.0	12.7
	Acceleration Tower	[m s^{-2}]	-0.15	0.0	0.18
Cable force		[MN]	130	132	137
Tether force		[MN]	34.9	54.3	75.7
Barrier dof 1		[m]	-23.5	0	30.2
Barrier dof 3		[m]	0	0	6.5
Ship indentation		[m]	0	0	10.5
Peak force		[MN]	0	0	44.1

Key results Diameter=10[m] and thickness=50 [mm]

Item		Units	Min	Average	Max
Floater 1	Displacement Bridge Girder	[m]	-14.2	0	19.2
	Acceleration Bridge Girder	[m s^{-2}]	-0.24	0.0	0.40
	Displacement Tower	[m]	-14.1	0.0	19.0
	Acceleration Tower	[m s^{-2}]	-0.24	0.0	0.37
Floater 2	Displacement Bridge Girder	[m]	-11.7	0.0	13.0
	Acceleration Bridge Girder	[m s^{-2}]	-0.07	0.0	0.08
	Displacement Tower	[m]	-11.5	0.0	12.8
	Acceleration Tower	[m s^{-2}]	-0.08	0.0	0.07
Cable force		[MN]	130	132	135
Tether force		[MN]	38.4	51.8	65.6
Barrier dof 1		[m]	-24.9	0	32.3
Barrier dof 3		[m]	0	0	7.1
Ship indentation		[m]	0	0	11.6
Peak force		[MN]	0	0	44.1

E   Additional results Environmental loads

Results from simulations with environmental loads

| Seed | Floater 1 | | Tower 1 | Floater 2 | |
	displacement [m]	acceleration [m s^{-2}]	acceleration [m s^{-2}]	displacement [m]	acceleration [m s^{-2}]
1	27.7	0.21	0.49	30.5	0.18
2	27.0	0.19	0.52	31.0	0.20
3	26.4	-0.18	-0.48	29.2	-0.18
4	28.2	0.20	-0.50	32.1	-0.19
5	25.5	0.19	0.50	29.1	-0.22
6	28.5	0.21	0.49	27.9	-0.19
7	30.8	0.19	0.46	32.1	-0.18
8	29.0	0.18	0.47	30.4	0.19
9	27.3	-0.20	-0.48	35.0	-0.20
10	26.3	-0.19	-0.47	29.5	0.18
11	26.7	0.18	0.46	32.9	0.18
12	30.3	0.20	-0.54	28.8	0.20
13	26.4	-0.18	-0.45	28.2	0.20
14	29.5	-0.21	-0.51	30.7	0.18
15	29.0	-0.22	0.53	30.2	0.20
16	27.2	0.19	-0.49	32.4	0.18
17	26.5	-0.17	-0.46	29.8	0.19
18	26.3	0.18	0.40	28.4	-0.19
19	28.4	-0.23	-0.57	28.4	0.17
20	24.7	0.21	0.52	32.7	-0.16
21	25.6	0.23	0.52	27.5	0.18
22	28.9	0.25	0.63	28.7	0.19
23	27.3	0.21	-0.48	28.7	-0.20
24	28.9	0.19	-0.46	28.5	-0.17
25	25.5	-0.19	-0.48	30.5	0.23
26	26.9	0.17	0.45	29.4	0.19
27	26.0	-0.17	-0.43	31.8	0.20
28	26.3	0.23	0.60	27.7	0.20
29	29.4	-0.20	0.50	30.3	0.20
30	28.3	0.19	-0.49	31.1	0.18

Results from simulations with environmental loads

Seed	Midspan deflection [m]	Midspan acceleration [m s^{-2}]	Tether force Maximum [N]	Tether force Minimum [N]	Tower 2 acceleration [m s^{-2}]
1	35.9	-0.81	-7.82E+07	8.90E+06	0.51
2	34.5	-0.70	-6.98E+07	-3.99E+05	0.49
3	35.0	-0.92	-7.59E+07	1.47E+07	0.50
4	35.4	-0.79	-7.21E+07	8.40E+06	-0.50
5	34.3	0.74	-6.81E+07	3.81E+06	-0.54
6	35.9	-0.66	-6.68E+07	4.92E+06	-0.51
7	37.1	0.68	-6.42E+07	1.15E+06	0.47
8	36.9	-0.72	-7.29E+07	2.69E+06	-0.46
9	37.4	-0.73	-7.48E+07	1.33E+07	-0.48
10	34.9	0.69	-6.00E+07	-2.83E+06	-0.43
11	34.3	-0.74	-7.58E+07	1.42E+07	-0.51
12	34.9	0.72	-6.90E+07	3.17E+06	0.50
13	34.0	-0.85	-6.69E+07	5.50E+06	0.53
14	35.2	-0.59	-7.23E+07	1.82E+06	-0.53
15	35.8	-0.82	-6.69E+07	2.77E+06	0.50
16	35.5	0.73	-7.64E+07	1.05E+07	-0.50
17	35.7	-0.69	-7.53E+07	7.32E+06	-0.51
18	32.8	-0.72	-6.53E+07	3.10E+06	-0.51
19	34.5	0.67	-6.45E+07	5.47E+05	-0.44
20	33.1	0.74	-6.55E+07	2.92E+06	-0.44
21	34.6	0.65	-7.08E+07	3.70E+06	-0.47
22	34.8	-0.73	-6.59E+07	7.72E+04	0.51
23	35.3	0.75	-8.06E+07	1.62E+07	-0.53
24	36.1	-0.68	-7.08E+07	3.93E+06	-0.47
25	34.6	-0.65	-6.50E+07	-4.31E+05	0.53
26	37.4	-0.68	-6.31E+07	6.42E+04	0.45
27	34.1	0.66	-6.98E+07	7.81E+06	-0.50
28	34.7	0.66	-6.60E+07	9.55E+05	-0.54
29	36.8	-0.78	-6.70E+07	4.36E+06	0.53
30	36.1	0.72	-6.80E+07	4.21E+06	0.46